

CHAPTER 4

RESULTS AND DISCUSSION

Chapter 4

Results and discussion

This chapter deals with the reporting and analysis of results obtained for various experimental procedures followed, as stated in previous chapter.

Following abbreviations will be used hereafter for powders of different processing routes and the consolidated compacts of Ag-ZnO and Ag-CdO systems :

Processing route	Abbreviation used
Conventional PM route of blending	B
Spray-coprecipitation route	C
Electroless coating route	E
Freeze-drying route	F
Mechanical - Alloying route	MA

Accordingly, typical nomenclature for Ag-10 wt% CdO powder or consolidated compact prepared by conventional PM route of blending would be Ag-10 CdO (B). Sameway, Ag-10.8 wt% ZnO powder or compact prepared by Mechanical Alloying process will be designated as Ag 10.8 ZnO (MA).

4.1 Powder characterization :

4.1.1 : Chemical analysis of powders :

The powders of Ag-ZnO and Ag-CdO of different processing routes were chemically analysed by EDTA titration. Purpose of this analysis was to ensure that the powders

produced by different routes were of required stoichiometry. By and large, no major deviation from stoichiometry was observed in each case.

4.1.2 : Na and K estimation :

It is observed that the control of alkali metal impurity level is a governing factor in deciding the contact performance of Ag-MeO materials. These impurities govern contact properties such as losses due to arc erosion, contact weldability and the arc reignition voltage. Table 4.1 (a) and 4.1 (b) give the measured values of Na and K, respectively, in the final powders for different processing routes. The relatively higher level of potassium (although less than the maximum permissible limit of 50 ppm) as against that of sodium in the reported results, is attributed to lower solubility of KNO_3 (31.2 gm/100 ml of distilled water at $20^{\circ}C$) as compared to $NaNO_3$ (88.0 gm/100 ml of distilled water at $20^{\circ}C$), leaving behind higher amounts of K in the final powders than Na even after vigorous washing [138]. These results clearly indicate that the powders with controlled amounts of Na and K impurities can be produced by procedures adopted in each process route.

4.1.3. XRD analysis :

Fig. 4.1 – 4.3 show the XRD profiles for the starting materials Ag, CdO and ZnO. They are similar to those for respective pure materials. Fig. 4.4 – 4.11 represent the multiple plots for X-ray diffraction of Ag-ZnO and Ag-CdO powder samples for different process routes. The peaks marked '1' indicate silver peaks whereas those marked as '2' are for ZnO or CdO phase.

**Table 4.1 (a) : Estimated values of Na by AAS
for different process routes**

Sample	Sample wt. (g)	Reading	Na ppm
Ag	0.0113	--	--
CdO	0.0125	0.072	5.76
ZnO	0.0114	--	--
Ag 7.1 ZnO (B)	0.0110	--	--
Ag 8.6 ZnO (B)	0.0104	--	--
Ag 10.8 ZnO (B)	0.0108	--	--
Ag 7.1 ZnO (C)	0.0113	--	--
Ag 8.6 ZnO (C)	0.0101	--	--
Ag 10.8 ZnO (C)	0.0124	--	--
Ag 7.1 ZnO (E)	0.0114	0.018	1.58
Ag 8.6 ZnO (E)	0.0099	0.021	2.12
Ag 10.8 ZnO (E)	0.0117	--	--
Ag 7.1 ZnO (F)	0.0125	0.236	18.88
Ag 8.6 ZnO (F)	0.0102	--	--
Ag 10.8 ZnO (F)	0.0101	--	--
Ag 10.8 ZnO (MA)	0.0112	--	--
Ag 10 CdO (B)	0.0110	--	--
Ag 12 CdO (B)	0.0119	--	--
Ag 15 CdO (B)	0.0119	--	--
Ag 10 CdO (C)	0.0130	--	--
Ag 12 CdO (C)	0.0123	--	--
Ag 15 CdO (C)	0.0130	--	--
Ag 10 CdO (E)	0.0130	0.074	5.69
Ag 12 CdO (E)	0.0110	0.097	8.82
Ag 15 CdO (E)	0.0122	0.214	17.54
Ag 10 CdO (F)	0.0112	0.560	50.00
Ag 12 CdO (F)	0.0113	0.315	27.90
Ag 15 CdO (F)	0.0103	0.134	13.00
Ag 15 CdO (MA)	0.0119	--	--

Table 4.1(b) : Estimated values of K by AAS for different process

sample	sample wt. In g	reading	K in ppm
Ag (SRL make)	0.0113	0.425	37.60
CdO (SD make)	0.0125	0.488	38.88
ZnO(EMerck make)	0.0114	0.340	29.82
Ag 7.1 ZnO (B)	0.0110	0.407	37.00
Ag 8.8 ZnO (B)	0.0104	0.380	36.50
Ag 10.8 ZnO (B)	0.0108	0.396	36.70
Ag 7.1 ZnO (C)	0.0113	0.396	35.04
Ag 8.8 ZnO (C)	0.0101	0.508	50.29
Ag 10.8 ZnO (C)	0.0124	0.388	31.29
Ag 7.1 ZnO (E)	0.0114	0.358	31.40
Ag 8.8 ZnO (E)	0.0099	0.345	34.85
Ag 10.8 ZnO (E)	0.0117	0.240	20.51
Ag 7.1 ZnO (F)	0.0125	0.405	32.40
Ag 8.8 ZnO (F)	0.0102	0.341	33.43
Ag 10.8 ZnO (F)	0.0101	0.127	12.57
Ag 10.8 ZnO (MA)	0.0107	0.400	37.40
Ag 10 CdO (B)	0.0110	0.418	38.00
Ag 12 CdO (B)	0.0119	0.419	37.70
Ag 15 CdO (B)	0.0119	0.449	37.70
Ag 10 CdO (C)	0.0130	0.240	18.46
Ag 12 CdO (C)	0.0123	0.330	26.83
Ag 15 CdO (C)	0.0130	0.491	37.77
Ag 10 CdO (E)	0.0130	0.390	30.00
Ag 12 CdO (E)	0.0110	0.121	11.00
Ag 15 CdO (E)	0.0122	0.327	26.80
Ag 10 CdO (F)	0.0112	0.493	44.02
Ag 12 CdO (F)	0.0113	0.444	39.29
Ag 15 CdO (F)	0.0103	0.474	46.02
Ag 15 CdO (MA)	0.0115	0.440	38.26

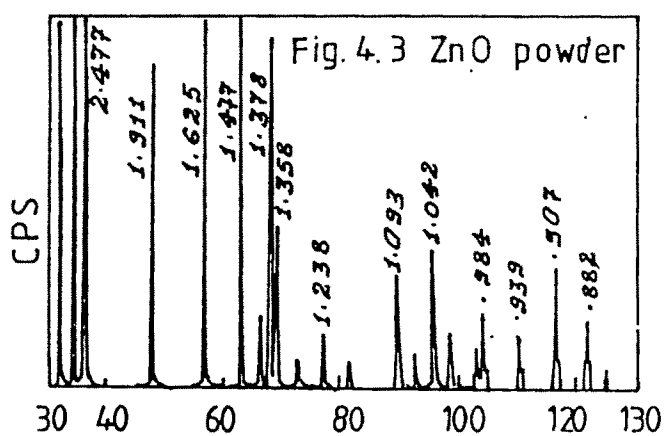
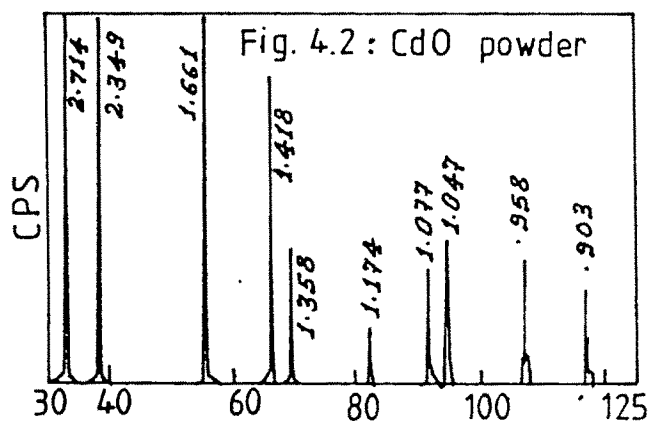
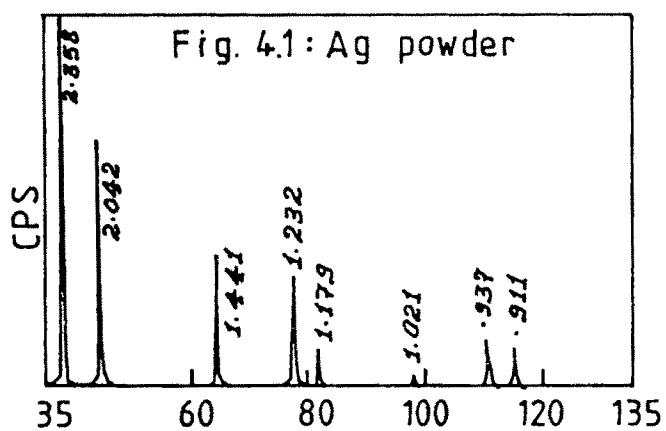


Fig. 4.1-4.3 XRD profiles for starting powders Ag, CdO and ZnO

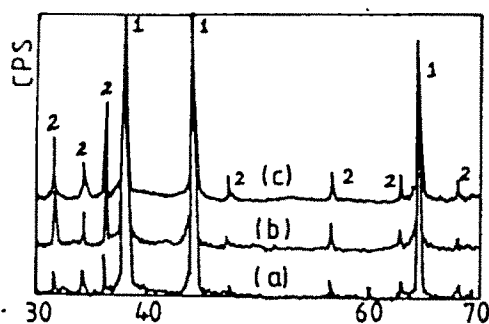


Fig.4.4: XRD profiles for blended powders

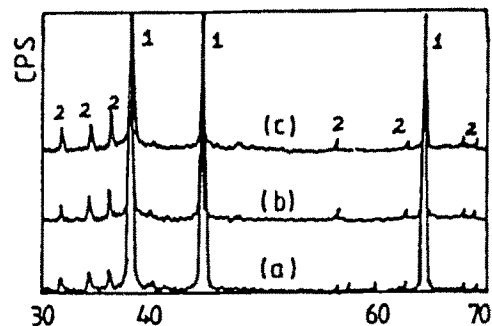


Fig. 4.5 XRD profiles for coprecipitated powders.

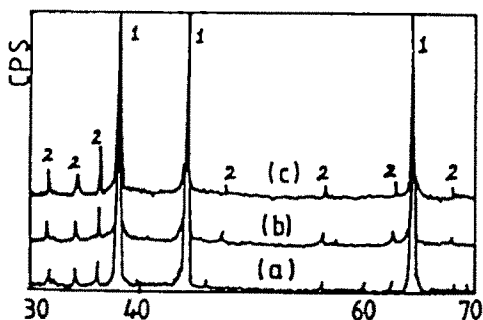


Fig. 4.6 :XRD profiles for electroless-coated powders.

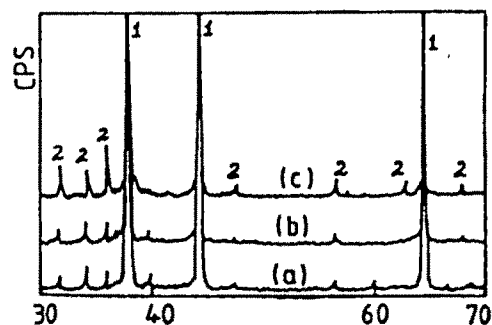


Fig.4.7 :XRD profiles for freeze-dried powders.

Fig 4.4-4.7 Multiple XRD profiles for (a) Ag 7.1ZnO, (b) Ag 8.6 ZnO and (c) Ag 10.8 ZnO powders of different processing routes.

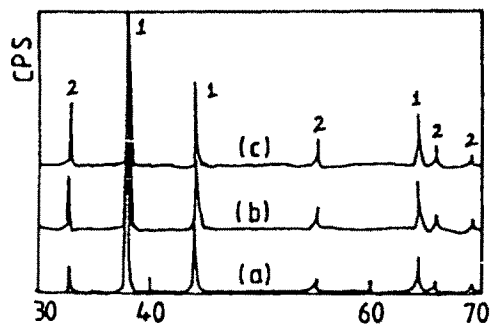


Fig. 4.8 : XRD profiles for blended powders.

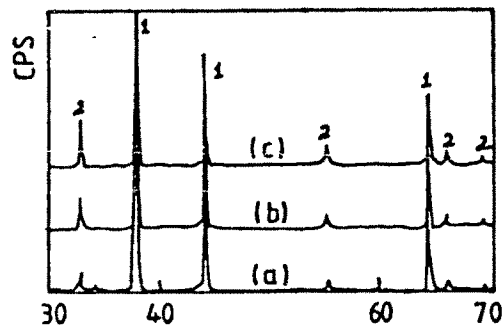


Fig. 4.9 : XRD profiles for coprecipitated powders.

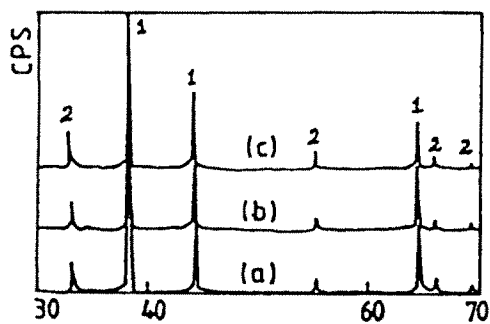


Fig. 4.10 : XRD profiles for electroless coated powders.

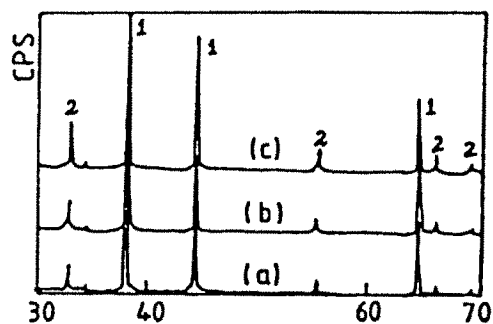


Fig. 4.11 : XRD profiles for freeze-dried powders.

Fig. 4.8 - 4.11 : Multiple XRD profiles for (a) Ag₁₀CdO (b) Ag₁₂CdO and (c) Ag₁₅CdO powders for different processing routes.

These profiles thus confirm the presence of Ag and ZnO and Ag and CdO phases in the powders. The absence of Fe contamination in MA powders of both AgZnO and AgCdO was confirmed by the XRD profiles as well as by chemical analysis by standard Phenanthroline method. Both tests gave negative results.

The effect of mechanical alloying (MA); on XRD line intensities of ZnO peaks from (101) diffracting plane, for powders corresponding to Ag 10.8 ZnO (MA) for two different attrition milling conditions viz. 11 : 1 ball to charge ratio and 180 rpm speed of attrition (named as condition 1) and 17 : 1 ball to charge ratio and 300 rpm speed (named as condition 2); is shown after various milling times in Table 4.2. With progressive milling, one notices, for each condition a reduction in peak height for the diffraction lines from ZnO (101) with time. For condition 1, the drop in relative peak intensity is significant after 12 hrs. of milling. Similar effect is observed for condition 2, only after 4 hrs. of milling. This is in view of the higher attrition energy transmitted in condition 2 as against that in condition 1, giving rise to similar end results at much shorter time. In both the cases, the decrease in relative peak intensities of ZnO is due to alloying of ZnO with Ag or the peaks becoming too broad (through particle size reduction and residual strains) to be visible above the background radiation. Fig.4.12 shows the plots of relative peak intensity (%) of ZnO phase for condition 1 and 2 for various milling times.

Similar findings for Ag 15 CdO (MA) are reported in Table 4.3 and Fig. 4.13 indicating the effect of milling time on degree of alloying by MA.

Mechanical alloying also leads to changes in the morphology of matrix. The major change noticed during MA of Ag-ZnO and Ag-CdO systems has been the drop in the peak intensities and the line broadening for silver peaks. Table 4.4 (a) shows change

Table 4.2 : Variation of XRD line intensity for ZnO peaks with milling time for AgZnO (MA) powders

Milling time hrs.	Condition I		Condition II	
	Actual peak intensity	Relative peak intensity (%)	Actual peak intensity	Relative peak intensity (%)
0	823	100	942	100
0.5	503	61.1	418	44.4
1	368	44.7	324	34.4
2	264	32.1	-	-
3	-	-	227	24.1
3.5	-	-	219	23.2
4	200	24.3	174	18.5
7	174	21.1	-	-
12	140	17.0	-	-

in relative peak intensity and the peak broadening in terms of the value of full width at half maximum (FWHM) for Ag (200) diffraction line with milling time for condition 1 and 2. There is a complementary variation between the peak height and the FWHM for Ag (200) diffraction lines for different milling times indicating the predominating phenomena occurring during MA, (particularly during early stages), as line broadening. This could arise either from residual stresses or a reduction in particle size or both.

Table 4.3 : Variation of XRD line intensity for CdO peaks with milling time for Ag CdO (MA) powders

time hrs.	peak intensity	peak intensity(%)
0	1454	100
0.5	923	63.5
1	767	52.8
2	300	20.6
3.5	238	16.4

Similar effect of milling time on the relative peak intensity and FWHM value for Ag (200) diffraction lines is demonstrated in Table 4.4 (b) for Ag 15 CdO (MA) system. Fig 4.14 and 4.15 show the variation of relative peak intensity (%) and FWHM for Ag (200) diffraction lines for both AgZnO (MA) and Ag CdO (MA) powders.

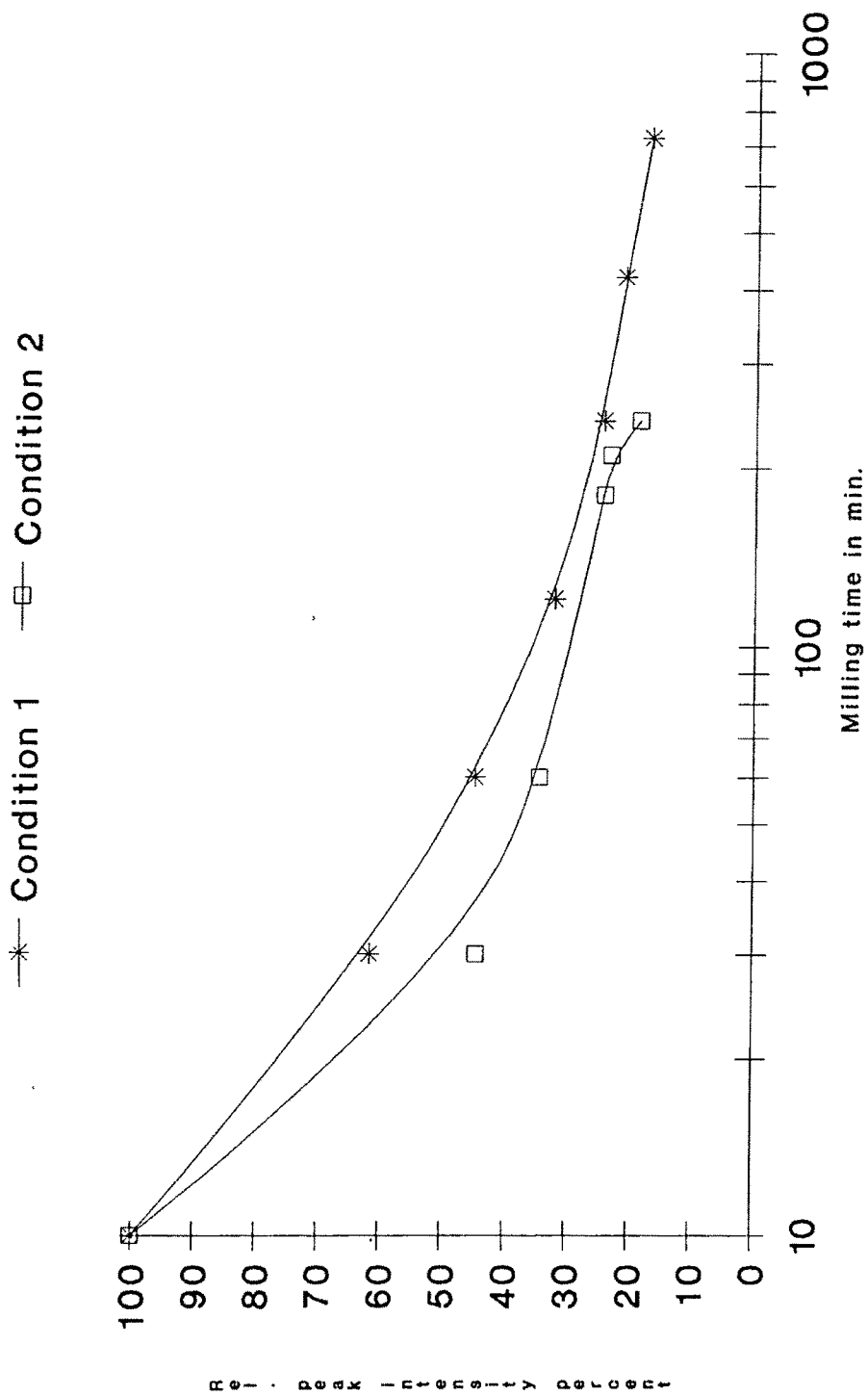


Fig.4.12 : Variation of rel. peak intensity (%) of ZnO phase with milling time for Ag ZnO (MA) powders.

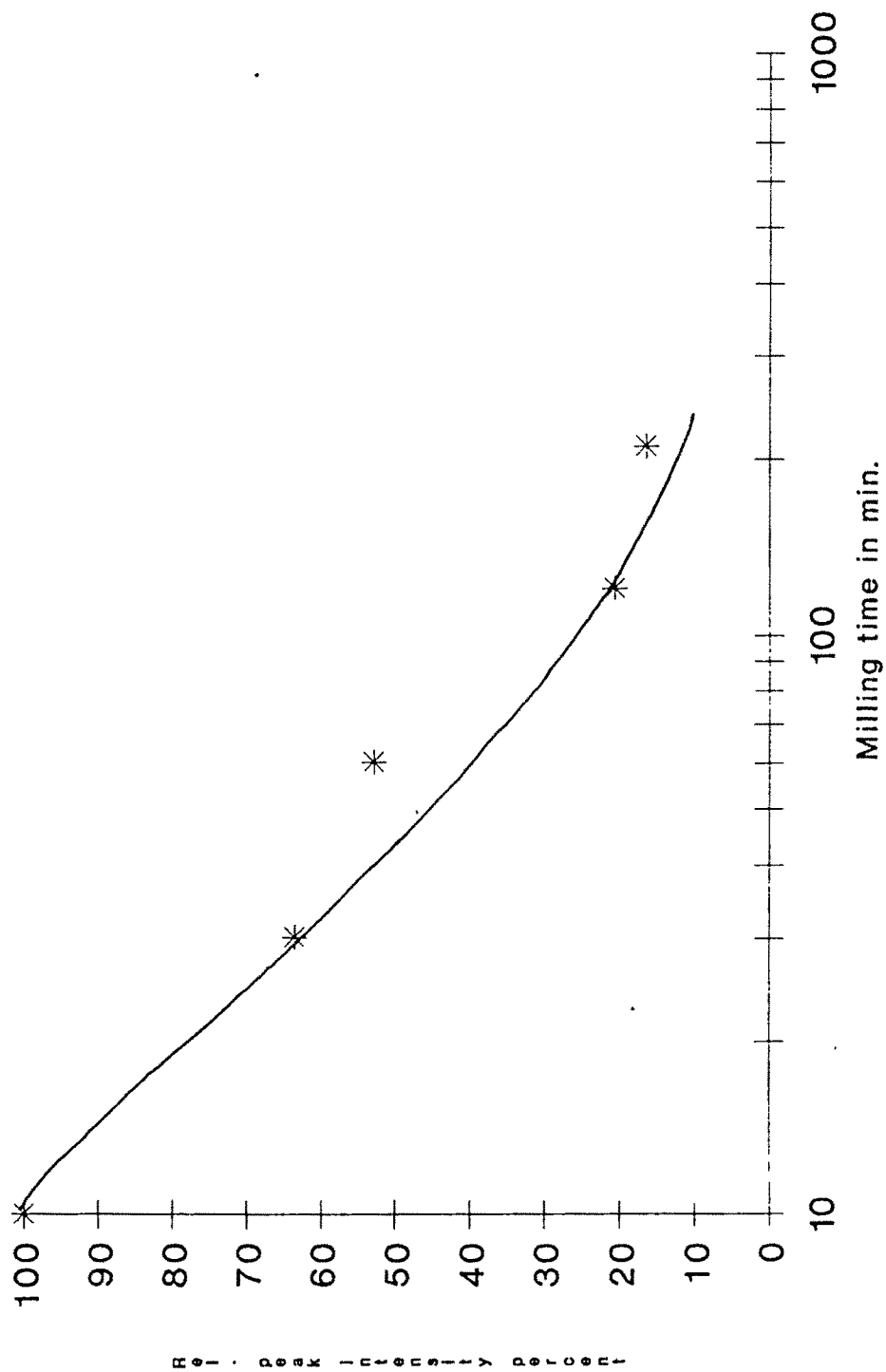


Fig.4.13 : Variation of rel. peak intensity (%) of CdO phase with milling time for Ag CdO (MA) powders.

Table 4.4 (a) : Variation of XRD line intensity and FWHM for Ag (200) peaks with milling time for Ag ZnO (MA) powders

Milling time	Ag 10.8 ZnO (MA)					
	CONDITION 1			CONDITION 2		
	Actual peak intensity	Relative peak intensity(%)	FWHM value	Actual peak intensity	Relative peak intensity(%)	FWHM value
0	3713	100	0.0098	3178	100	0.0105
0.5	2822	76.0	0.0215	1898	59.8	0.0166
1	1871	50.4	-	1570	49.4	0.0189
2	1341	36.1	0.0177	-	-	-
3	-	-	-	1186	37.3	0.0180
3.5	-	-	-	1048	33.0	0.0174
4	1332	35.9	0.0187	1056	33.2	0.0183
7	1152	31.0	0.0183	-	-	-
12	900	24.3	0.0224	-	-	-

Table 4.4 (b) : Variation of XRD line intensity and FWHM for Ag (200) peaks with milling time for Ag CdO (MA) powders

Milling time hrs.	Actual peak intensity	Relative peak intensity(%)	FWHM value
0	2156	100	0.0050
0.5	1463	67.9	0.0224
1	1278	59.3	0.0192
2	585	27.1	0.0174
3.5	520	24.1	0.0140

The above results of XRD analysis are in conformity with the findings of optical microscopy of MA powder samples in respect of their particle morphologies discussed later in section 4.1.7.

4.1.4. Particle size analysis :

Fig. 3.1 - 3.3 reported in Ch.3 show the probability number distribution plots for Ag, CdO and ZnO powders. These powders ; which are starting raw materials for conventional PM route and MA route ; are of much finer particle size & size distribution. As per these plots, silver powder is of 99% - 6.06 microns & 55% - 0.98 microns, CdO powder is 99% - 4.93 microns and 65% - 0.97 microns and ZnO powder is 100% < 1.0 micron size. As a result of this, the blends prepared out of Ag

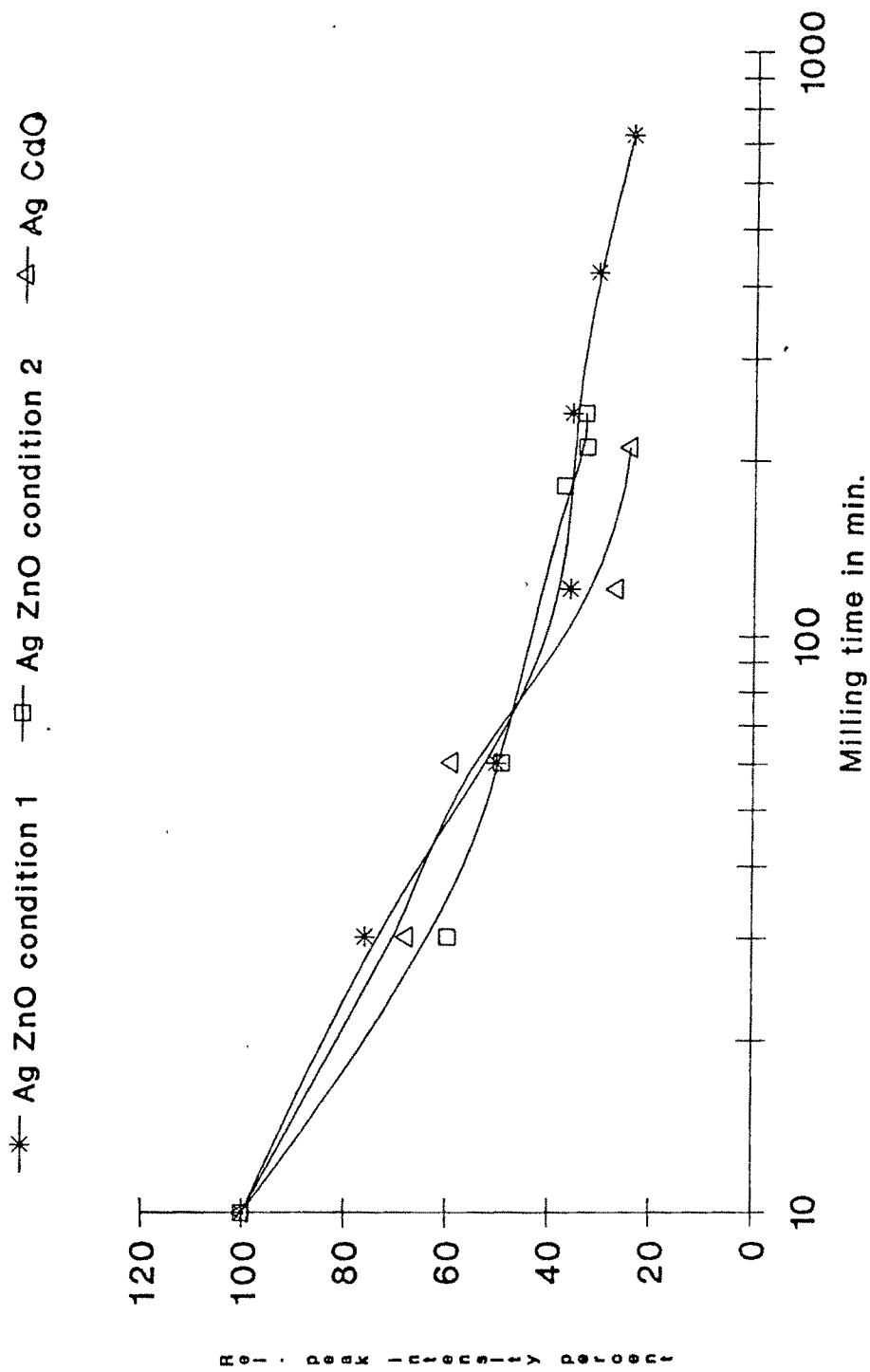


Fig.4.14 : Variation of rel. peak intensity for Ag(200) line with milling time for Ag ZnO (MA) and AgCdO (MA) powders.

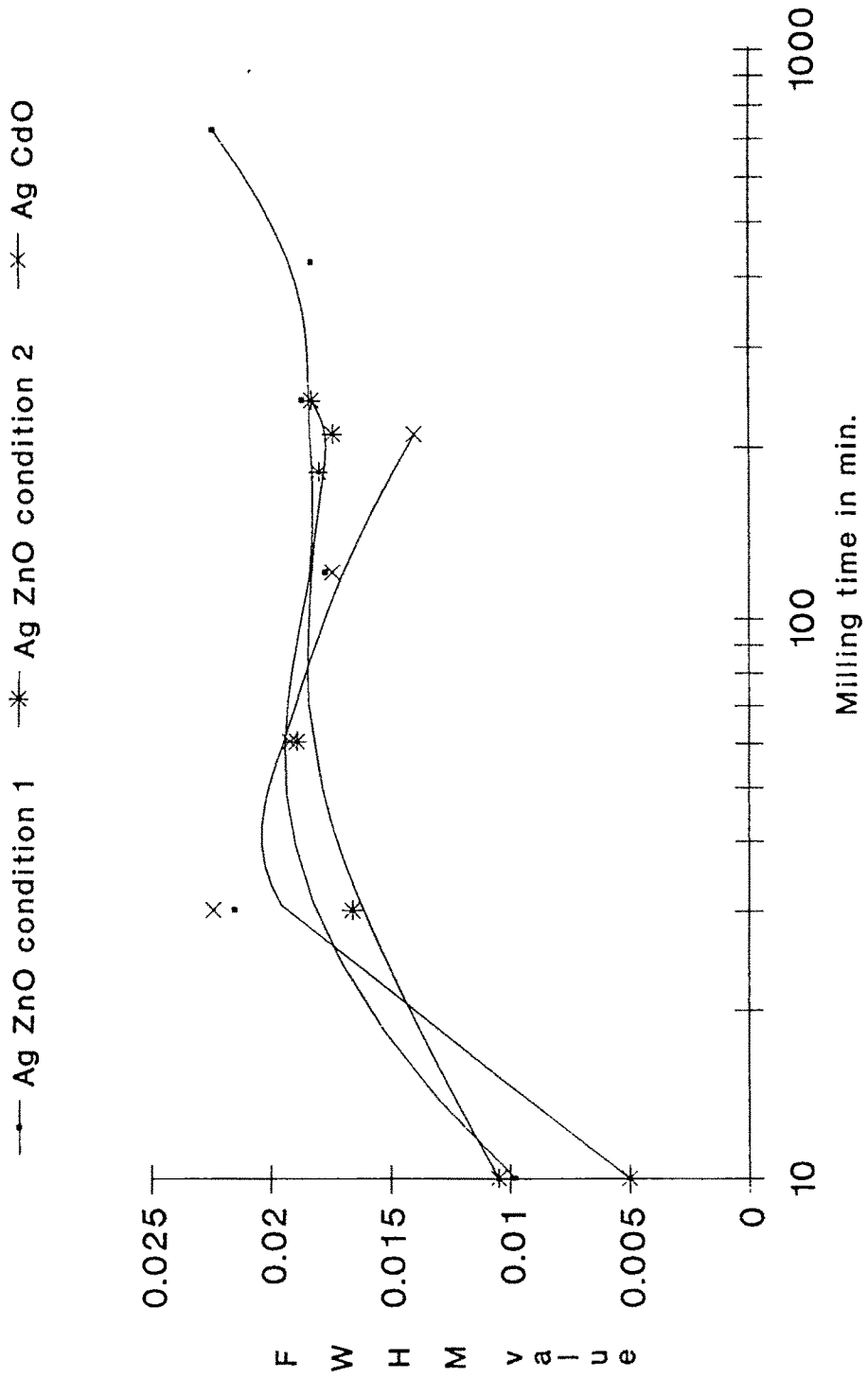


Fig.4.15 : Variation of FWHM value for Ag(200) line with milling time for Ag ZnO(MA) and Ag CdO (MA) powders.

and ZnO and Ag and CdO powders for further use in conventional PM route gave low apparent and tap density values.

Fig. 4.16 - 4.21 display the multiple plots for probability number distribution for powders of different processing routes for Ag-ZnO and Ag-CdO systems. These plots showed a very high degree of overlap amongst one another indicative of more or less similar particle size distribution attained by different process routes. By and large all the powders belonged to subsieve size range and had 99% particles of less than 10 micron size. The blended powders (mainly those of Ag ZnO group) displayed their tendency to skewness towards fineness.

4.1.5 : Apparent and tap density of powders :

Table 4.5 (a) and 4.5 (b) give the data on apparent and tap density measurements and Fig. 4.22 and Fig.4.23 show the corresponding histograms. These results clearly indicate lowest apparent density and tap density values for Ag ZnO(B) and Ag CdO(B) powders. The fine particle size and size distribution of the starting powders (i.e. Ag, CdO and ZnO powders) and their eventual high surface area are the reasons for such behaviour.

Table 4.5(a): Apparent and tap density data for Ag ZnO powders

Processing route	Ag-7.1wt% ZnO			Ag-8.6 wt% ZnO			Ag-10.8 wt% ZnO		
	A.D. g/cc	T.D. g/cc	% rise	A.D. g/cc	T.D. g/cc	% rise	A.D. g/cc	T.D. g/cc	% rise
Blending	0.83	1.32	37.1	0.89	1.39	36.0	0.88	1.32	34.8
Co-precipitation	1.47	2.50	41.2	1.25	2.27	44.9	1.47	2.77	48.9
Electroless coating	1.67	3.13	48.8	1.47	2.78	47.1	1.58	2.78	43.9
Freeze drying	1.06	1.79	39.1	1.25	1.92	34.9	1.25	2.08	39.9
Mechanical alloying	-	-	-	-	-	-	1.50	3.13	52.1

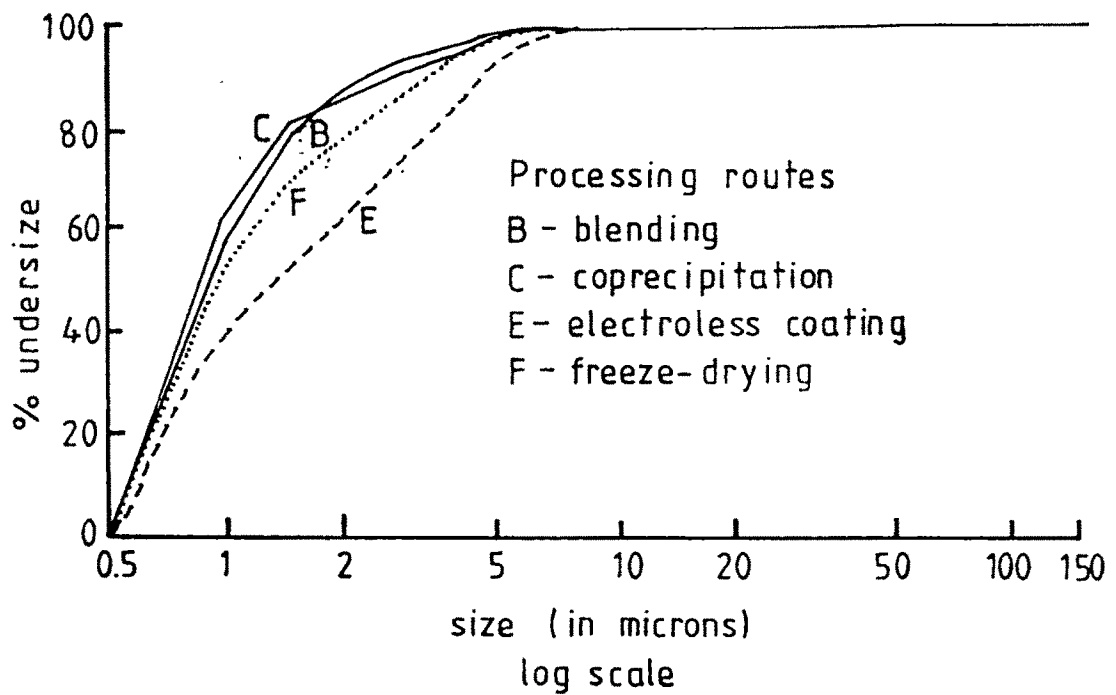


Fig.4.16 : Multiple plots for probability number distribution for different process routes for Ag 7.1 ZnO system.

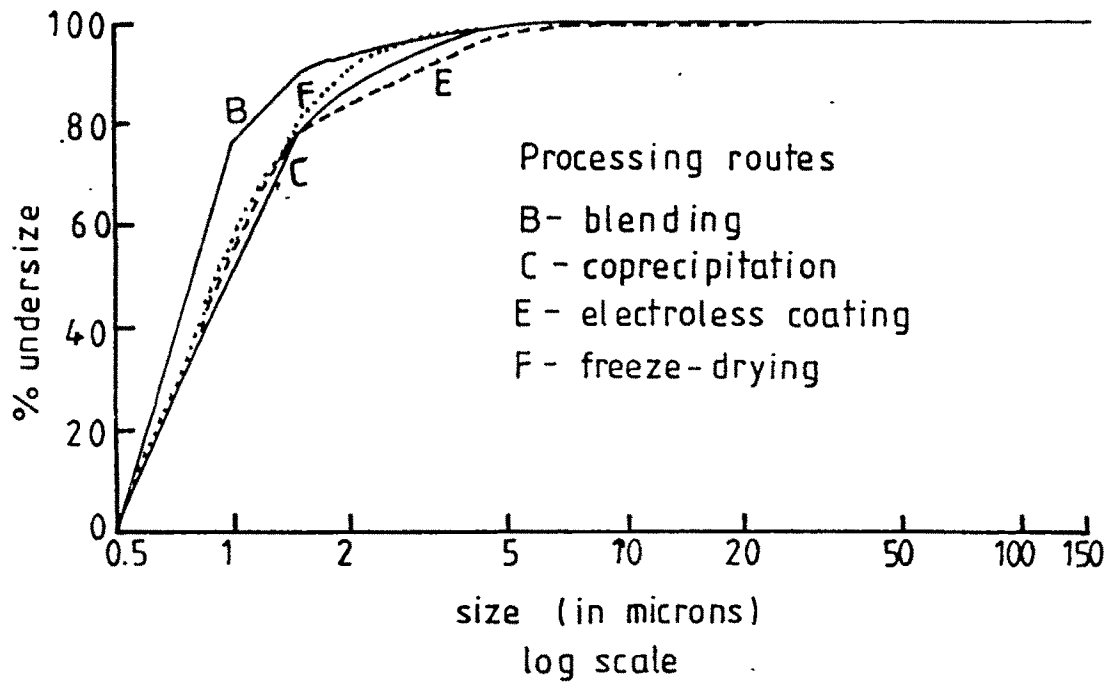


Fig. 4.17: Multiple plots for probability number distribution for different process routes for Ag 8.6 ZnO system.

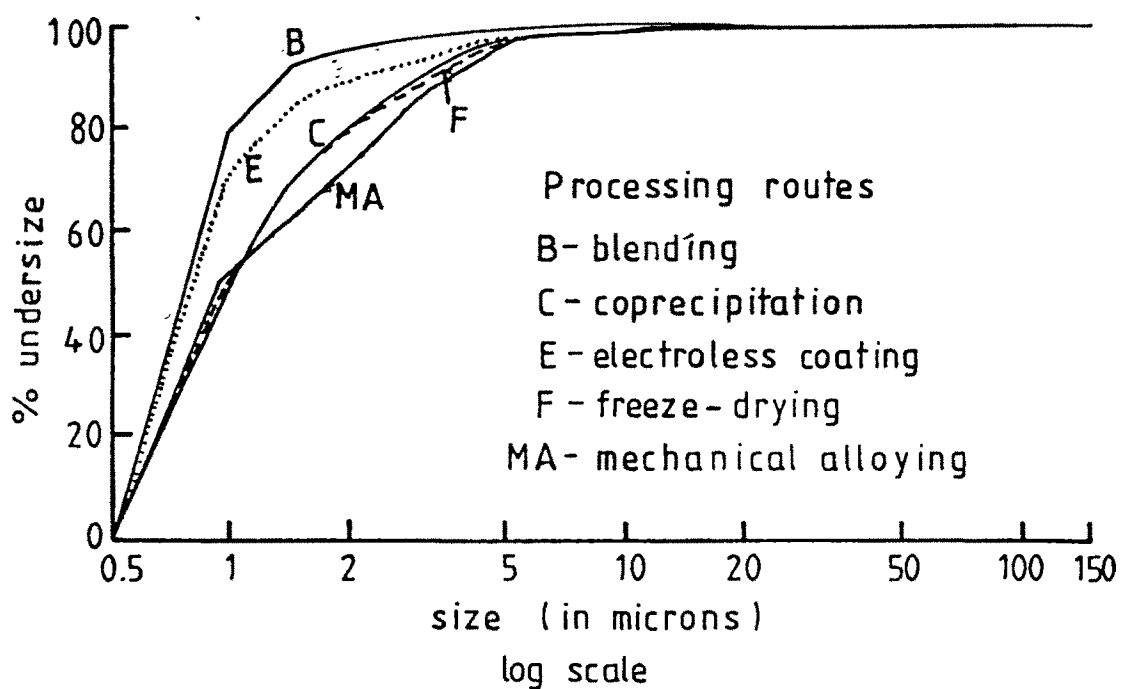


Fig. 4.18. Multiple plots for probability number distribution for different process routes for Ag 10.8 ZnO system.

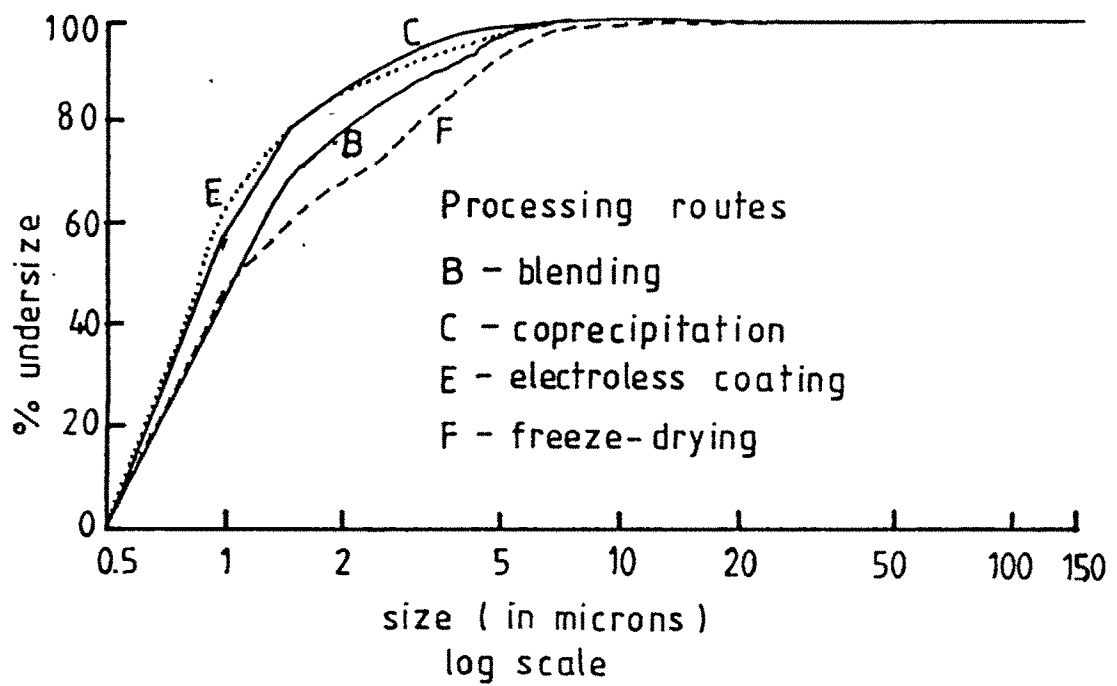


Fig. 4.19 Multiple plots for probability number distribution for different process routes for Ag₁₀CdO system.

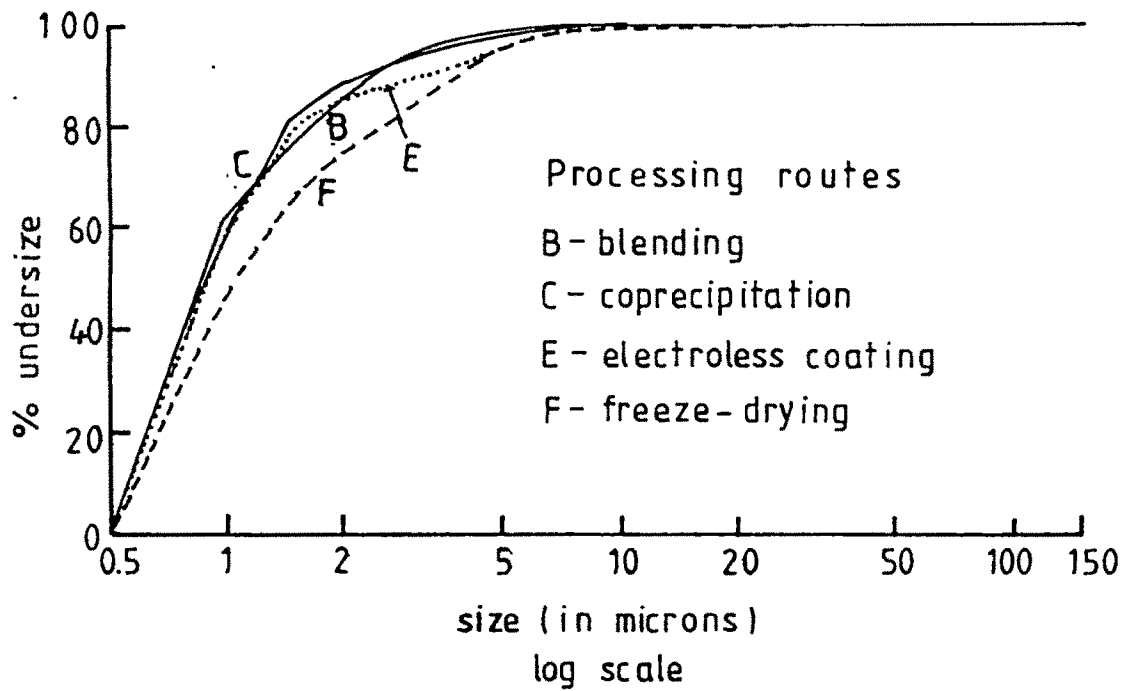


Fig. 4.20: Multiple plots for probability number distribution for different process routes for Ag₁₂CdO system.

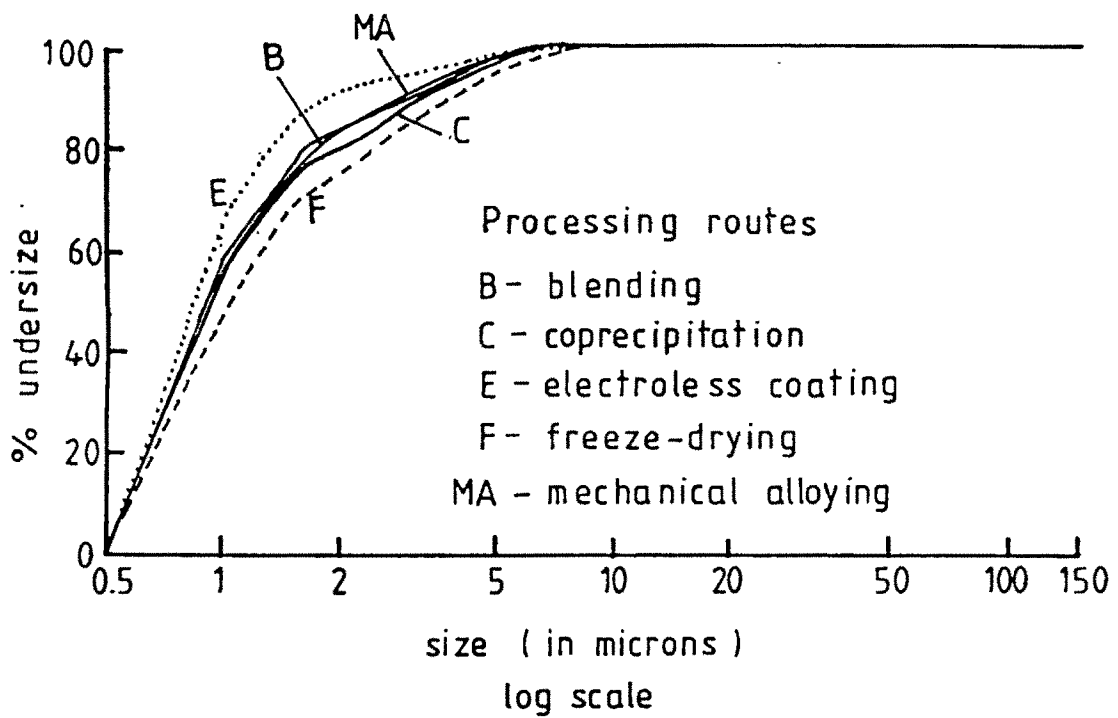


Fig.4.21 Multiple plots for probability number distribution for different process routes for Ag₁₅CdO system.

- B - Blending route
- C - Coprecipitation route
- E - Electroless coating route
- F - Freeze - drying route
- MA - Mechanical alloying route

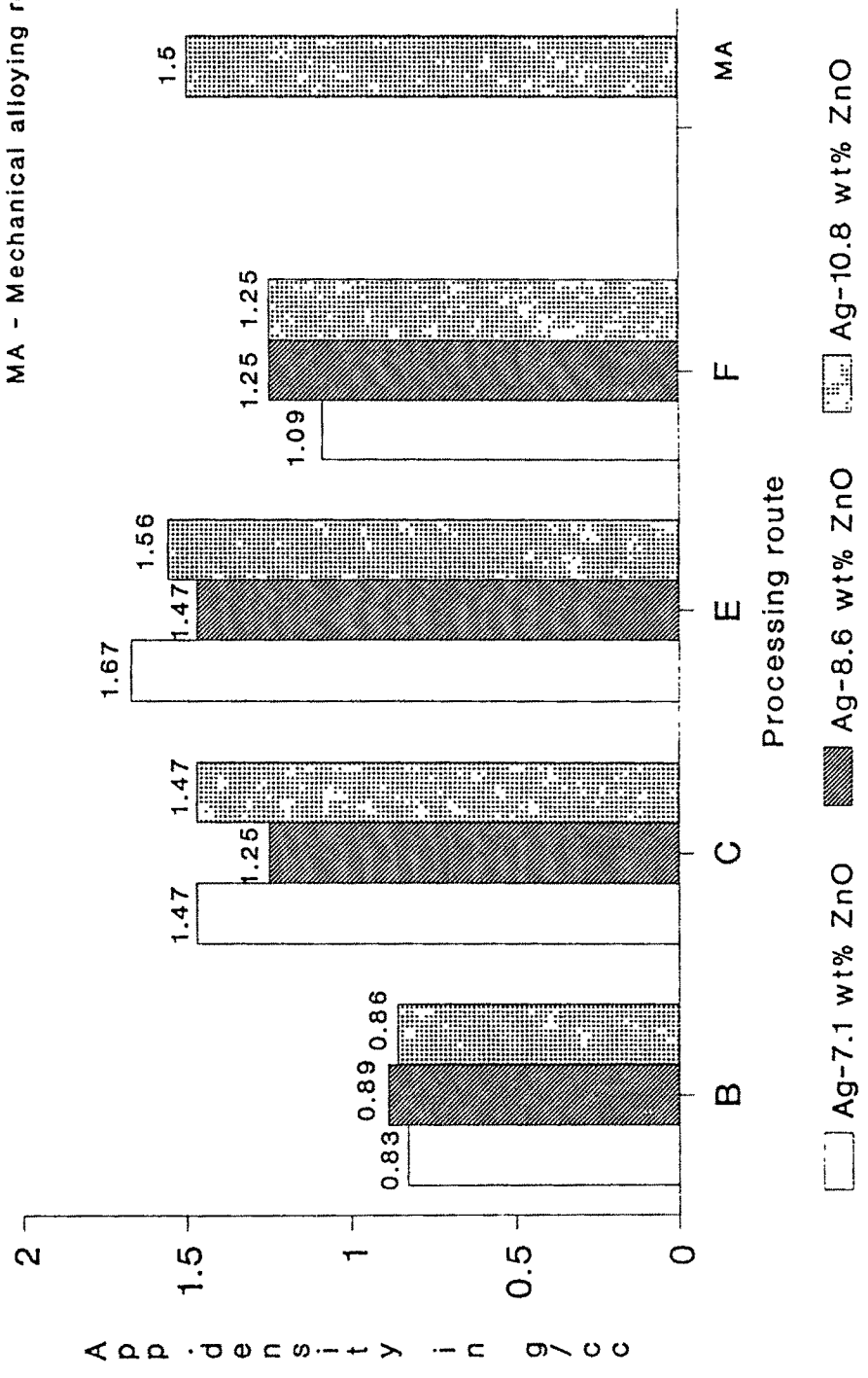


Fig. 4.22(a) : Histograms for apparent density of Ag ZnO powders

- B - Blending route
- C - Coprecipitation route
- E - Electroless coating route
- F - Freeze-drying route
- MA - Mechanical alloying route

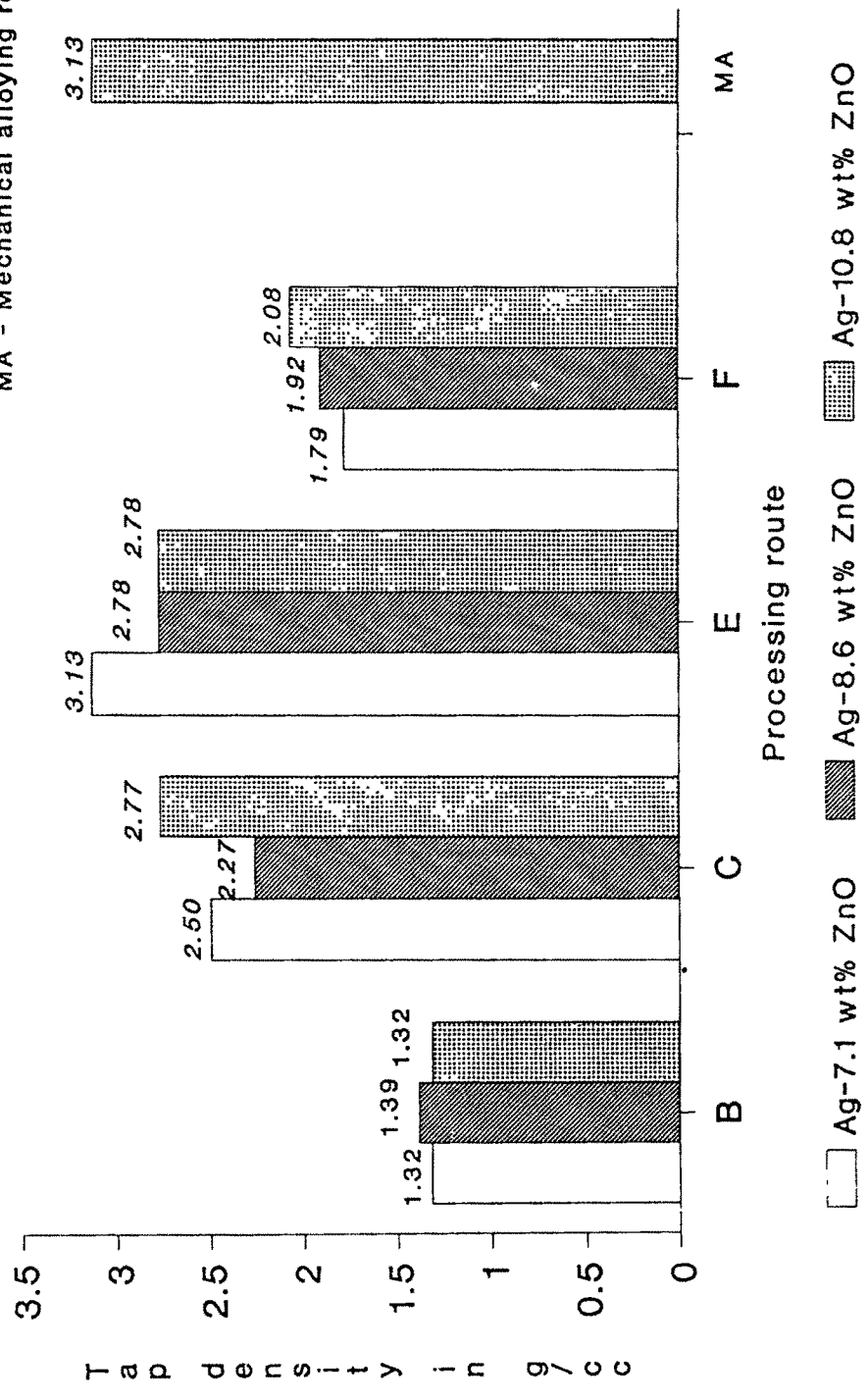


Fig.4.22(b) : Histograms for tap density of Ag ZnO powders.

- B - Blending route
- C - Coprecipitation route
- E - Electroless coating route
- F - Freeze - drying route
- MA - Mechanical alloying route

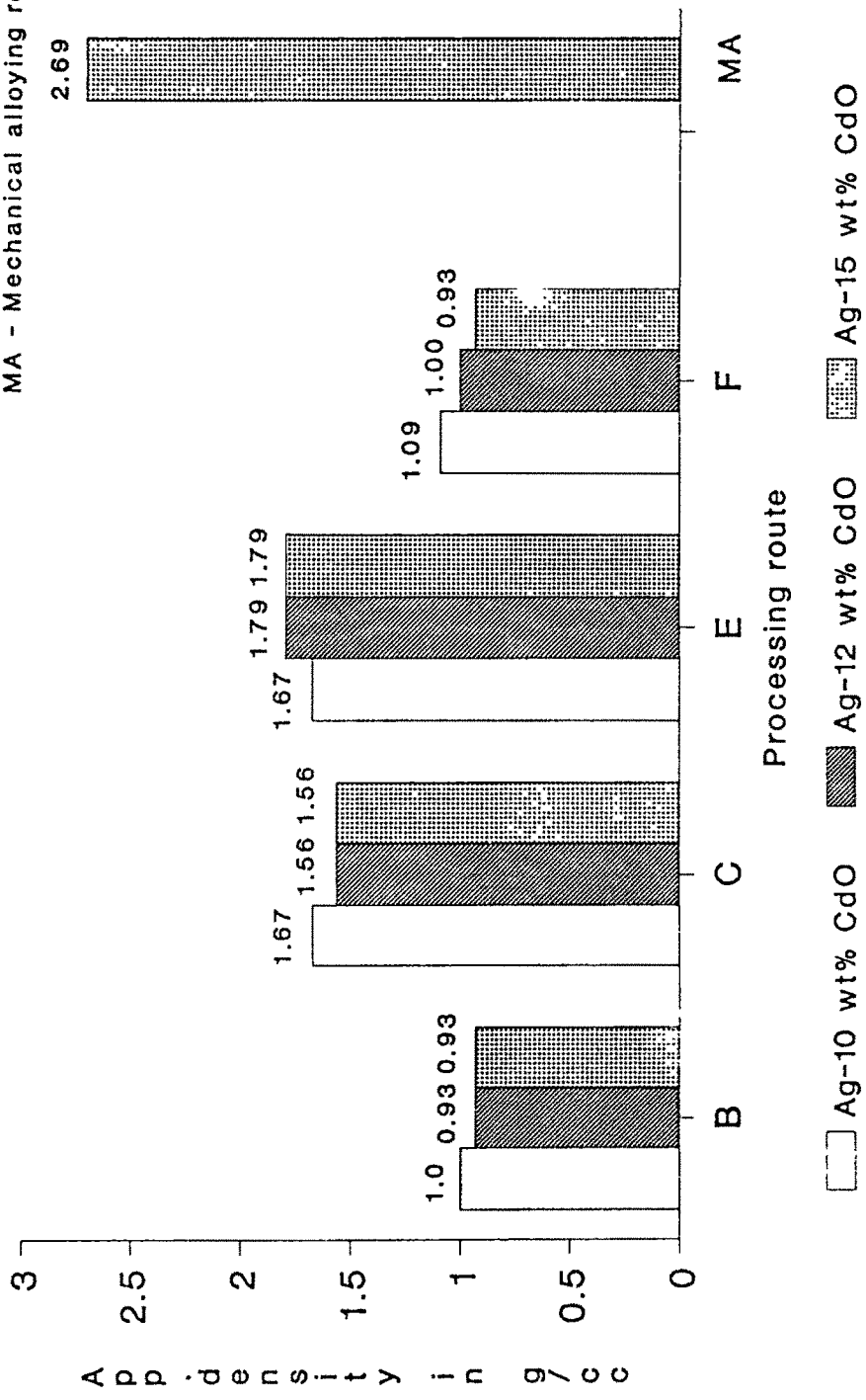


Fig. 4.23(a) : Histograms for apparent density of Ag CdO powders

- B - Blending route
- C - Coprecipitation route
- E - Electroless coating route
- F - Freeze-drying route
- MA - Mechanical alloying route

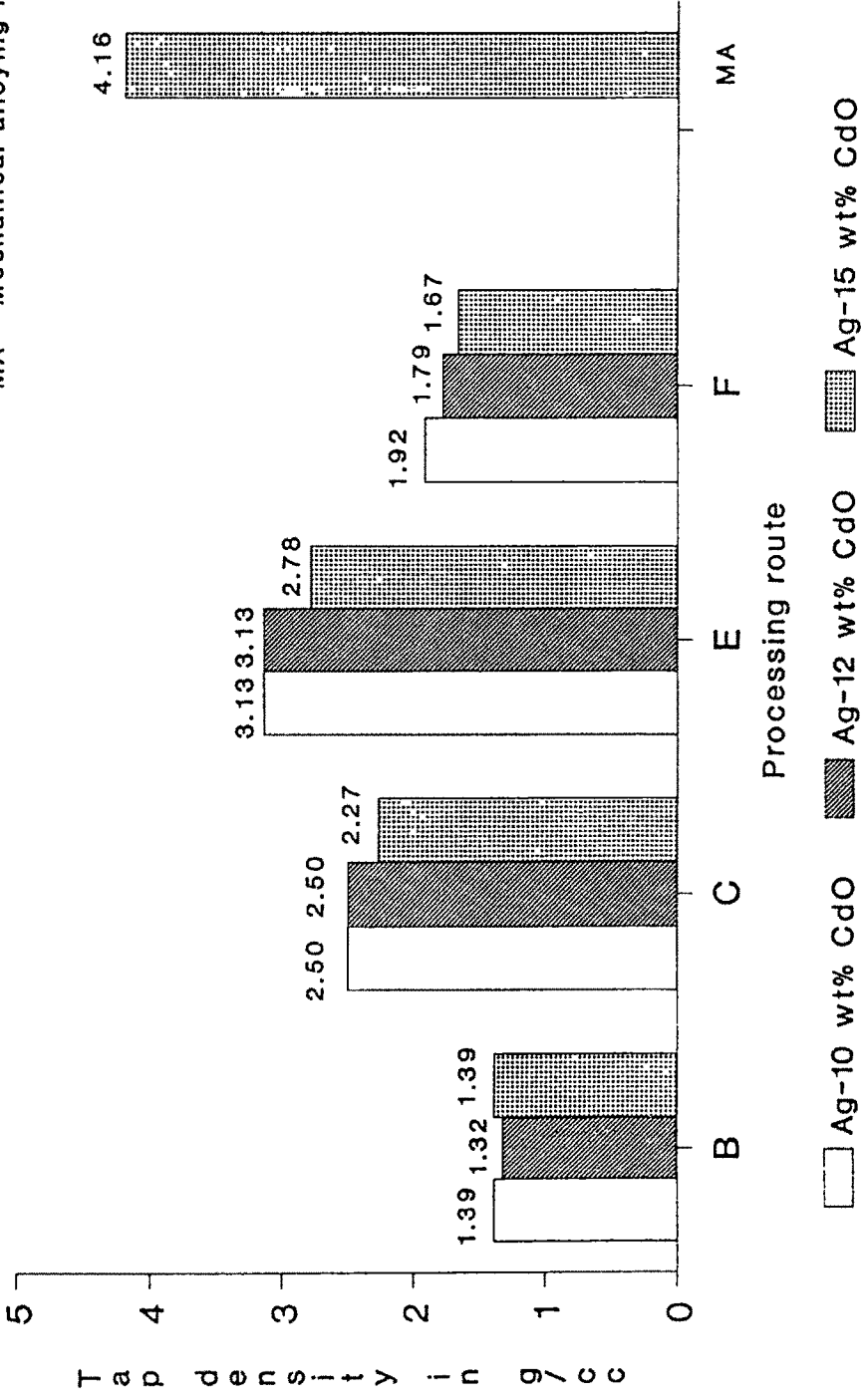


Fig.4.23(b) : Histograms for tap density of Ag CdO powders.

Table 4.6 (b): Apparent and tap density for Ag CdO powders

Processing route	Ag-10 wt%CdO			Ag-12 wt%CdO			Ag-15 wt%CdO		
	A.D g/cc	T.D. g/cc	% rise g/cc	A D g/cc	T D. g/cc	% rise	A D. g/cc	T D g/cc	% rise
Blending	1.00	1.39	28.1	0.93	1.32	29.5	0.93	1.39	33.1
Co-precipitation	1.67	2.50	33.2	1.56	2.50	37.6	1.56	2.27	31.3
Electroless coating	1.67	3.13	46.7	1.79	3.13	42.9	1.79	2.78	35.6
Freeze drying	1.09	1.92	43.2	1.00	1.79	44.1	0.93	1.67	44.3
Mechanical alloying	-	-	-	-	-	-	2.69	4.16	35.3

$$\% \text{Rise in density} = \frac{\text{T.D.} - \text{A.D.}}{\text{T.D.}} \times 100$$

Freeze-dried powders also gave low apparent density and tap density values. A comparative assessment of powder particles' morphology for different process routes as displayed in various SEM photographs and discussed in section 4.1.8 explains these findings. The freeze-dried samples were highly spongy and had greater surface area. A sample estimation of surface area for Ag 10.8 ZnO (F) and Ag 10.8 ZnO (B) powders was done by BET method. The former gave the value of 15.240 m²/g whereas the later gave 7.720 m²/g for specific surface area. The microporosity was also computed for these two samples from the adsorption - desorption isotherms obtained during BET surface area measurements. Freeze -dried sample reported higher microporosity than the blended powder. Higher surface area and microporosity accounted for the low apparent & tap densities of freeze dried powders. (see table 4.6)Mechanically alloyed powders exhibited better apparent and tap density values and in some cases even the best. The higher apparent and tap density of such mechanically comminuted powders are obviously on account of their broad particle size distribution, clean particle surfaces free from any adsorbed gas layer, dense nature of their powder particles and better packing properties.

Fig.4.24 and 4.25 show in histogrammic form the results of percentage rise in density on tapping for different powders. Maximum improvement in density on tapping was found

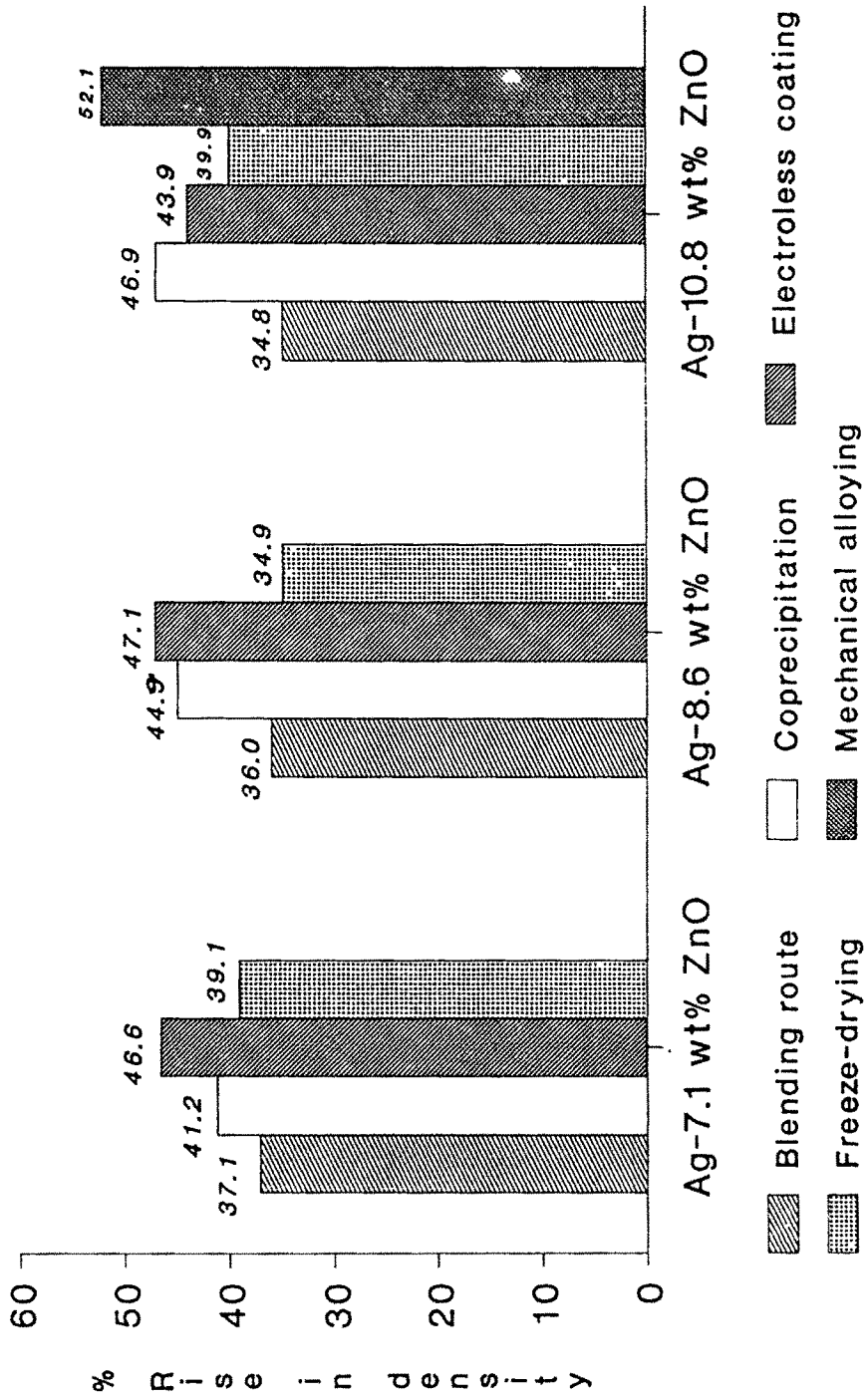


Fig.4.24 : Histograms for percentage rise in density on tapping for Ag ZnO powders.

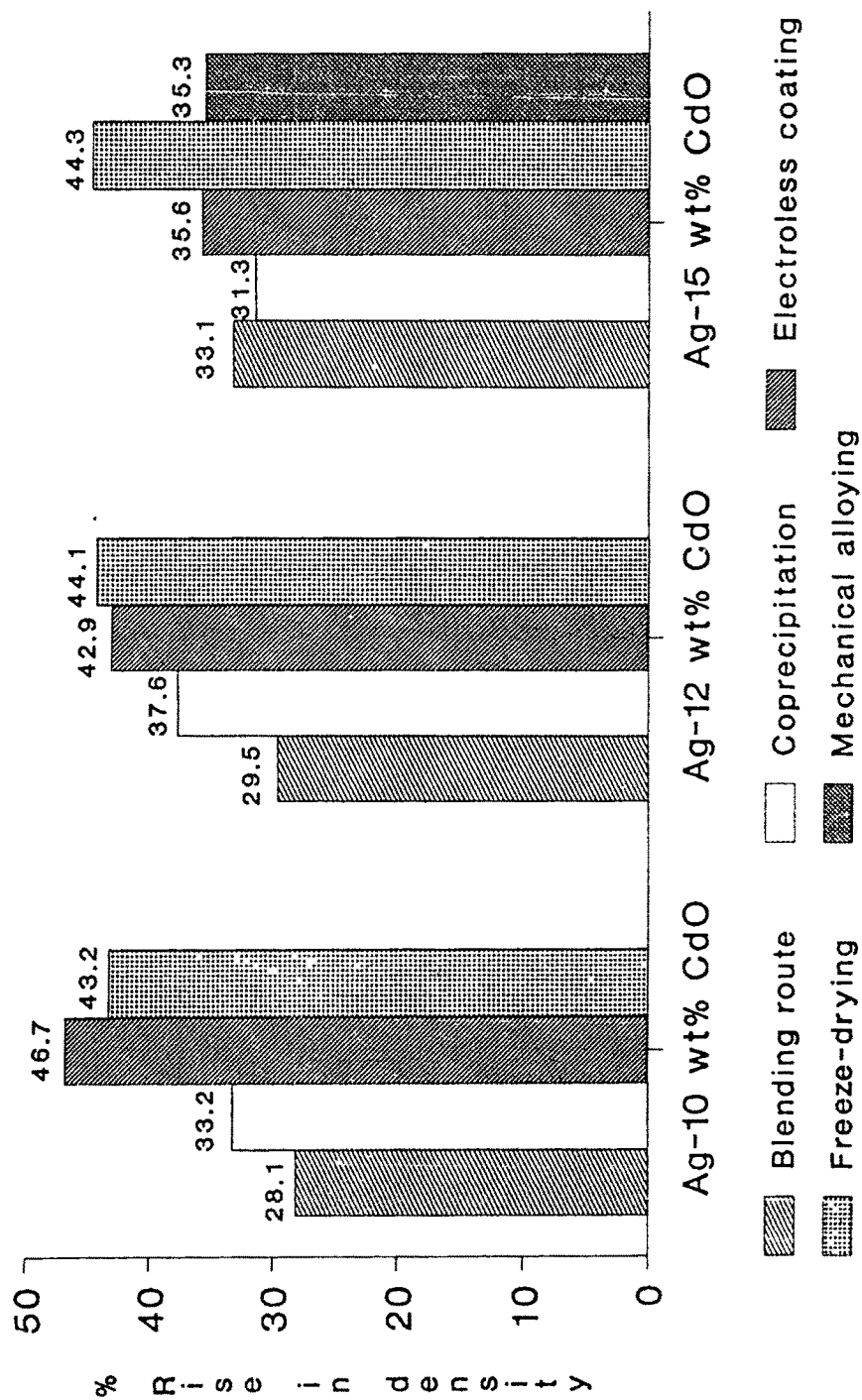


Fig.4.25 : Histograms for percentage rise in density on tapping for Ag CdO powders.

for Ag ZnO (MA), Ag ZnO (E), Ag CdO (E) and Ag ZnO (C) powders whereas less improvement was observed for Ag-ZnO (B), Ag-CdO (B) and Ag-ZnO (F) powders.

Inconsistent behaviour was noticed in case of Ag 12 CdO (F), Ag 15 CdO (F) and Ag 15 CdO (B) powders. The inconsistency may partly be attributed to insufficient quantity of powder sample taken for tap density measurements than recommended by standards. About 25g powder sample was used in each case for tap density measurement as against the recommended quantity of 50g by standards. This was in view of limitations in processing of powders in bulk amounts (in particular the processing of freeze dried powders), as well as the higher cost of material owing to silver.

Finally it may be inferred that the substantial improvement in density on tapping a powder (vis a vis its apparent density) is possible only when the powder particles are relatively coarse (offering low specific surface area and hence less interparticle friction); have broad particle size distribution (yielding greater packing density) and possess low surface roughness (giving greater flowability).

4.1.6. Specific surface area of powders :

Representative powder samples of Ag 10.8 ZnO (B) and Ag 10.8 ZnO (F) were subjected to measurement of specific surface area by BET method using Sorptomatic 1900 Surface Area Analyser of Fisons, Italy. Following table gives the values for specific surface area and the amount of microporosity for these powders.

Table 4.6 : Specific surface area and porosity of powders

Powder sample	Specific surface area m ² /g	Microporosity (%)
Ag 10.8 ZnO (B)	7.720	34.70
Ag 10.8 ZnO (F)	15.240	60.00

Higher specific surface area and microporosity of freeze-dried powders impart greater inter-particle friction and hence give lower apparent and tap density values. This is also confirmed by SEM micrographs for freeze-dried powders (Fig. 4.33 & 4.34) indicating highly spongy powder morphology compared to coarse and granular powder morphology for blended powders (Fig. 4.29 & 4.30). The bridging tendency of spongy freeze-dried powders during property evaluation could also be the cause of low apparent and tap density for these powders.

4.1.7 Optical microscopy of MA powders :

Mechanical alloying leads to changes in the morphology of powder particles and the degree of dispersion of oxide phase in silver matrix with attrition milling. Ag 10.8 ZnO (MA) of condition 2 and Ag15CdO (MA) powder samples drawn at regular time intervals during attrition milling were subjected to optical microscopy. The powder samples were mounted by means of cold setting compound, and were subsequently ground and polished as per standard metallographic practices. The ground and polished embedded particles were examined in unetched condition at 100 - 500 X magnification on a metallograph. Microscopic examination of these embedded particles revealed the change in particle size, particle shape and dispersion of oxide phase with milling time. According to Fig. 4.26 and 4.27, the Ag-MeO (MA) composite particles first underwent deformation giving rise to formation of elongated rod or flake like particles. Finally, towards the end of milling, the fracturing of particles appears to have occurred. Thus there has been a change in particle shape, size and size distribution during MA. Not only this, a more homogeneous distribution of oxide-phase was produced in silver-matrix as displayed by these photographs. The gradual but definite improvement in dispersivity of oxide-phase occurred with increasing milling time.

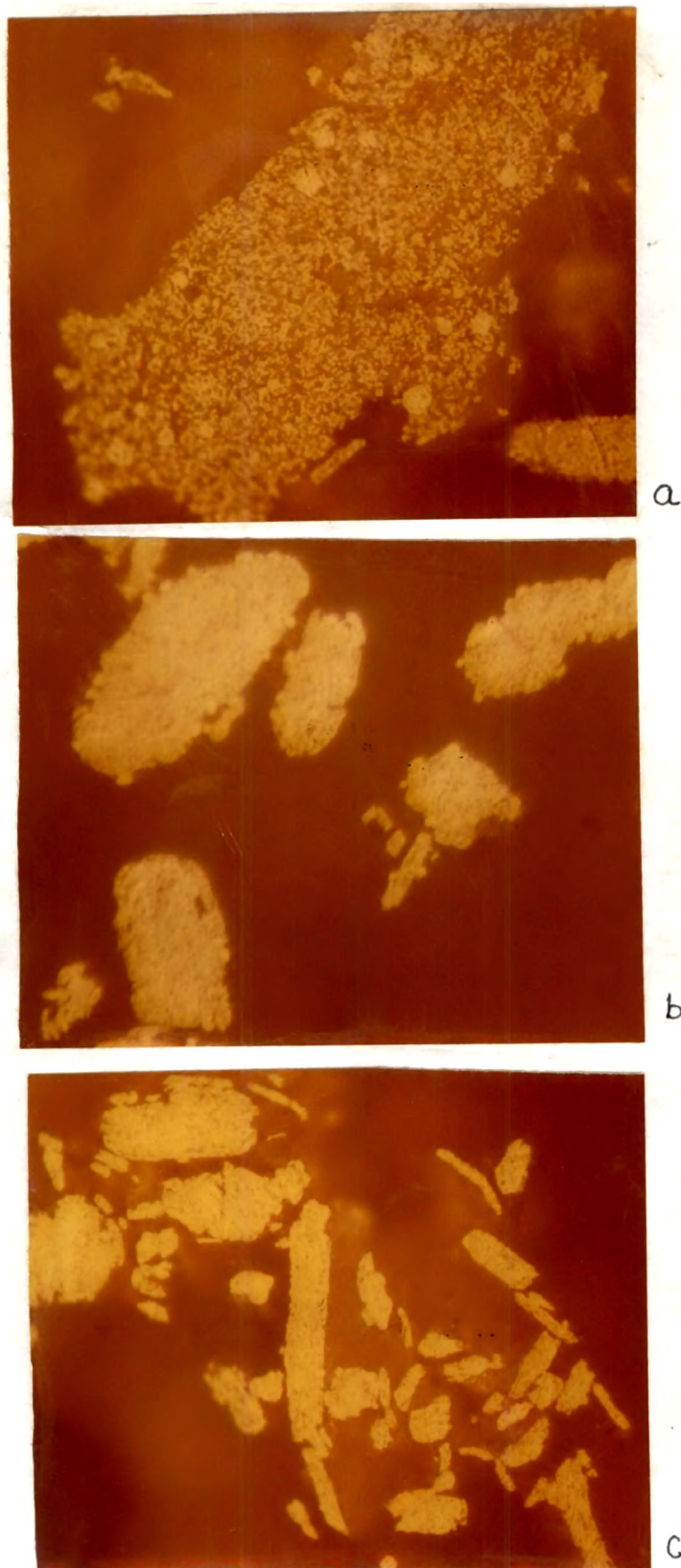


Fig. 4.26 : Optical micrographs for Ag_{10.8}ZnO (MA) powders of condition 2 after (a) annealing, (b) 1 h milling (c) 4 h of attrition milling. (500X)

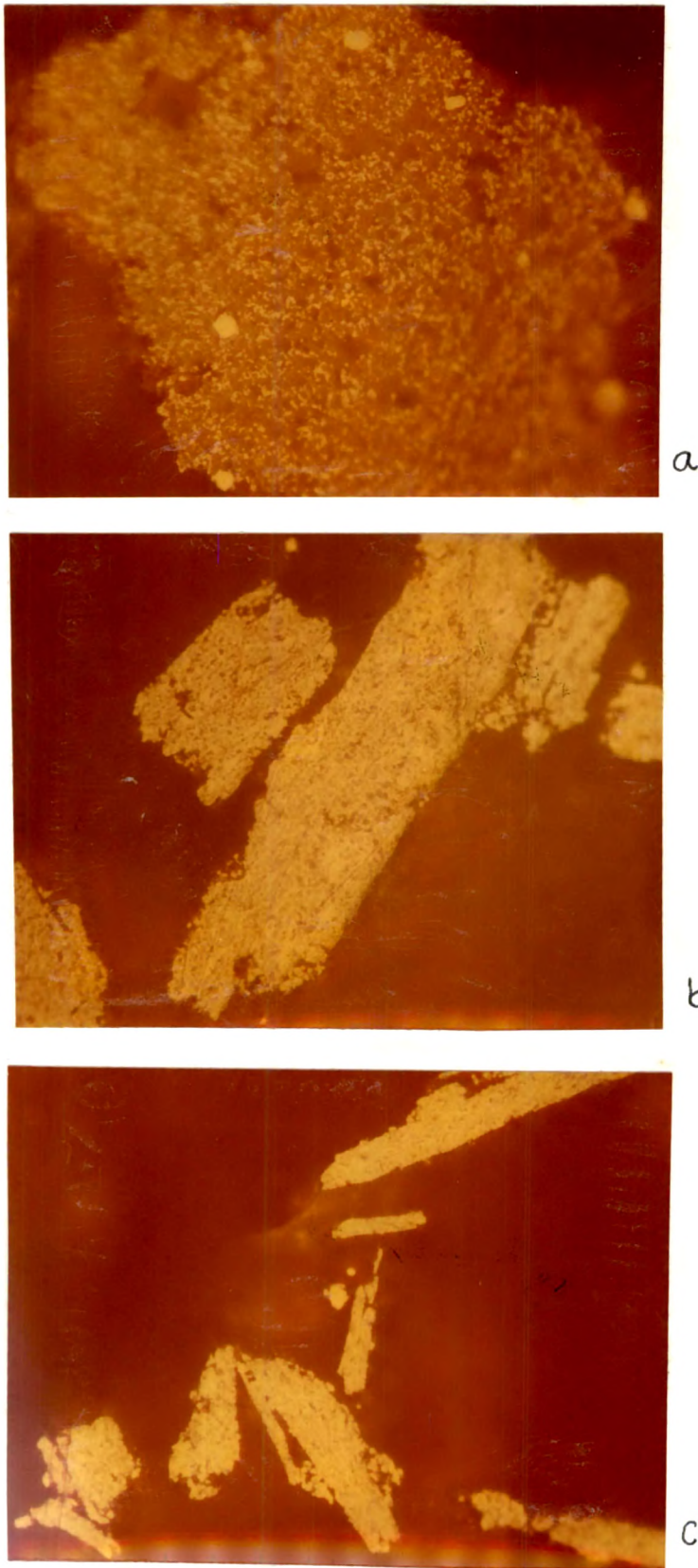


Fig. 4.27 : Optical micrograph for Ag₁₅CdO (MA) powders after (a) annealing, (b) 1 h milling (c) 3.5 h attrition milling. (500X)

The above results are in agreement with Benjamin's theory of welding - fracturing - steady state process for MA of ductile metal-matrix composites.

4.1.8. SEM morphology of powders :

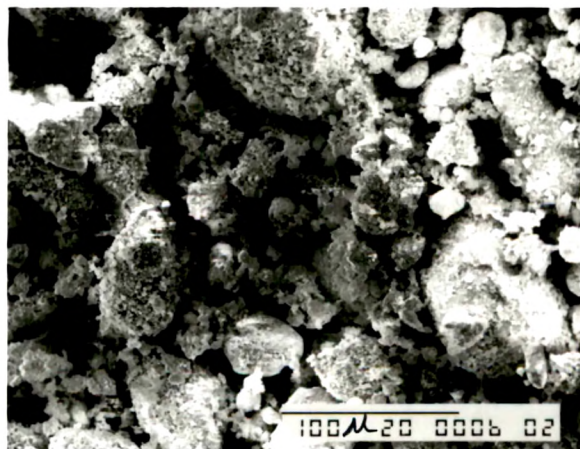
Scanning electron microscopy was done for the powder samples of different process routes to study the change in particle morphology with method of powder production. Both SRL make silver powder and SD make cadmium oxide powder had granular shape ; with silver powder exhibiting greater tendency to agglomeration (Fig. 4.28(a) and (b)). Fig. 4.28 (c) shows the SEM photograph of the E-Merck grade zinc oxide powder showing membranous spongy powder morphology.

As the overall morphology of powder particles is largely governed by that of major phase in a blend, the Ag CdO (B) and Ag ZnO (B) powders of different compositions showed similar granular morphology to that of silver powder, as presented in SEM micrographs of Fig. 4.29 and Fig. 4.30.

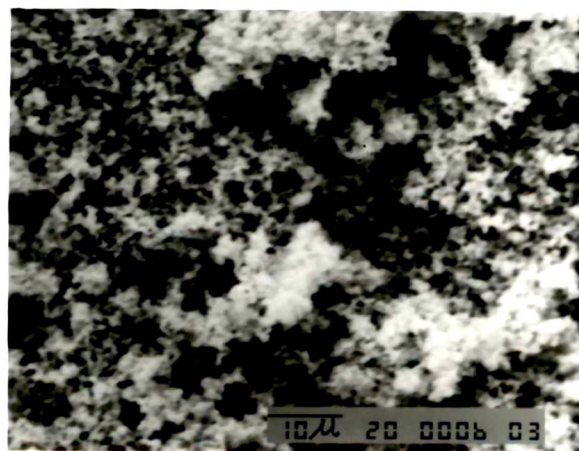
The powders processed by chemical routes such as spray-coprecipitation and freeze-drying exhibited a well dispersed, fine and rounded particle morphology. The coprecipitated Ag-ZnO and Ag-CdO powders showed a gradual transition from rounded particle shape to a ligament or rod like morphology with increasing oxide content as per Fig. 4.31 and Fig. 4.32. The sponginess and hence related surface area was more for freeze-dried powders as compared to coprecipitated Ag-ZnO and Ag-CdO powders (Fig. 4.33 and Fig. 4.34). This is attributed mainly to the absence of hydrogen bonds in freeze-dried powders reducing their tendency to agglomeration.



a

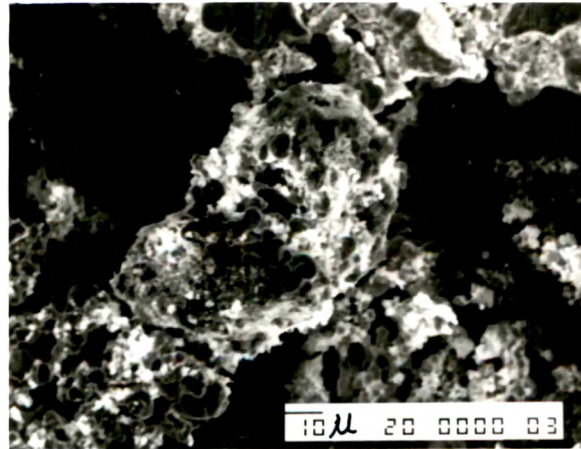


b

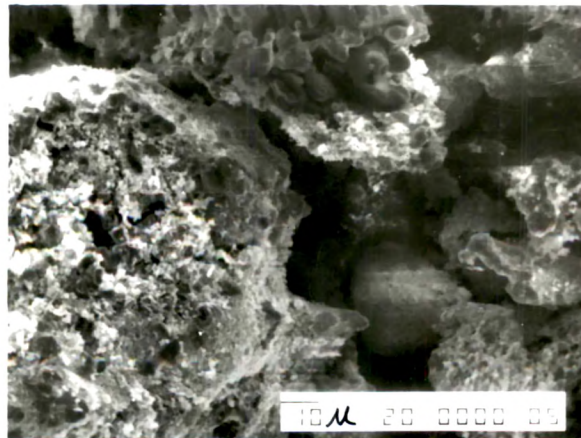


c

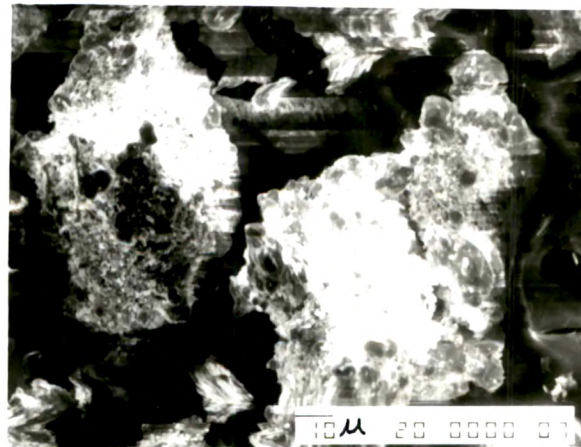
Fig. 4.28 : SEM micrographs for (a) silver, (b) cadmium oxide and (c) Zinc oxide powders.



a

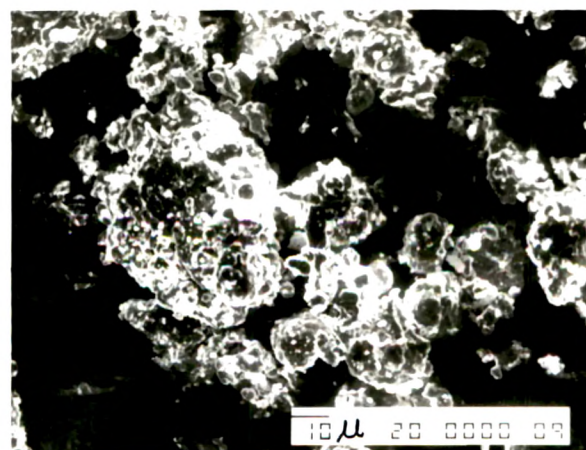


b



c

Fig. 4.29 : SEM micrographs for (a) Ag 7.1 ZnO (B), (b) Ag 8.6 ZnO(B) and (c) Ag 10.8 ZnO (B) powders.



a

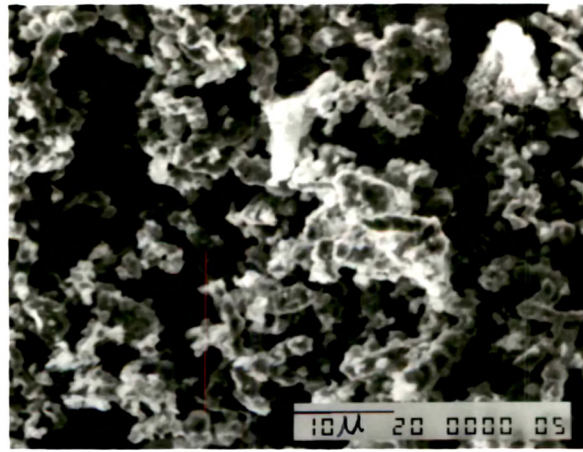


b

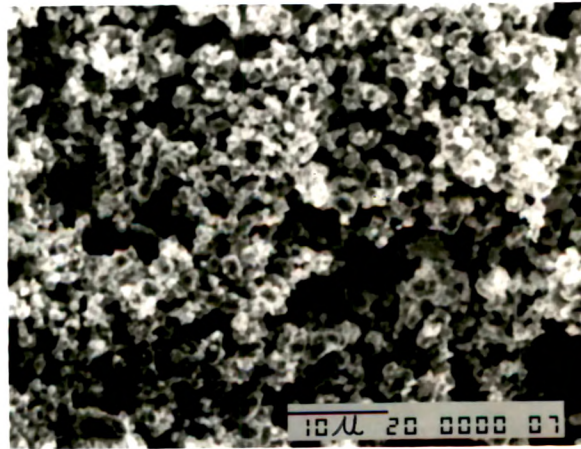


c

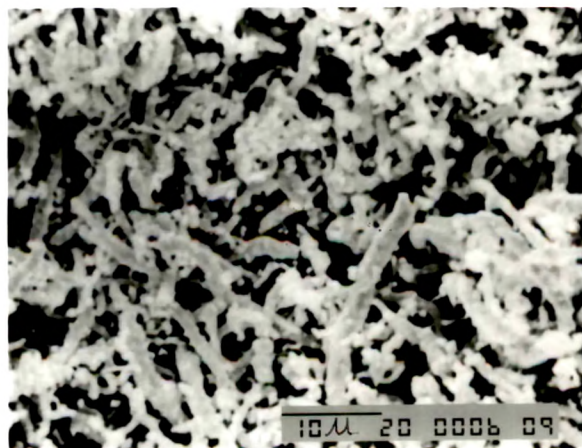
Fig. 4.30 : SEM micrographs for (a) Ag 10CdO (B), (b) Ag 12 CdO (B) and (c) Ag 15 CdO (B) powders.



a

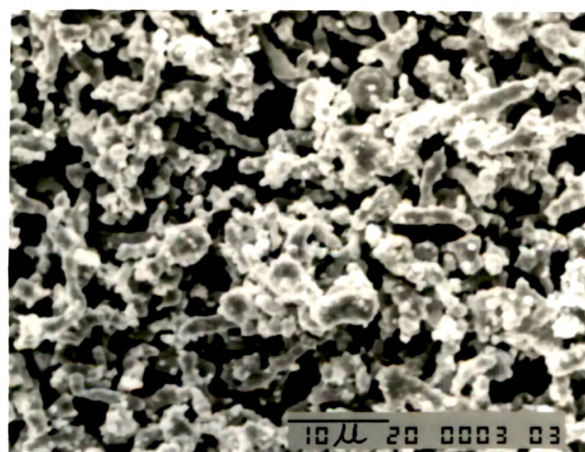


b

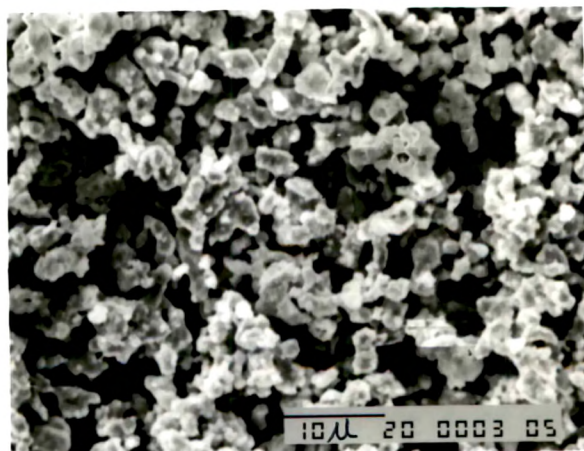


c

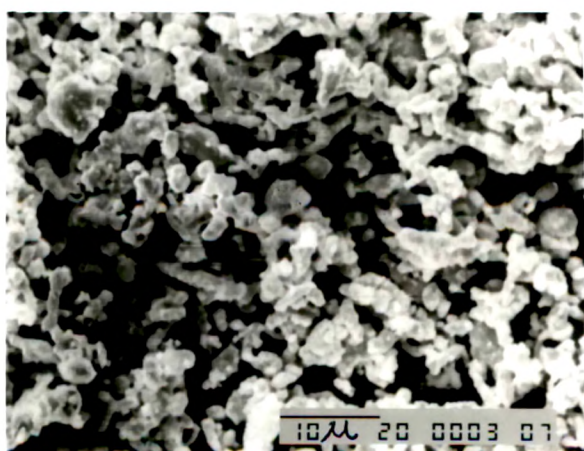
Fig. 4. 31 : SEM micrographs for (a) Ag_{7.1}ZnO (C), (b) Ag_{8.6}ZnO (C) and (c) Ag_{10.8}ZnO (C) powders.



a



b



c

Fig. 4.32 : SEM micrographs for (a) Ag 10 CdO (C), (b) Ag 12 CdO (C) and (c) Ag 15 CdO (C) powders.

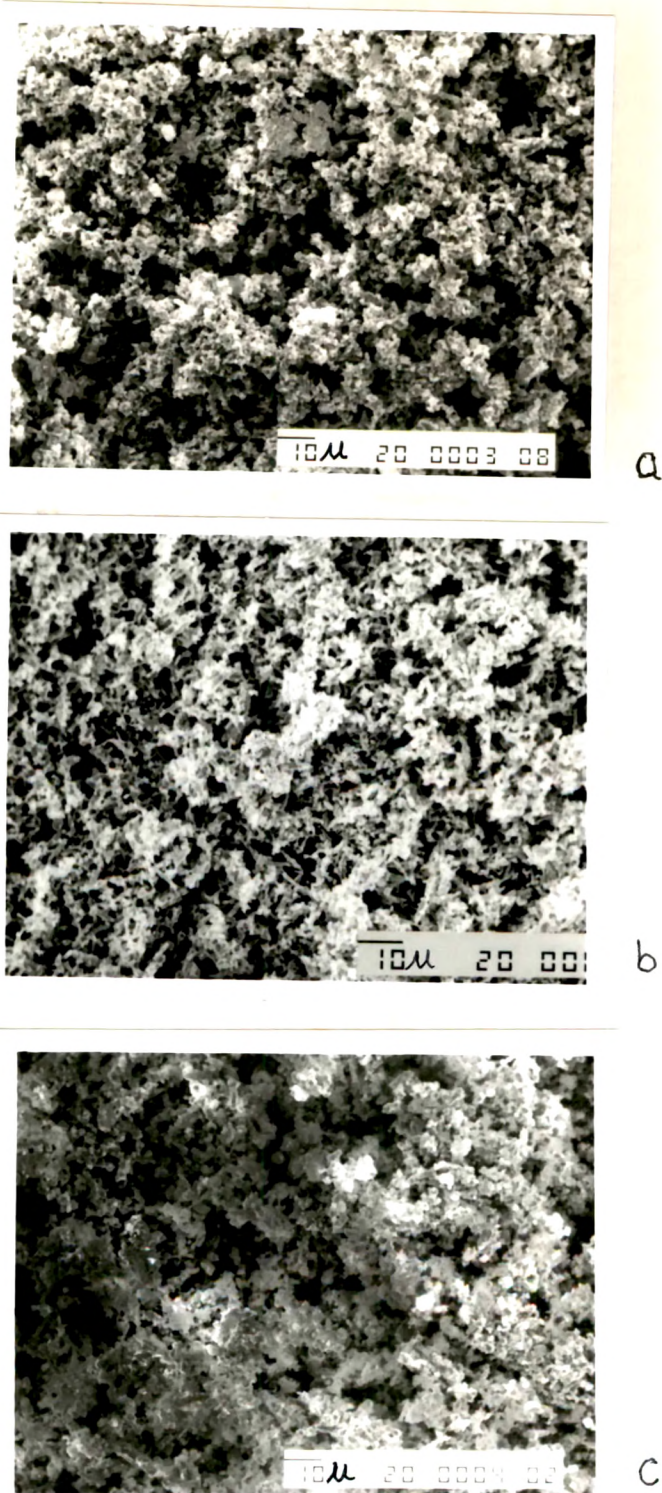


Fig. 4. 33 : SEM micrographs for (a) Ag_{7.1}ZnO (F), (b) Ag_{8.6}ZnO (F) and (c) Ag_{10.8}ZnO (F) powders.

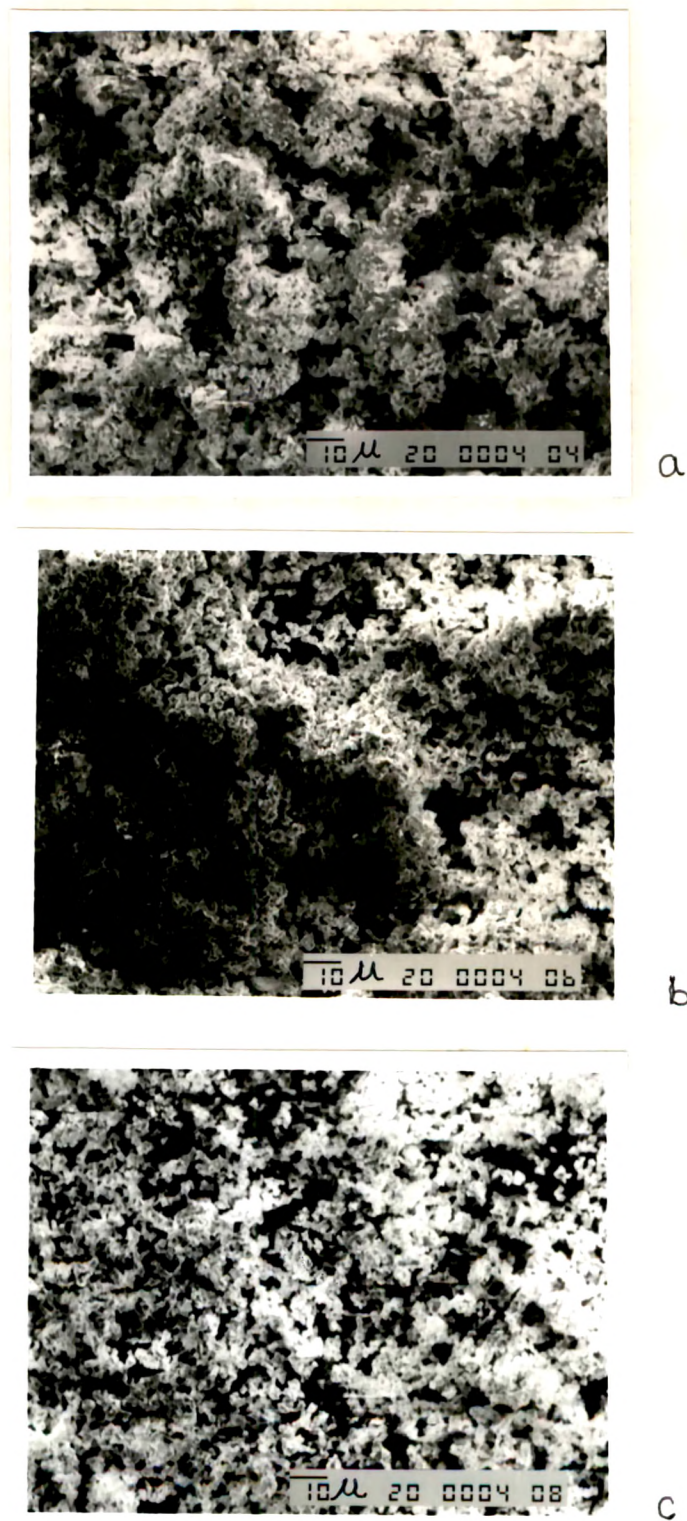
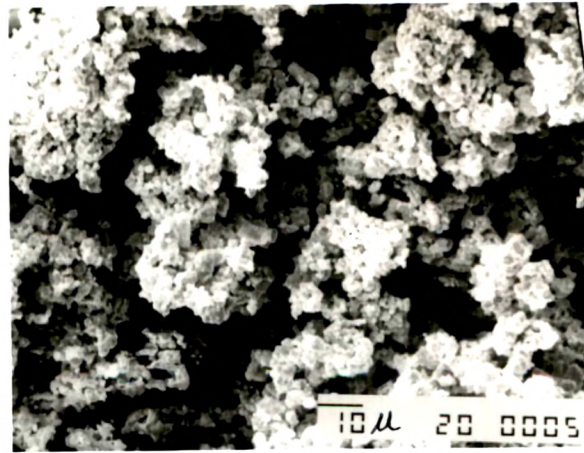


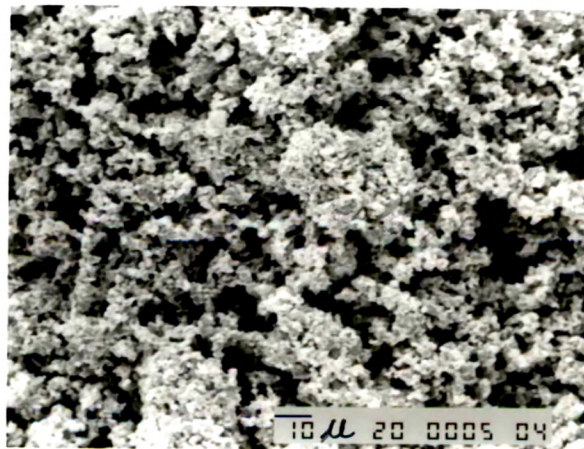
Fig. 4.34 : SEM micrographs for (a) Ag 10 CdO (F), (b) Ag 12 CdO (F) and (c) Ag 15 CdO (F) powders.



a



b

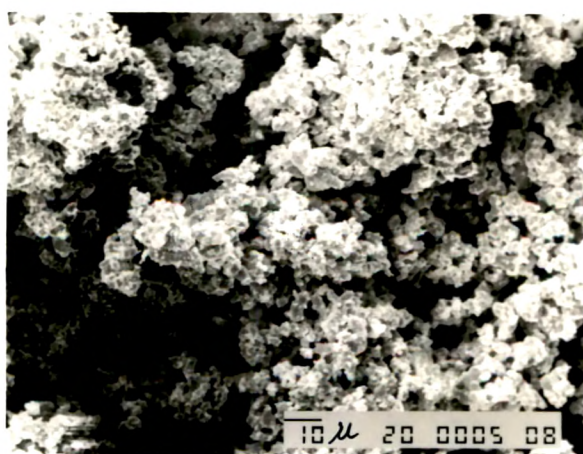


c

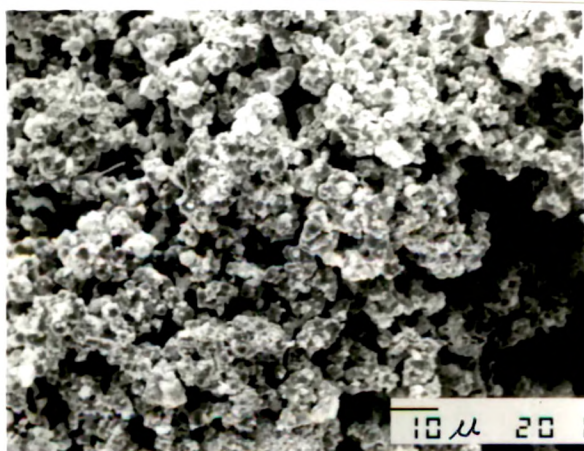
Fig. 4.35 : SEM micrographs for (a) Ag 7.1 ZnO (E), (b) Ag 8.6 ZnO (E) and (c) Ag 10.8 ZnO (E) powders.



a



b



c

Fig. 4.36 : SEM micrographs for (a) Ag 10 CdO (E), (b) Ag 12 CdO (E) and (c) Ag 15 CdO (E) powders.

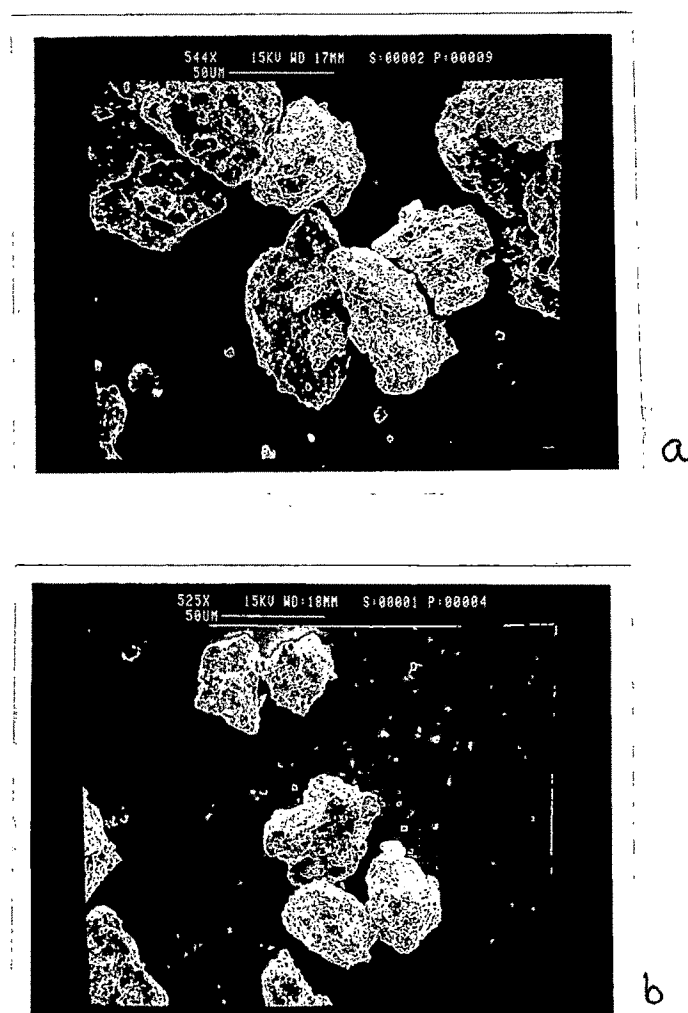


Fig. 4.37 : SEM micrographs for (a) Ag 10.8 ZnO (MA) and (b) Ag 15 CdO (MA) powders

The electroless-coated powders had particle morphologies more or less similar to those of blended powders. i.e. of granular nature. However, the granules were more dispersed and deagglomerated than those observed in blended powders. The powder particle shapes for electroless-coated powders are given in Fig. 4.35 and Fig. 4.36.

A noteworthy observation is that the particle roundness (i.e.the tendency to spherodization) is greater in Ag-CdO compositions than in Ag-ZnO powders processed by spray-coprecipitation, electroless-coating and freeze-drying.

SEM micrographs were also taken for Ag_{10.8}ZnO (MA) and Ag₁₅CdO (MA) powders and are as per Fig.4.37(a) and (b).The coarse and granular morphology of MA powders is well displayed in these photographs.

4.1.9. ESCA analysis of electroless coated powders :

XPS spectra of Ag-ZnO (E) and Ag-CdO (E) samples are shown in Fig. 4.38 and Fig. 4.39. The Ag (3d), Zn (2p), Cd (3d) and O (1s) photoelectron lines arising from these elements are marked on the spectra. XPS and Auger measurements confirmed the surface phase of silver, zinc and cadmium as silver, zinc oxide and cadmium oxide, respectively. Since the dispersion of silver on zinc oxide or cadmium oxide substrates is a factor governing the electrical properties of these materials, the Ag/Zn and Ag/Cd atomic ratios were estimated for all the samples prepared by electroless coating process. These ratios (shown in Table 4.7) indicate an increase in electrical conductivity with an increase in silver dispersion on zinc oxide and cadmium oxide substrates.

Although better silver dispersion was attainable on zinc oxide than on cadmium oxide substrates in the present investigation, it is worth mentioning that the conductivity values are better for the Ag-CdO systems compared with the Ag-ZnO systems for similar dispersion of silver on these substrates as per data given in Table 4.7. This is in

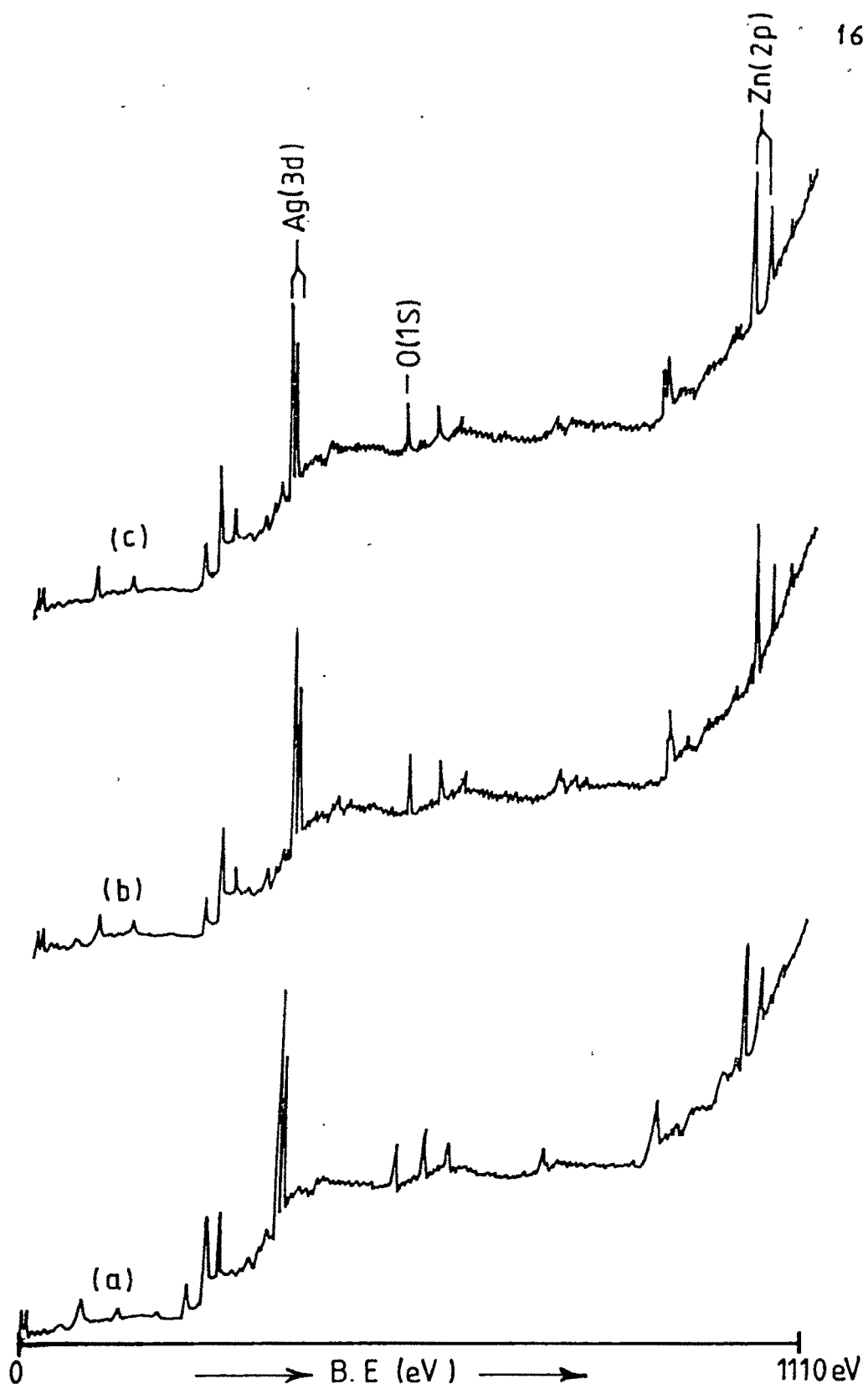


Fig. 4.38: XPS survey spectra of electroless coated powders (a) Ag 7.1 ZnO, (b) Ag 8.6 ZnO and (c) Ag 10.8 ZnO.

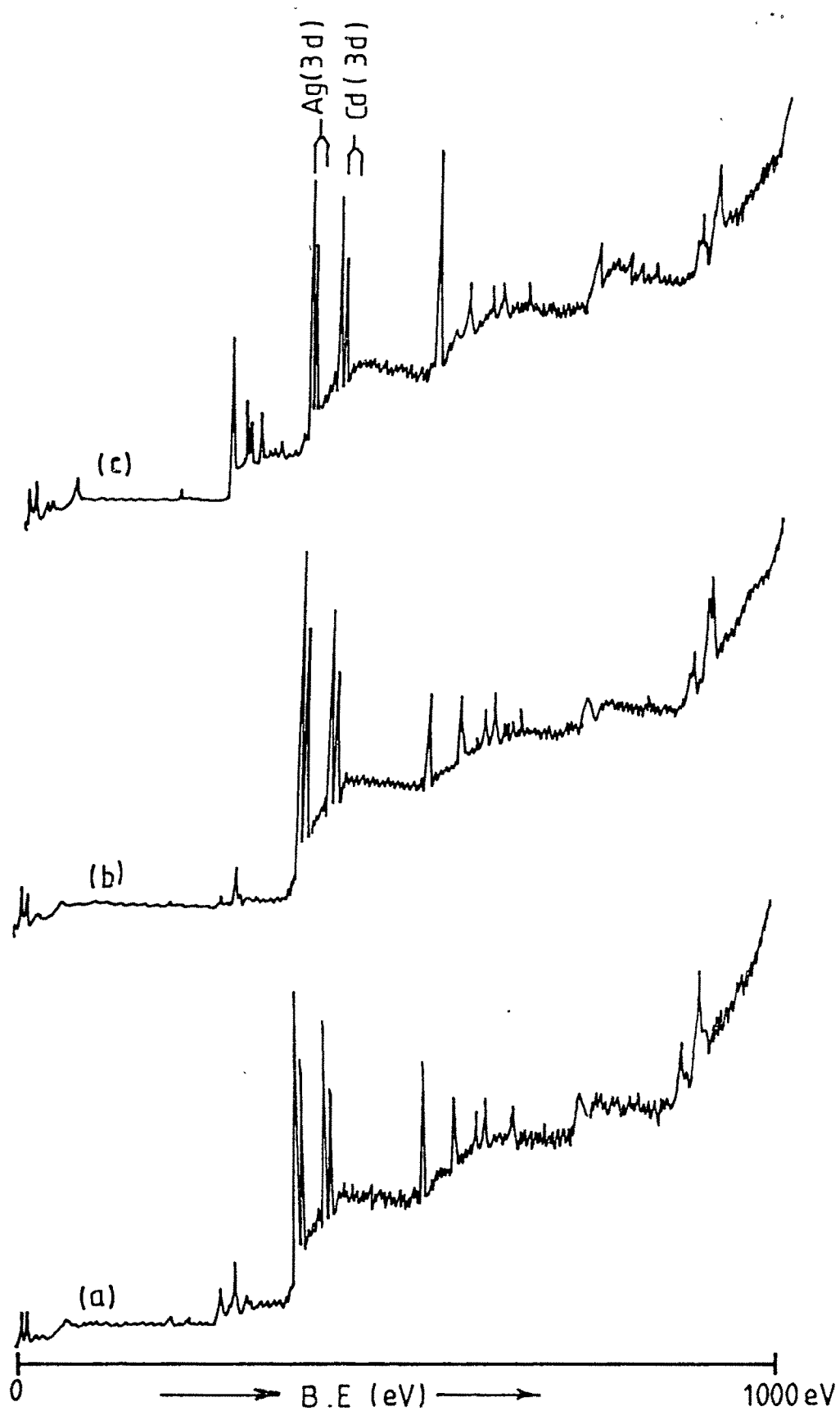


Fig.4.39: XPS survey spectra of electroless coated powders (a) Ag₁₀CdO, (b) Ag₁₂CdO and Ag₁₅CdO.

agreement with the lower resistivity of cadmium oxide as compared to zinc oxide thereby offering better conductivity for the Ag-CdO composites compared to the Ag-ZnO composite systems [139]. Of course, the difference is marginal.

Table 4.7 : Data on relative atomic ratios for different electroless coated powders

System	Composition	Relative atomic ratio	Elect. cond. %IACS
Ag - ZnO		Ag/Zn atomic ratio	
	Ag 7.1 ZnO	2.33	85
	Ag 8.6 ZnO	1.64	77
	Ag 10.8 ZnO	1.30	77
Ag - CdO		Ag/Cd atomic ratio	
	Ag 10 CdO	1.22	91
	Ag 12 CdO	1.05	76
	Ag 15 CdO	0.96	73

4.1.10. DTA / TGA of powders :

The DTA and TGA traces for Ag_{8.6}ZnO(C) and Ag₁₂CdO (C) powders as shown in Fig.4.40 and Fig.4.41 indicate an exothermic peak around 170-180 °C for decomposition of Ag₂O to silver and oxygen in these traces [65]. Two endothermic peaks are also observed in the ranges of 190-195 °C and 330-360 °C corresponding to slow decomposition of carbonates of silver and zinc or silver and cadmium in two samples.

Both the traces show almost complete decomposition of mixed carbonates by about 500 °C and on the basis of which the firing temperature of 550 °C was selected.

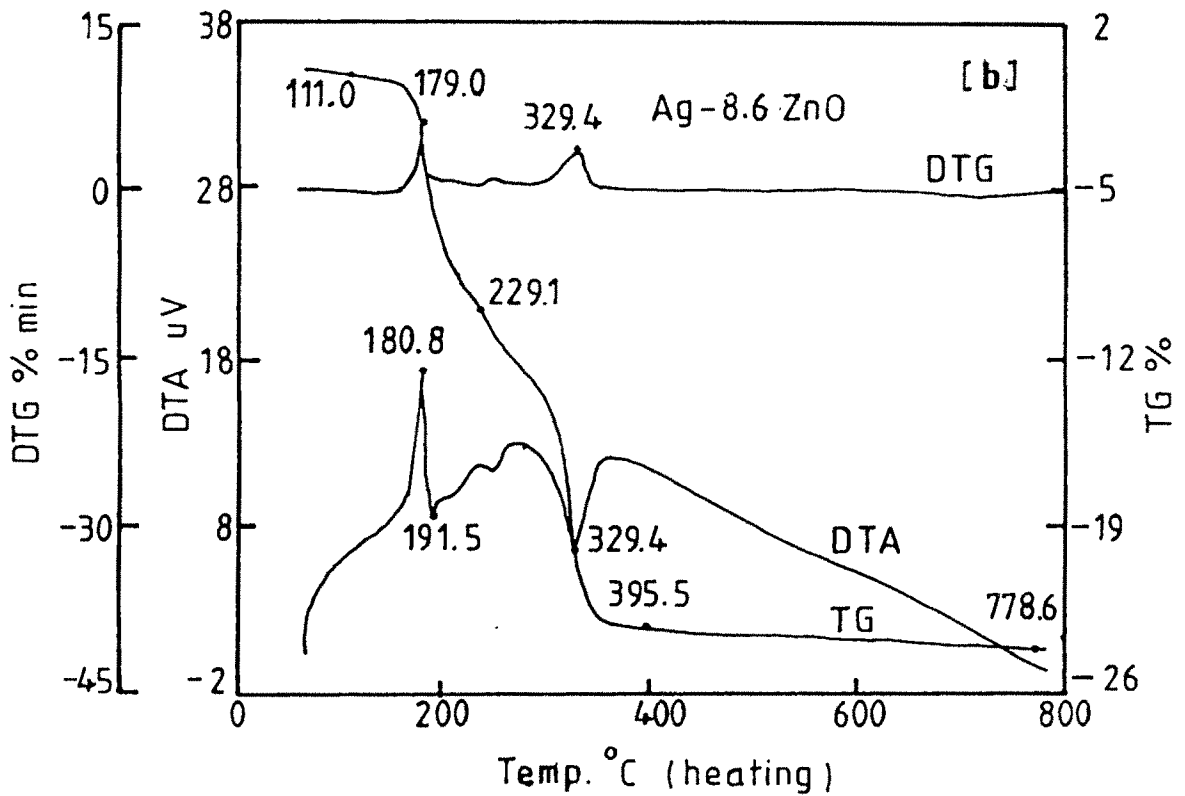
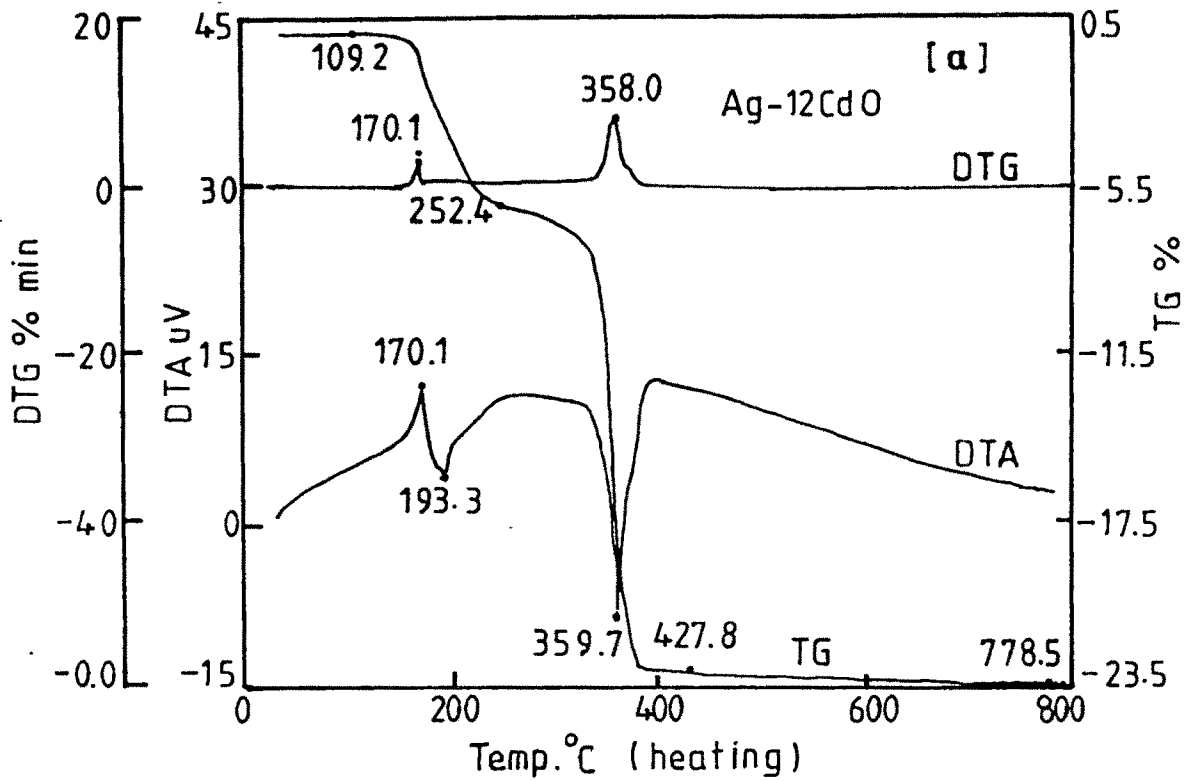


Fig. 4.40 & 4.41 : DTA /TGA profiles for carbonates of [a] Ag and Cd and [b] Ag and Zn powder samples.

4.2. Compaction, sintering and hot-pressing of powders :

Experiments were conducted to study the effect of various variables of compaction and sintering on density. Ag 8.6 ZnO (B) and Ag 12 CdO (B) were the compositions selected for this study (being the middle compositions).

4.2.1 Effect of compaction pressure on green and sintered density :

Table 4.8 (a) and (b) show the values for compaction pressure and resultant green and sintered density for Ag 8.6 ZnO (B) and Ag 12 CdO (B) systems.

The data clearly indicates increase in green and sintered density for Ag 8.6 ZnO (B) with increasing compaction pressure. However, with Ag 12 CdO (B) for compacts pressed at 300 MPa, the sintered density was found to decrease. This may be attributed to the expansion of the compact (pressed at higher values of pressure) occurring during sintering. In rare cases, even blistering or exfoliation of compacts was observed. These changes may be in view of the thermal decomposition of CdO above 900°C into cadmium and oxygen. The liberated oxygen in process of effusion out of the compact must be giving rise to expansion. Fig.4.42 and Fig.4.43 show the variation of density with compaction pressure for two systems.

TABLE 4.8 (a) Effect of compaction pressure on green and sintered density of Ag-8.6 ZnO(B)

Sample	Compaction pressure MPa	Green density g/cc	G.D.as % T.D.	Sintered density g/cc	S.D. as % T.D.
P1	50	5.49	58.50	7.32	74.92
P2	200	7.19	73.59	8.17	83.62
P3	450	8.47	86.69	8.82	90.28

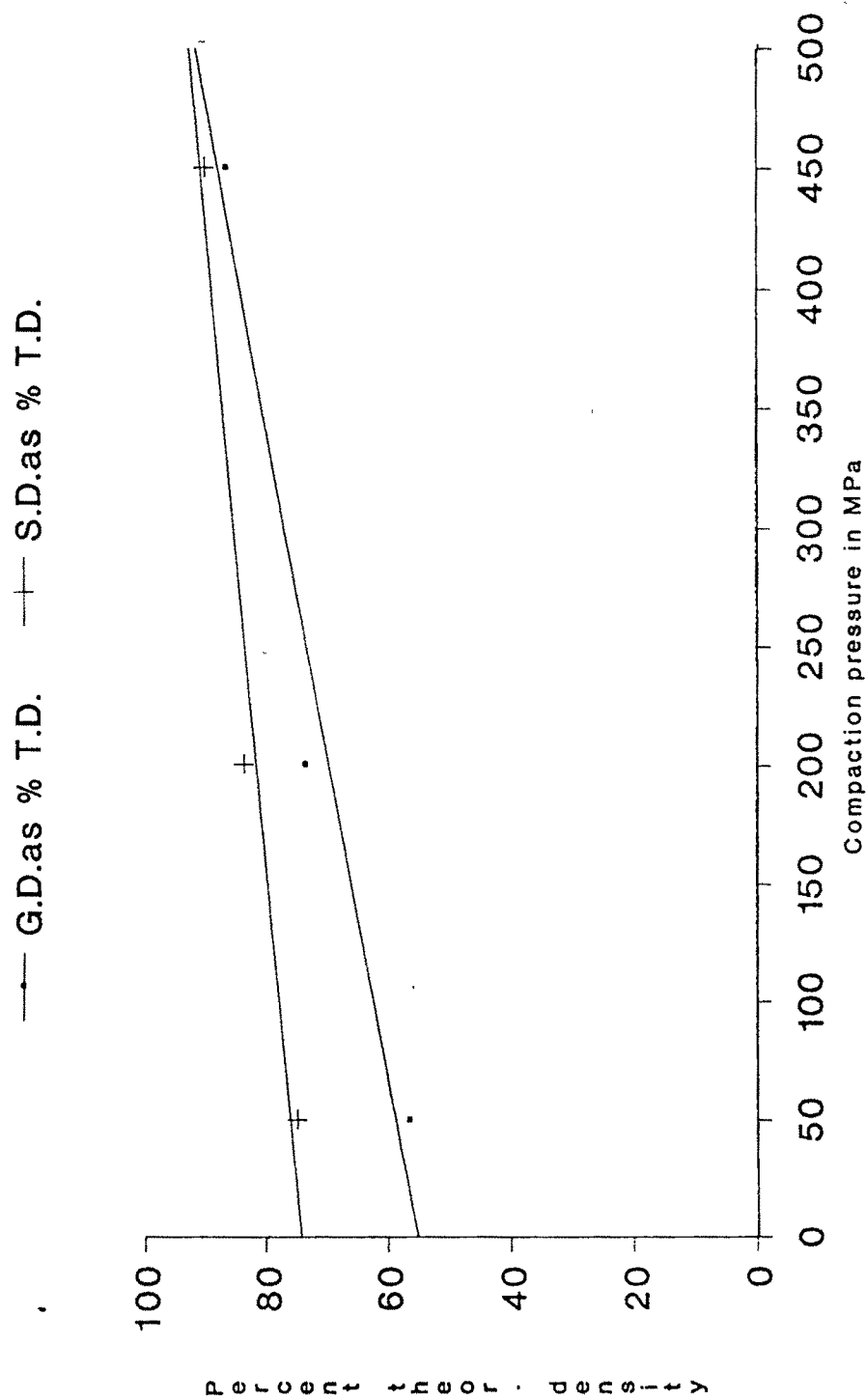


Fig.4.42 : Variation of density with compaction pressure for Ag8.6ZnO (B) system.

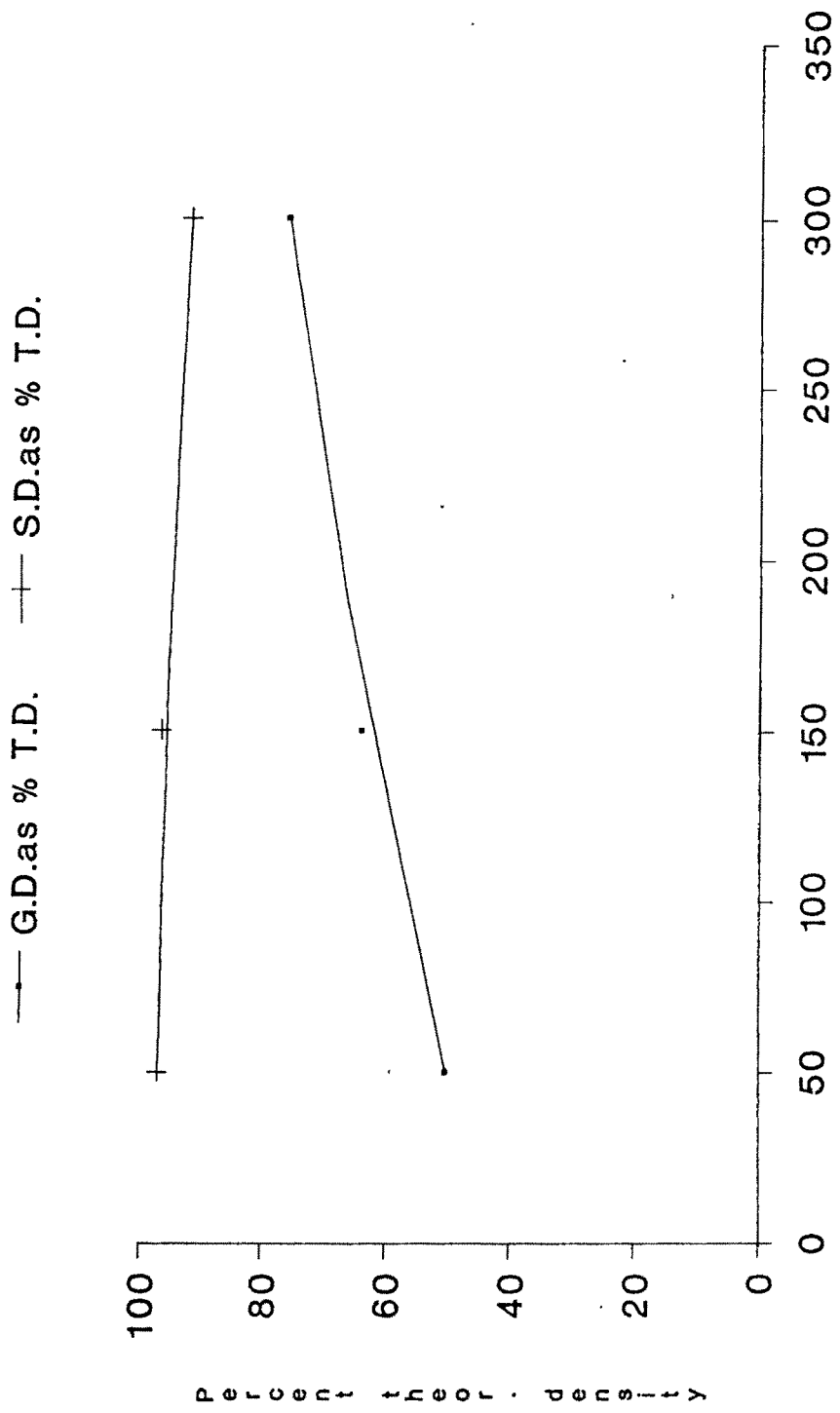


Fig.4.43 :Variation of density with compaction pressure for Ag12 Cdo (B) system.

TABLE : 4.8 (b) Effect of compaction pressure on green and sintered density of Ag 12 CdO(B)

Sample	Compaction pressure MPa	Green density g/cc	G.D.as % T.D.	Sintered density g/cc	S.D. as % T.D.
P4	50	5.11	50.35	9.84	96.95
P5	150	6.49	63.94	9.79	96.45
P6	300	7.71	75.96	9.32	91.82

4.2.2. Effect of sintering temperature on the sintered density :

Experiments were conducted to examine the effect of sintering temperature on as-sintered density. For the range of temperature selected in this investigation, no significant change in sintered density with respect to sintering temperature was noticed. The results of this study are as per Table 4.9 (a) and (b) and Fig. 4.44.

Table 4.9 (a) : Effect of sintering temperature on sintered density of Ag 8.6 ZnO (B)

Sample	Sintering temp. °C	Green density g/cc	G.D. as %T.D.	Sintered density,g/cc	S.D. as % T.D.
S 1	850	8.43	86.30	8.51	87.10
S 2	900	8.44	86.39	8.44	86.39
S 3	930	8.47	86.69	8.82	90.28

Table 4.9 (b) : Effect of sintering temperature on sinter on sintered density of Ag 12 CdO(B)

Sample	Sintering temp, °C	Green density g/cc	G.D. as %T.D.	Sintered density,g/cc	S.D. as % T.D.
S 4	850	7.59	74.78	9.35	92.12
S 5	900	7.74	76.26	9.39	92.50
S 6	930	7.71	75.96	9.32	91.82

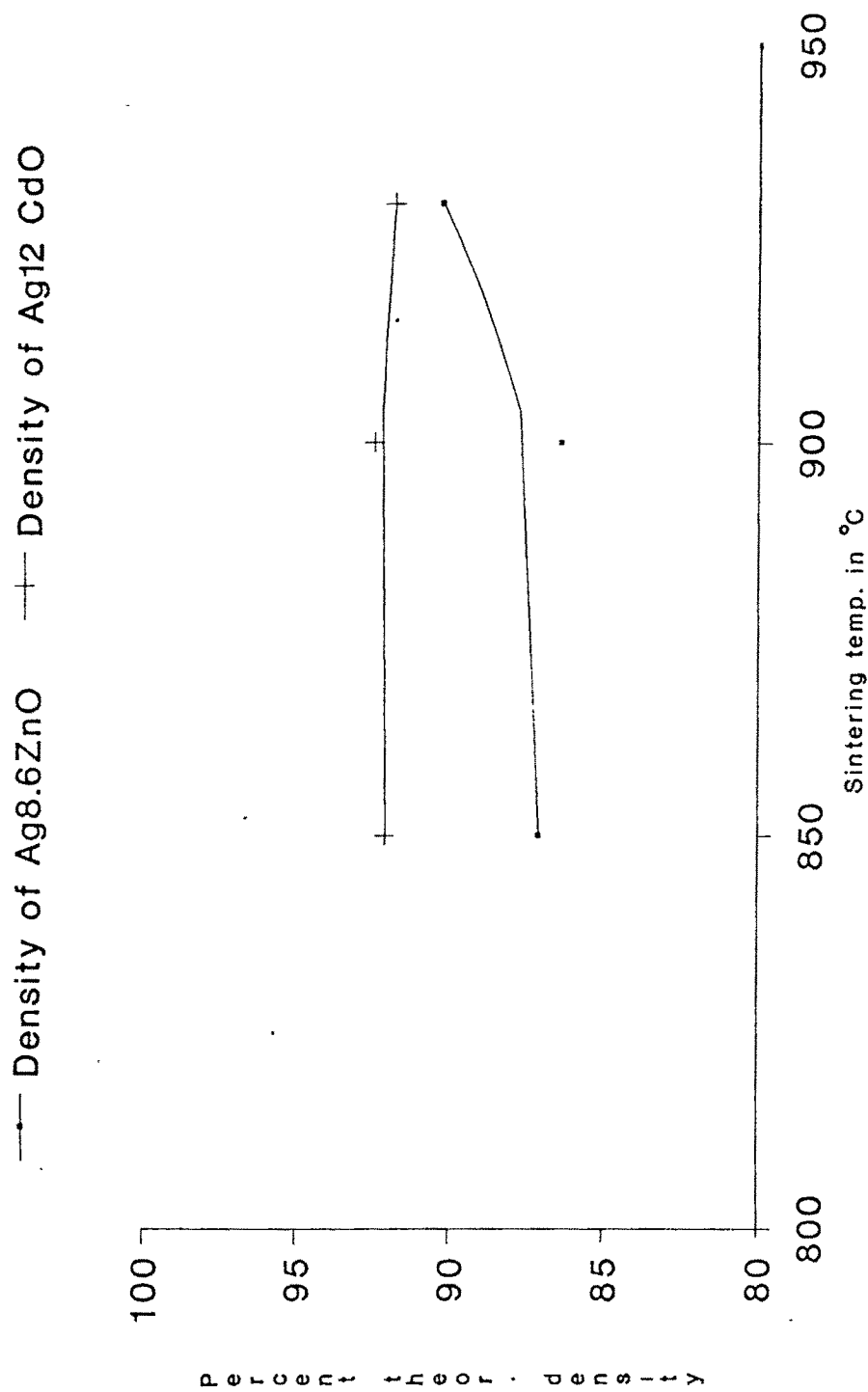


Fig.4.44 :Variation of sintered density with sintering temp. for Ag8.6ZnO (B) and Ag12 CdO (B) system.

4.2.3 Effect of sintering time on sintered density :

Table 4.10 (a) and (b) and Fig. 4.45 demonstrate the effect of sintering time on Ag 8.6 ZnO (B) and Ag 12 CdO (B) compacts pressed and sintered as per conditions stated in these tables. The final sintered density values for both Ag8.6ZnO (B) and Ag12CdO (B) in terms of % theoretical density are ranging from 87 to 93%. There is no specific trend in variation of sintered density with sintering time as per this investigation.

On the basis of these findings for all subsequent experiments, the sintering temperature of 930°C and sintering time equal to 60 min. were maintained.

Table 4.10(a): Effect of sintering time on sintered density of Ag 8.6 ZnO (B)

Sample	Compaction pressure MPa	Green Density g/cc	G.D. as % T.D.	Sintering Temp. C	Sintering Time minutes	Sintered Density g/cc	S.D. as % T.D.
T1	450	8.60	87.0	930	15	8.60	88.0
T2	450	8.48	86.8	930	60	8.90	91.1
T3	450	8.45	86.5	930	90	8.48	86.8
T4	450	8.37	85.7	930	120	8.75	89.8

Table 4.10 (b): Effect of sintering time on sintered density of Ag12 CdO(B)

Sample	Compaction pressure MPa	Green density g/cc	G.D. as % T.D.	Sintering temp C	Sintering time min	Sintered density g/cc	S.D. as % T.D.
T5	300	7.80	78.8	930	15	8.48	83.3
T6	300	7.73	78.2	930	60	9.24	91.0
T7	300	7.79	78.8	930	90	9.18	90.3
T8	300	7.58	74.8	930	120	9.47	93.3

4.2.4. Green density, sintered density and hot pressed density of compacts :

Measurement of green density, sintered density and hot-pressed density of Ag ZnO and Ag-CdO compacts were done and the results are reported in the Table 4.11(a) and 4.11 (b).

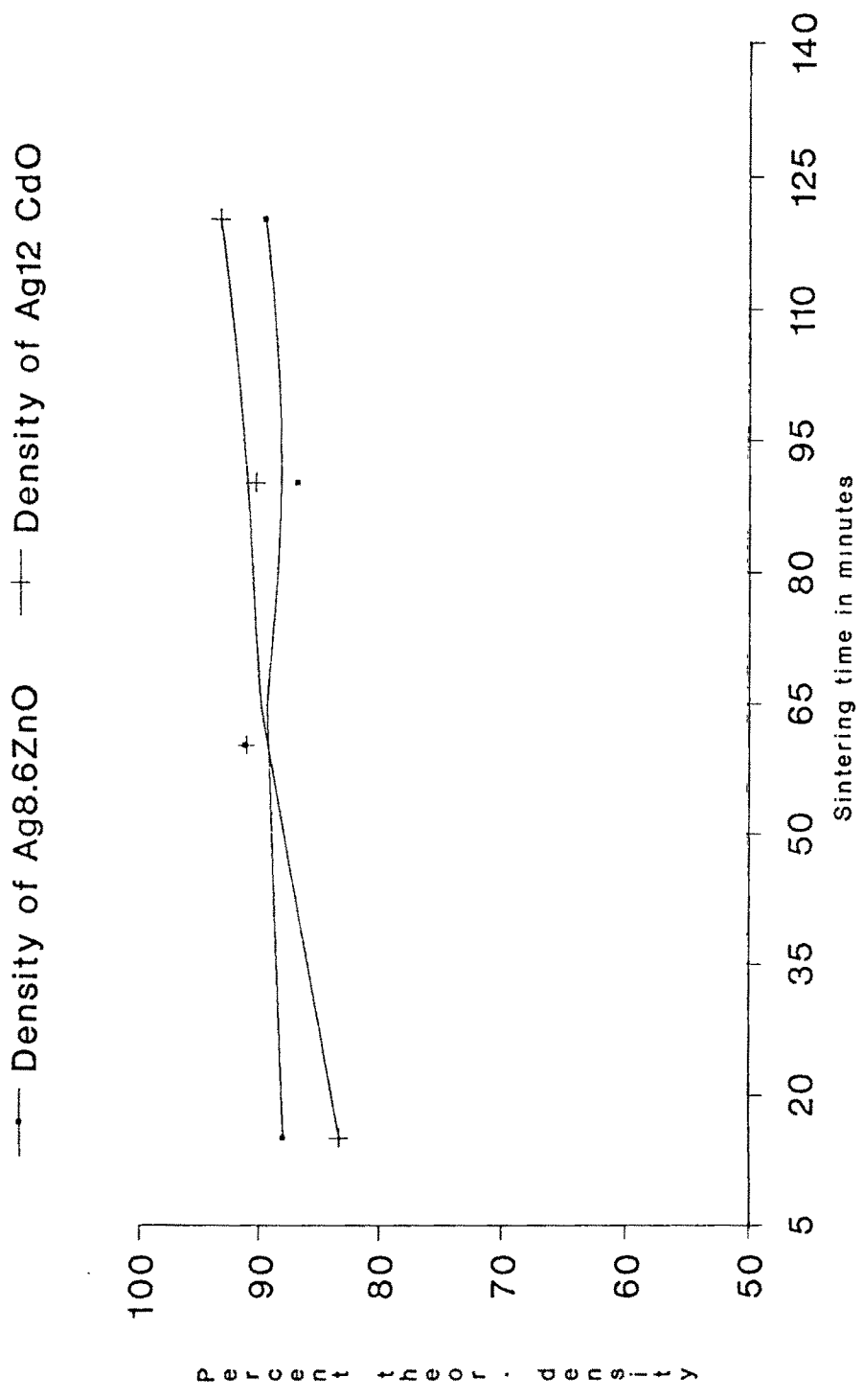


Fig.4.45 :Variation of sintered density with sintering time for Ag8.6ZnO (B) and Ag12 CdO (B) system.

Minimum three samples were tested for each condition. The figures in bracket indicate the values of density as percentage of theoretical density. The values for theoretical density for Ag-ZnO and Ag-CdO systems under study are as per those reported in Table 3.2.

In all forthcoming tables 'M' indicates mean value of that property whereas 'S' indicates the standard deviation for a sample size of three.

Table 4.11 (a) : Density data for Ag-ZnO systems
(in g/cc)

System	G.D. (%)		S.D. (%)		FD (%)	
	M	S	M	S	M	S
Ag 7.1 ZnO (B)	8.58 [86.7]	0.017	8.99 [90.8]	0.048	9.76 [98.6]	0.099
Ag 8.6 ZnO (B)	8.46 [86.6]	0.017	8.85 [90.8]	0.034	9.57 [98]	0.006
Ag 10.8 ZnO (B)	8.26 [86.0]	0.006	8.60 [89.6]	0.017	9.47 [98.6]	0.088
Ag 7.1 ZnO (C)	8.96 [90.7]	0.049	8.22 [83.0]	0.278	9.84 [99.4]	0.029
Ag 8.6 ZnO (C)	8.58 [87.8]	0.070	8.65 [88.5]	0.062	9.58 [98.1]	0.002
Ag 10.8 ZnO (C)	8.42 [87.7]	0.022	8.85 [92.2]	0.037	9.40 [97.9]	0.042
Ag 7.1 ZnO (E)	8.71 [88.0]	0.027	8.74 [88.3]	0.013	9.70 [98.0]	0.01
Ag 8.6 ZnO (E)	7.70 [78.8]	0.059	7.77 [79.5]	0.093	9.41 [96.3]	0.080
Ag 10.8 ZnO (E)	8.10 [84.4]	0.039	8.46 [88.1]	0.049	9.29 [96.8]	0.032
Ag 7.1 ZnO (F)	7.71 [77.9]	0.043	8.22 [83.0]	0.016	9.32 [94.1]	0.091
Ag 8.6 ZnO (F)	8.02 [82.1]	0.039	8.16 [83.5]	0.031	9.48 [96.8]	0.041
Ag 10.8 ZnO (F)	7.02 [73.1]	0.033	7.55 [78.6]	0.055	9.24 [96.3]	0.107
Ag 10.8 ZnO (MA) (condition 1)	7.85 [81.8]	0.014	7.23 [75.3]	0.054	9.53 [99.3]	0.057
Ag 10.8 ZnO (MA) (condition 2)	8.06 [84.0]	0.098	7.09 [73.9]	0.045	9.59 [99.9]	0.014

It is clear from these tables that it is possible to attain final densities in the range of 98-100% of theoretical by methods such as conventional PM route of blending, spray-

coprecipitation and mechanical alloying for both Ag-ZnO and Ag-CdO compacts of different chemical compositions under present investigation.

**Table 4.11 (b) : Density data for Ag-CdO systems
(in g/cc)**

System	G.D. (%)		S.D. (%)		F.D. (%)	
	M	S	M	S	M	S
Ag 10 CdO (B)	7.82 [76.7]	0.017	9.34 [91.8]	0.092	10.08 [98.8]	0.025
Ag 12 CdO (B)	7.76 [76.4]	0.039	9.31 [91.7]	0.054	10.0 [98.5]	0.049
Ag 15 CdO (B)	7.59 [75.4]	0.017	9.30 [92.4]	0.052	9.91 [98.5]	0.124
Ag 10 CdO (C)	8.91 [87.4]	0.008	8.43 [82.7]	0.022	9.99 [97.9]	0.013
Ag 12 CdO (C)	8.83 [87]	0.025	8.41 [82.9]	0.014	10.13 [99.8]	0.013
Ag 15 CdO (C)	8.68 [86.3]	0.004	8.54 [84.9]	0.016	9.96 [99.0]	0.019
Ag 10 CdO (E)	8.93 [87.5]	0.033	9.16 [89.8]	0.017	9.92 [97.3]	0.013
Ag 12 CdO (E)	8.81 [86.8]	0.003	9.35 [92.1]	0.029	9.99 [98.4]	0.013
Ag 15 CdO (E)	8.52 [84.7]	0.025	8.92 [88.7]	0.037	9.70 [96.4]	0.029
Ag 10 CdO (F)	6.53 [64.0]	0.008	6.49 [63.6]	0.084	8.96 [87.8]	0.103
Ag 12 CdO (F)	7.27 [71.6]	0.008	7.33 [72.2]	0.127	9.36 [92.2]	0.027
Ag 15 CdO (F)	6.86 [68.2]	0.010	5.90 [58.6]	0.061	9.17 [91.2]	0.071
Ag 15 CdO (MA)	8.42 [83.7]	0.028	7.09 [70.5]	0.140	10.0 [99.4]	0.050

Electroless coating offered densities in the range of 96-98% of theoretical. The optical micrographs for these samples shown in Fig. 4.60 and 4.61 indicated the presence of porosity in the final hot-pressed compacts, thereby justifying lower density for the compacts of this process route.

Abnormally low values of density were obtained for compacts of freeze-drying route (only 87-97% of theoretical value). Freeze-dried powders were highly spongy with high specific surface area and large amount of microporosity, leading to poor compressibility

and sinterability of freeze-dried powders. The optical micrographs for these samples showed much higher percentage of porosity (Fig. 4.62 and 4.63).

4.2.5. : Microhardness of as-sintered and final hot-pressed compacts :

The values for microhardness in kg/mm^2 are shown in Table 4.12 (a) and (b).

Mechanically alloyed samples showed the best results (the value of microhardness for Ag 10.8 ZnO (MA) being equal to 106 kg/mm^2). Matrix strengthening due to finely-dispersed ZnO particles may be related to this results.

Electroless coated powders also offered good microhardness ($92\text{-}93 \text{ kg/mm}^2$). This may be due to some very fine oxide phase particles getting dispersed in silver due to intense stirring during electroless coating process. The degree of strengthening due to dispersed oxide phase in ODS system is an inverse function of diameter of dispersed phase particles.

Lowest values of hardness for compacts of blending route could be explained with the help of optical micrographs for these samples (Fig 4.56 & Fig 4.57). These photographs clearly indicate islands of silver with oxide phase as grain boundary network. The indentation in the silver island during hardness measurement is the cause of low hardness.

Table 4.12 (b) summarizes the results of microhardness measurements on Ag-CdO compacts. In general Ag-CdO composite compacts showed lower values of microhardness than Ag-ZnO compacts by an order of 1-5 units. However, here also mechanically alloyed sample i.e Ag 15CdO (MA) gave much higher value of microhardness clearly bringing out the supremacy of the mechanical alloying route over other processes for silver-base contact material processing.

**Table 4.12 (a) : Microhardness data for Ag-ZnO systems.
(In Kg/mm²)**

System	Sintered & annealed		Final hot - pressed	
	M	S	M	S
Ag 7.1 ZnO (B)	66.57	1.115	73.30	0.00
Ag 8.6 ZnO (B)	68.70	0.00	73.30	7.267
Ag 10.8 ZnO (B)	68.20	0.707	76.73	1.429
Ag 7.1 ZnO (C)	80.93	2.407	86.27	1.432
Ag 8.6 ZnO (C)	84.20	0.00	86.93	1.933
Ag 10.8 ZnO (C)	82.87	0.471	87.57	1.037
Ag 7.1 ZnO (E)	91.27	1.084	92.03	1.084
Ag 8.6 ZnO (E)	92.03	1.108	92.80	0.00
Ag 10.8 ZnO (E)	92.80	0.00	92.80	0.00
Ag 7.1 ZnO (F)	80.00	0.00	80.00	0.00
Ag 8.6 ZnO (F)	84.50	0.424	91.27	1.084
Ag 10.8 ZnO (F)	84.20	0.00	84.90	2.539
Ag 10.8 ZnO (MA) (condition 1)	92.00	0.00	106.0	0.00
Ag 10.8 ZnO (MA) (condition 2)	92.00	0.00	106.0	0.00

**Table 4.12 (b) : Microhardness data for Ag - CdO system
(In Kg/mm²)**

System	Sintered & annealed		Final hot - pressed	
	M	S	M	S
Ag 10 CdO (B)	70.80	3.536	71.20	0.707
Ag 12 CdO (B)	74.43	1.603	73.87	0.807
Ag 15 CdO (B)	70.80	3.536	73.87	0.801
Ag 10 CdO (C)	82.87	0.943	82.87	0.943
Ag 12 CdO (C)	84.83	0.895	84.23	2.876
Ag 15 CdO (C)	81.57	0.896	82.20	0.00
Ag 10 CdO (E)	86.10	0.00	88.30	0.00
Ag 12 CdO (E)	81.57	0.896	86.10	0.00
Ag 15 CdO (E)	84.80	1.839	84.83	0.896
Ag 10 CdO (F)	88.30	1.796	85.53	2.522
Ag 12 CdO (F)	85.47	0.896	84.90	2.539
Ag 15 CdO (F)	85.47	0.896	84.80	1.838
Ag 15 CdO (MA).	92.00	0.00	106.0	0.00

Microhardness results are displayed in the form of histograms in Fig 4.46 and Fig 4.47 for their easy interpretation.

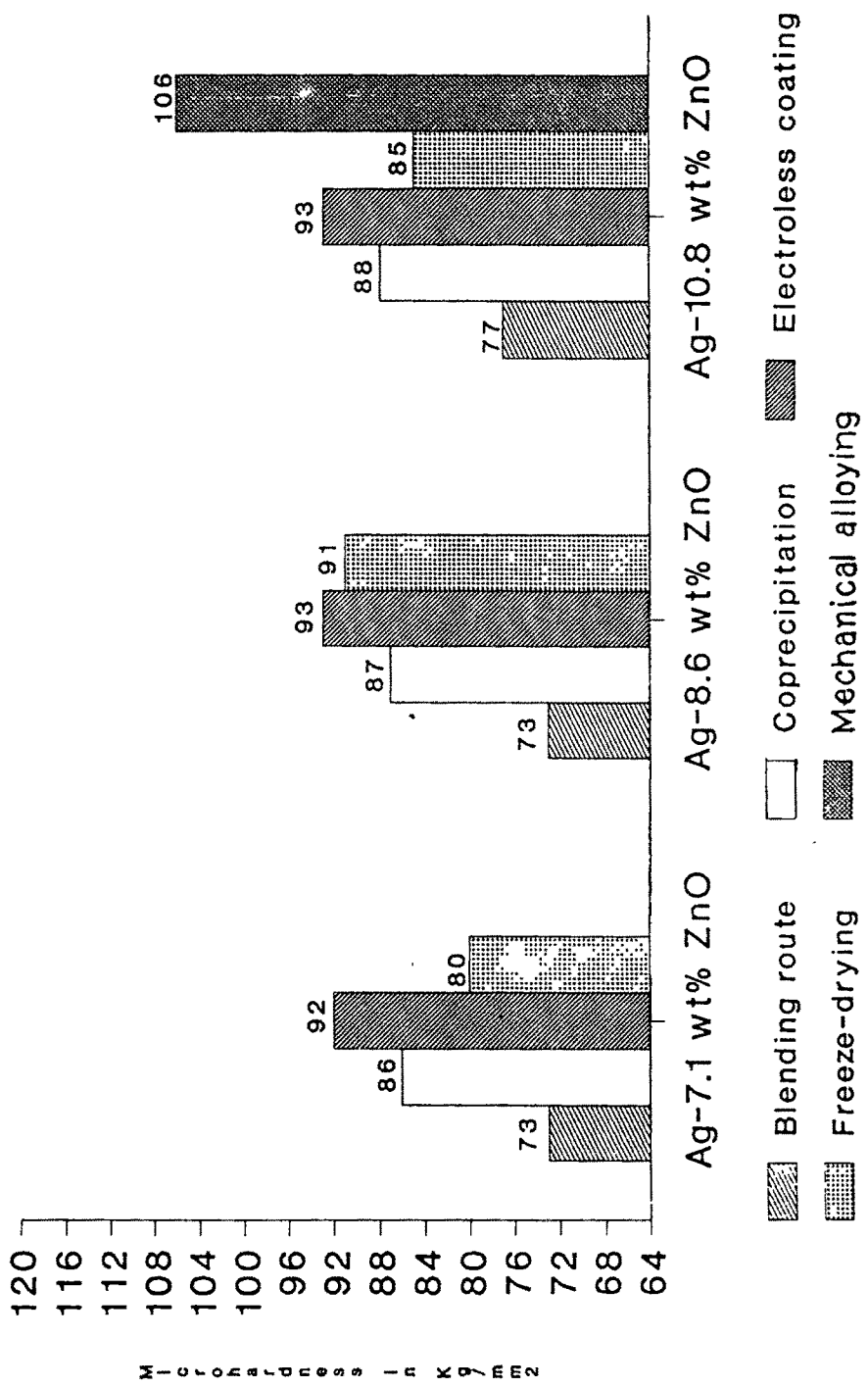


Fig.4.46 : Histograms showing microhardness for Ag ZnO systems.

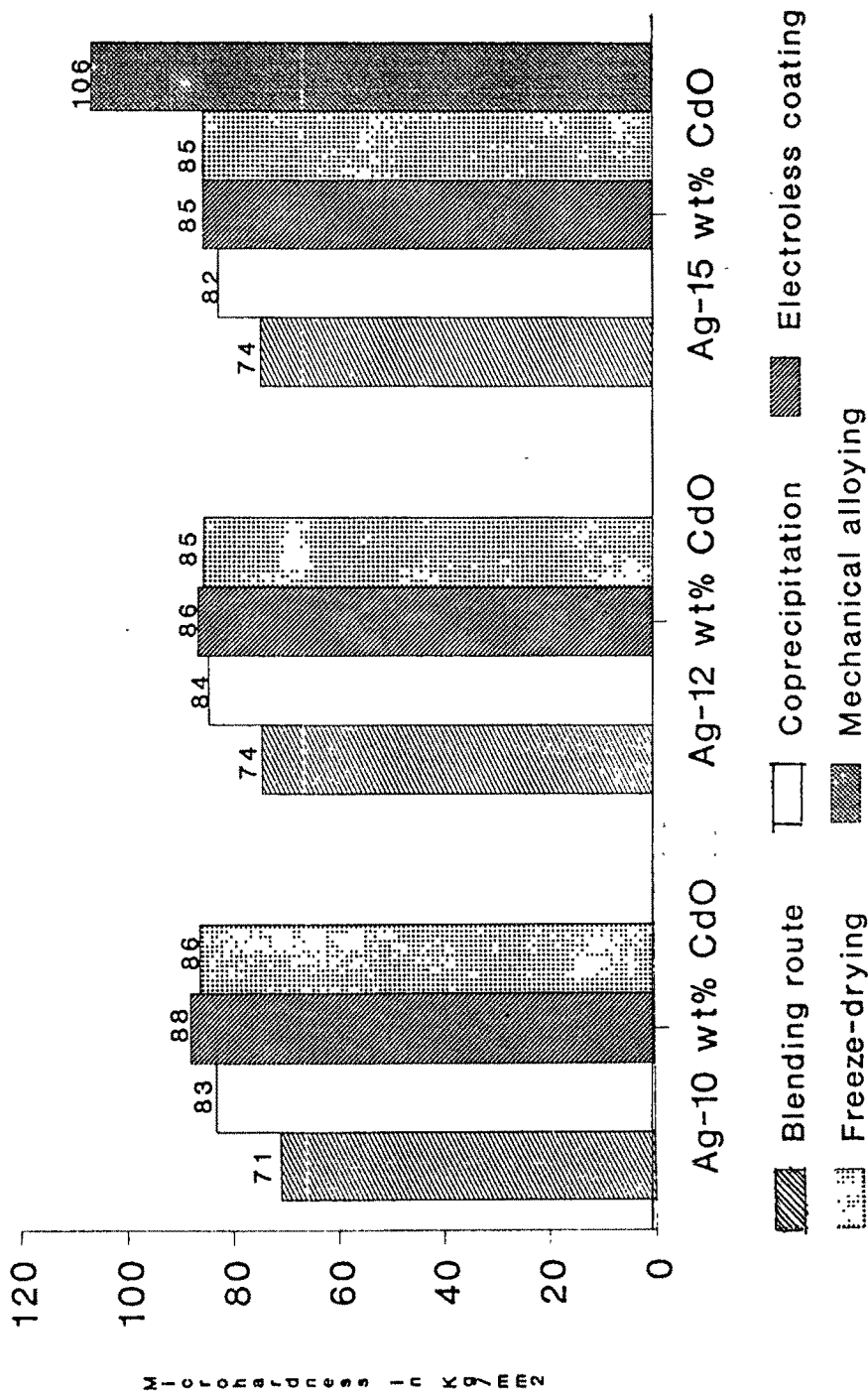


Fig.4.47 : Histograms showing microhardness for Ag CdO Systems.

4.2.6. : Electrical conductivity of as-annealed and hot-pressed compacts :

Electrical conductivity measurements were done on as-annealed as well as final hot-pressed 15 mm dia.samples. The % IACS values are given in Table 4.13 (a) and (b) for Ag ZnO and Ag CdO samples.

**Table 4.13 (a) : Electrical conductivity of Ag-ZnO systems
(In % IACS unit)**

Systems	Sintered & annealed		Final hot - pressed	
	M	S	M	S
Ag 7.1 ZnO (B)	81	0.00	85	0.00
Ag 8.6 ZnO (B)	76	0.417	81	0.471
Ag 10.8 ZnO (B)	66	0.00	72	0.00
Ag 7.1 ZnO (C)	80	0.817	85	0.471
Ag 8.6 ZnO (C)	76	0.471	80	0.00
Ag 10.8 ZnO (C)	68	0.471	73	0.00
Ag 7.1 ZnO (E)	81	0.471	85	0.471
Ag 8.6 ZnO (E)	73	0.471	77	0.943
Ag 10.8 ZnO (E)	65	0.00	73	0.579
Ag 7.1 ZnO (F)	76	0.817	78	0.00
Ag 8.6 ZnO (F)	75	0.00	77	0.00
Ag 10.8 ZnO (F)	61	0.943	63	0.00
Ag 10.8 ZnO (MA)	-	-	72	0.00
Ag 10.8 ZnO (MA)	-	-	72	0.00

Inspite of heterogeneous microstructure with discrete areas of silver and grain boundary oxide phase, greater conductivity values were obtained for Ag ZnO (B) and Ag CdO (B) compacts. Silver islands in these samples offer greater mean free path, λ , and hence more conductivity.

Freeze-dried samples with large amount of porosity as revealed by their optical photomicrographs gave large variation in conductivity and less conductivity compared to other samples.

**Table 4.13 (b) : Electrical conductivity of Ag - CdO systems
(In % IACS UNIT)**

Systems	Sintered and annealed		Final hot - pressed	
	M	S	M	S
Ag 10 CdO (B)	81	1.247	89	0.943
Ag 12 CdO (B)	77	0.943	85	0.00
Ag 15 CdO (B)	73	1.414	82	0.471
Ag 10 CdO (C)	80	0.471	86	0.00
Ag 12 CdO (C)	79	0.471	84	0.471
Ag 15 CdO (C)	73	0.471	76	0.471
Ag 10 CdO (E)	76	0.817	91	0.00
Ag 12 CdO (E)	71	1.001	81	0.471
Ag 15 CdO (E)	68	1.700	76	0.471
Ag 10 CdO (F)	53	4.500	70	2.829
Ag 12 CdO (F)	63	0.047	72	0.471
Ag 15 CdO (F)	53	2.160	68	0.471
Ag 15 CdO (MA)	-	-	74	0.00

The electrical conductivity values obtained for Ag-ZnO and Ag-CdO compacts of coprecipitation, electroless coating and mechanical alloying routes are comparable to those reported in the literature for similar compositions.

4.2.7 : Effect of amount of oxide phase on electrical conductivity :

In general it is observed that with the increasing percentage of oxide phase, the electrical conductivity of Ag-MeO composite compact decreases. The incorporation of the second phase (i.e. ZnO or CdO) of much less conductivity value into a highly conducting phase

(i.e. Ag), lowers the conductivity of composite structure as per equation stated in section 2.4.1.

Fig. 4.48-4.55 show the graphs for variation of electrical conductivity with percent oxide phase for both Ag-ZnO and Ag-CdO systems. Inconsistent trend in variation of conductivity with percent oxide phase is noticed for Ag15 CdO (F) compacts.

4.3 : Structural analysis of final compacts :

4.3.1 : Microstructural analysis :

Final hot-pressed compacts on examination at 100 X magnification under UNION microscope, revealed presence of silver and metal oxide phase and in some cases porosity also. Optical microscopy was done to assess the morphology of dispersion of oxide phase particles in silver matrix, qualitatively.

Optical micrographs for Ag-ZnO (B) samples showed dispersion of oxide phase in the form of a network (Fig 4.56). Similarly, Fig. 4.57 showed the microstructures for Ag-CdO (B) samples with CdO network and the agglomerates of CdO visible as black patches in the structure.

The microstructures for Ag-ZnO (C) and Ag-CdO (C) are displayed in Fig.4.58 and Fig.4.59. Fine and uniform dispersion of oxide phase in silver matrix was obtained for these samples.

The microstructures for Ag-ZnO (E) and Ag-CdO (E) showed an additional phase, ie porosity. Irregularly shaped black spots seen in photomicrographs (Fig. 4.60 and Fig. 4.61) are pores. Presence of porosity is cross checked by density data reported earlier.

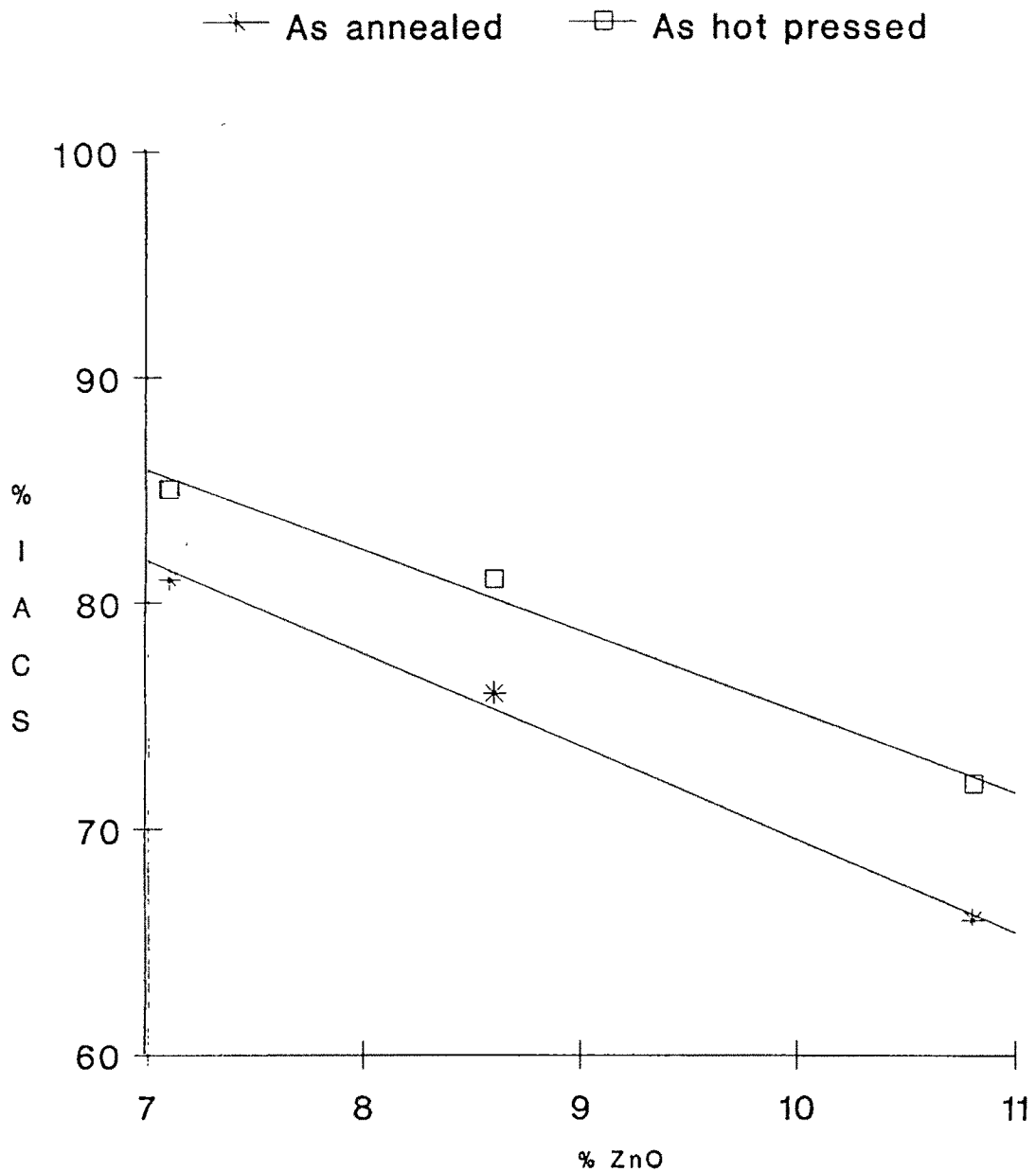


Fig.4.48 : Variation of electrical conductivity with percent oxide phase for Ag ZnO (B) system.

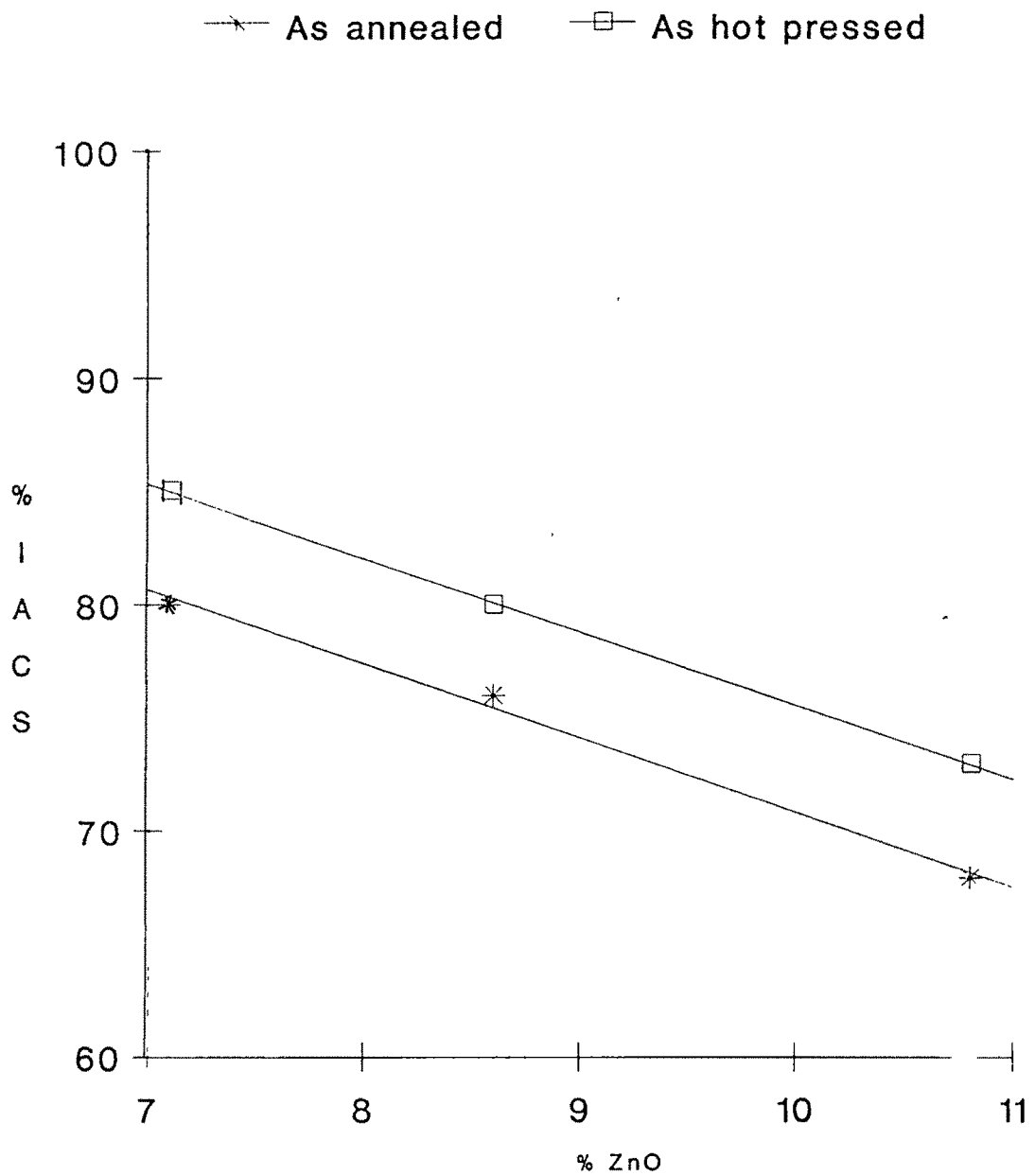


Fig.4.49 : Variation of electrical conductivity with percent oxide phase for Ag ZnO (C) system.

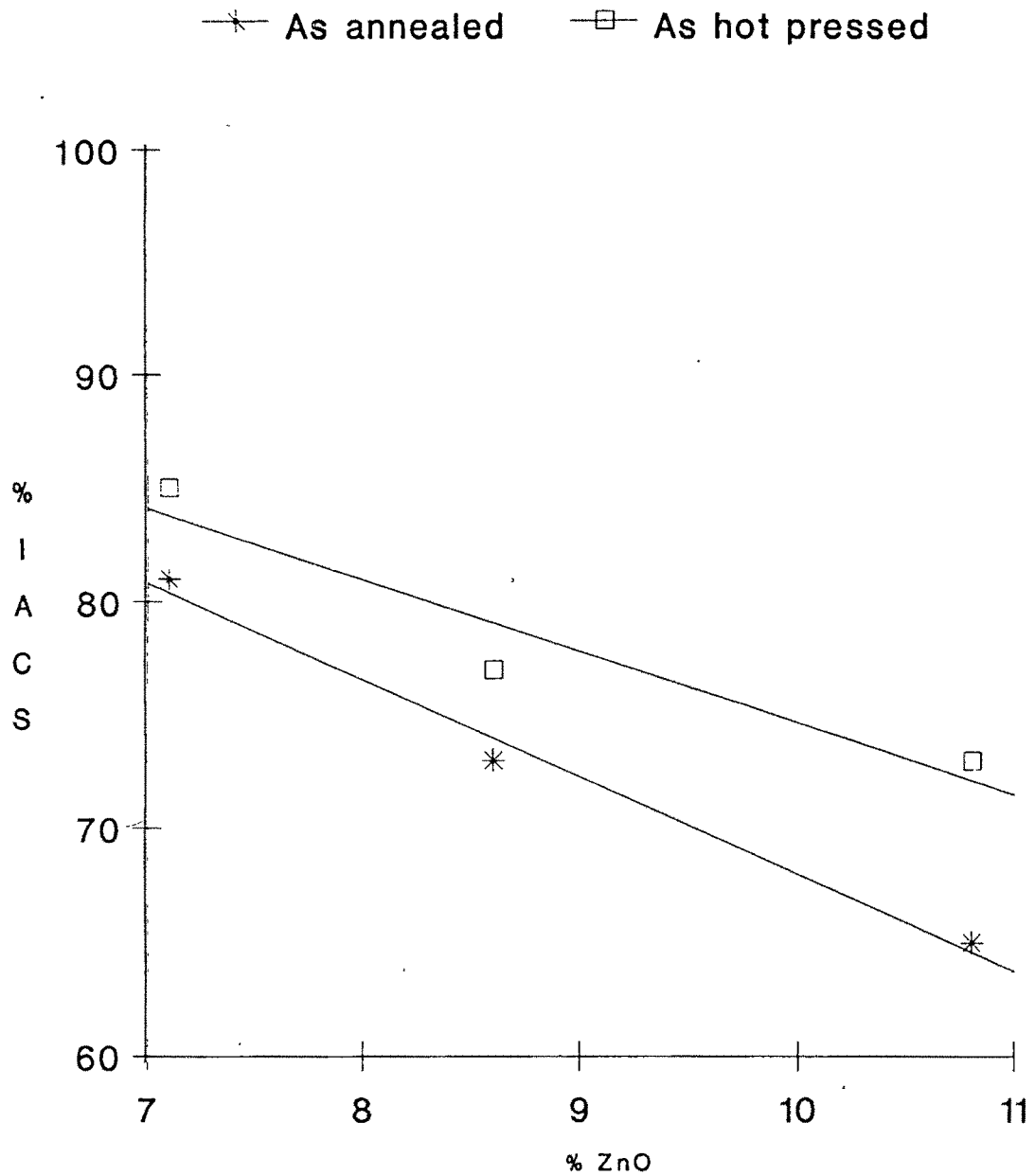


Fig.4.50 : Variation of electrical conductivity with percent oxide phase for Ag ZnO (E) system.

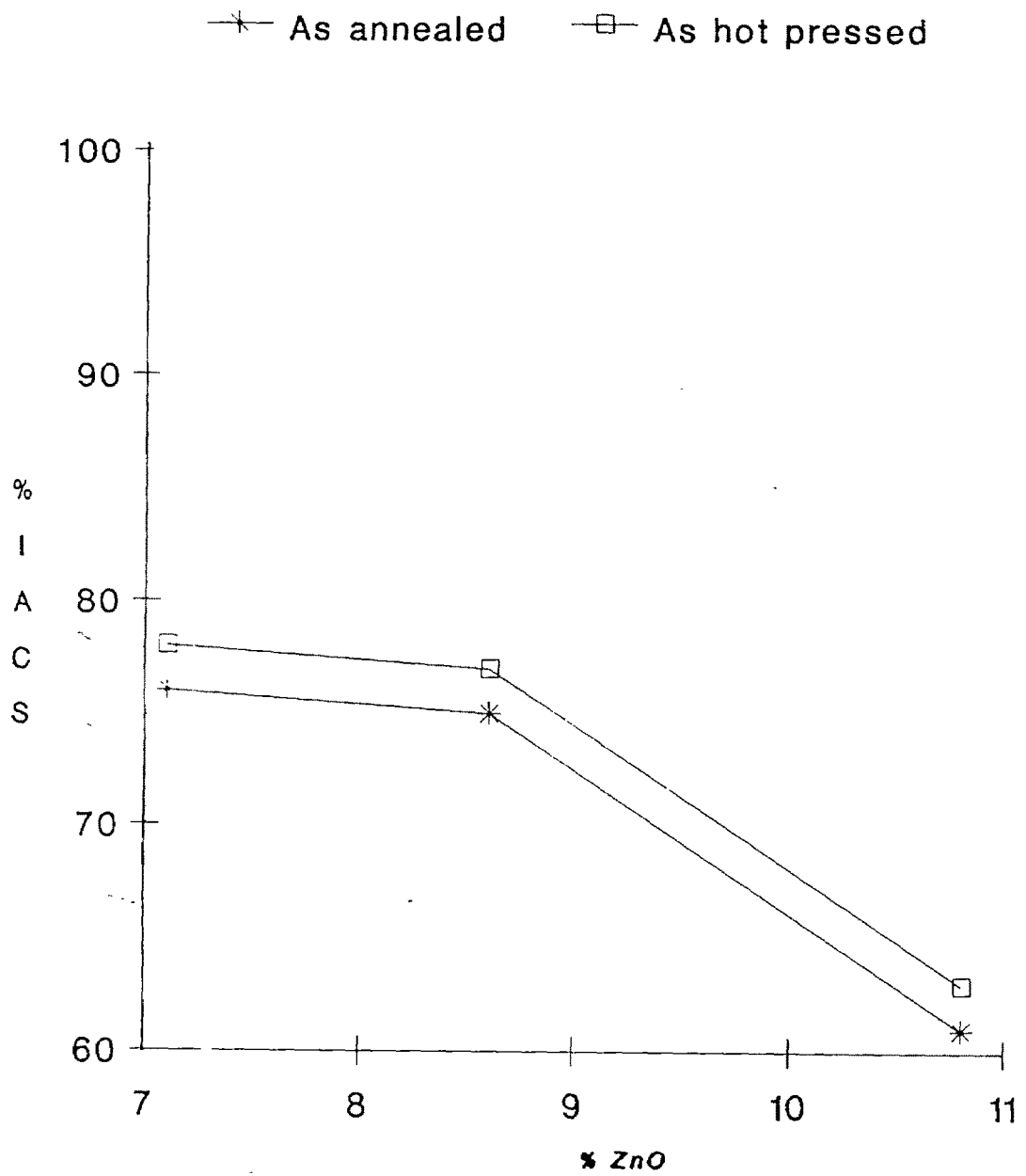


Fig.4.51 : Variation of electrical conductivity with percent oxide phase for Ag ZnO (F) system.

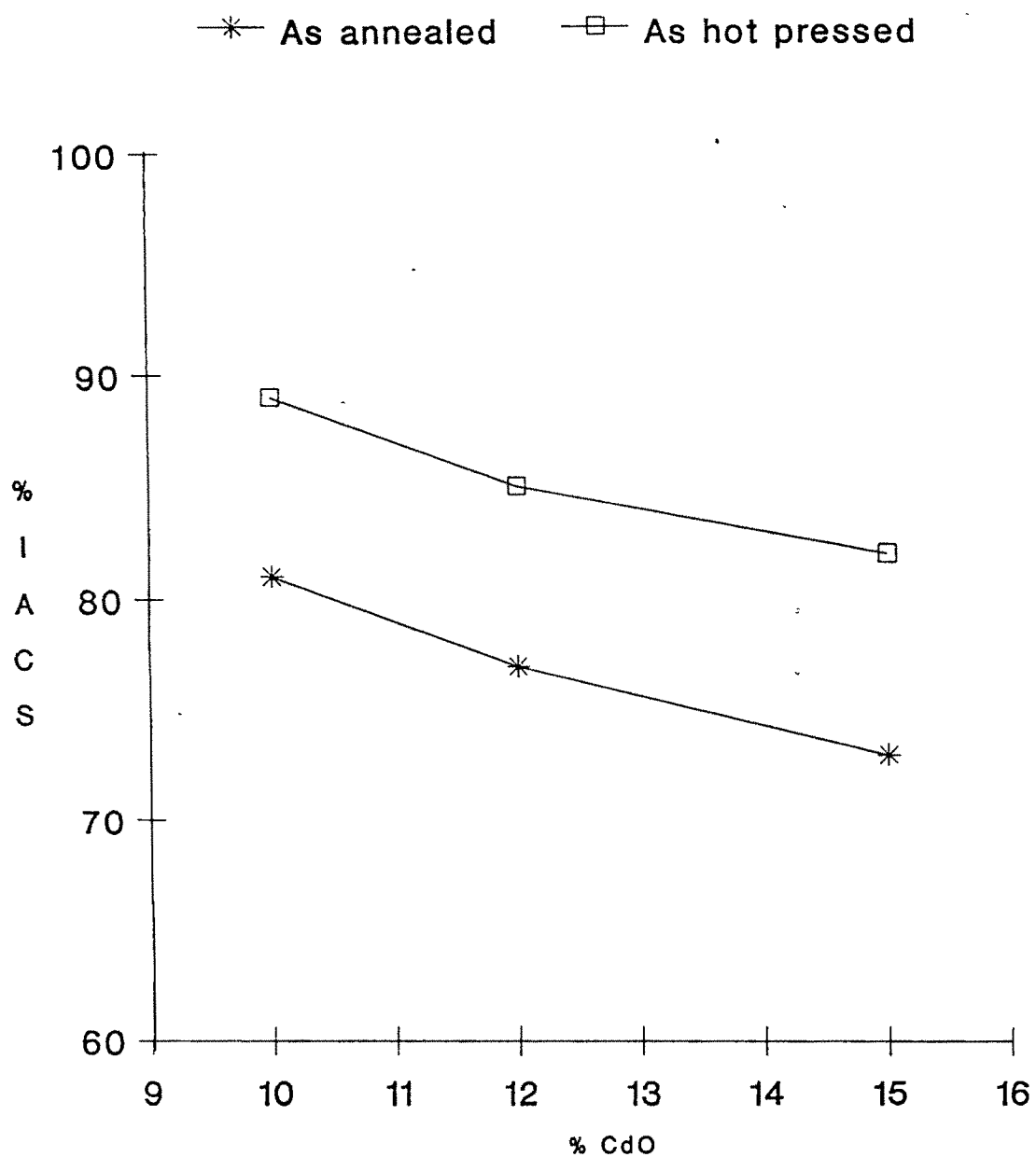


Fig.4.52 : Variation of electrical conductivity with percent oxide phase for Ag CdO (B) system.

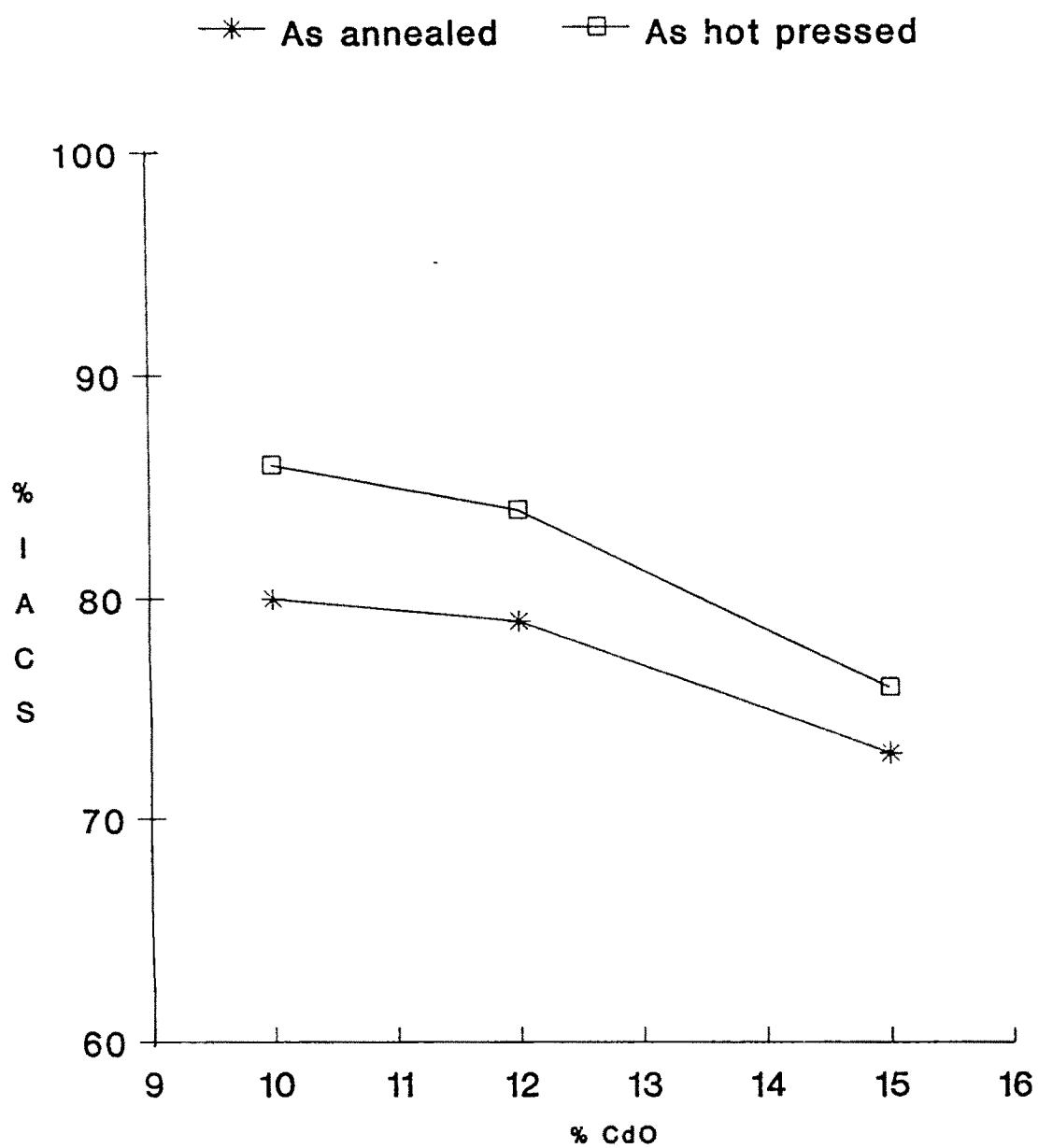


Fig.4.53 : Variation of electrical conductivity with percent oxide phase for Ag CdO (C) system.

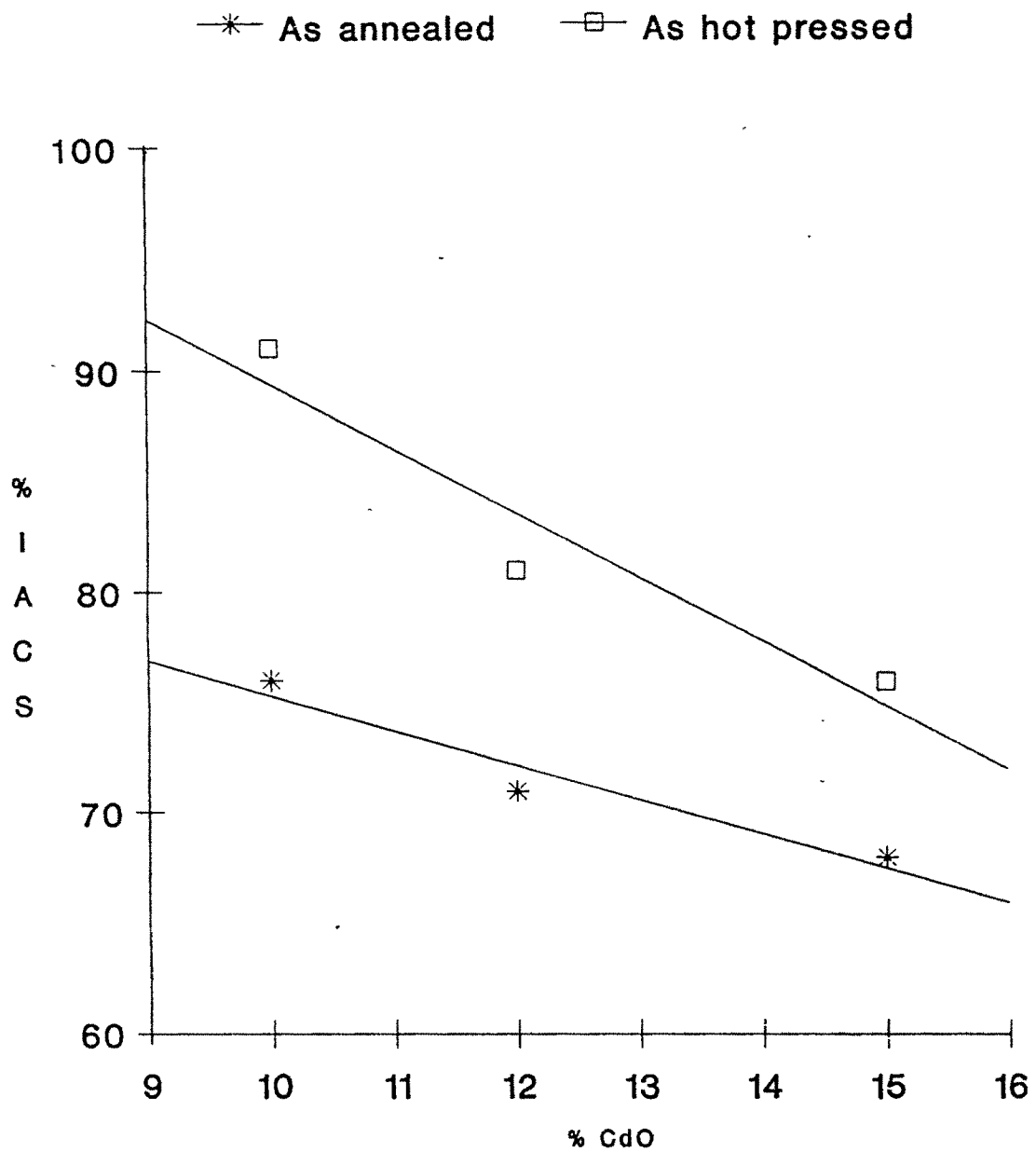


Fig.4.54 : Variation of electrical conductivity with percent oxide phase for Ag CdO (E) system.

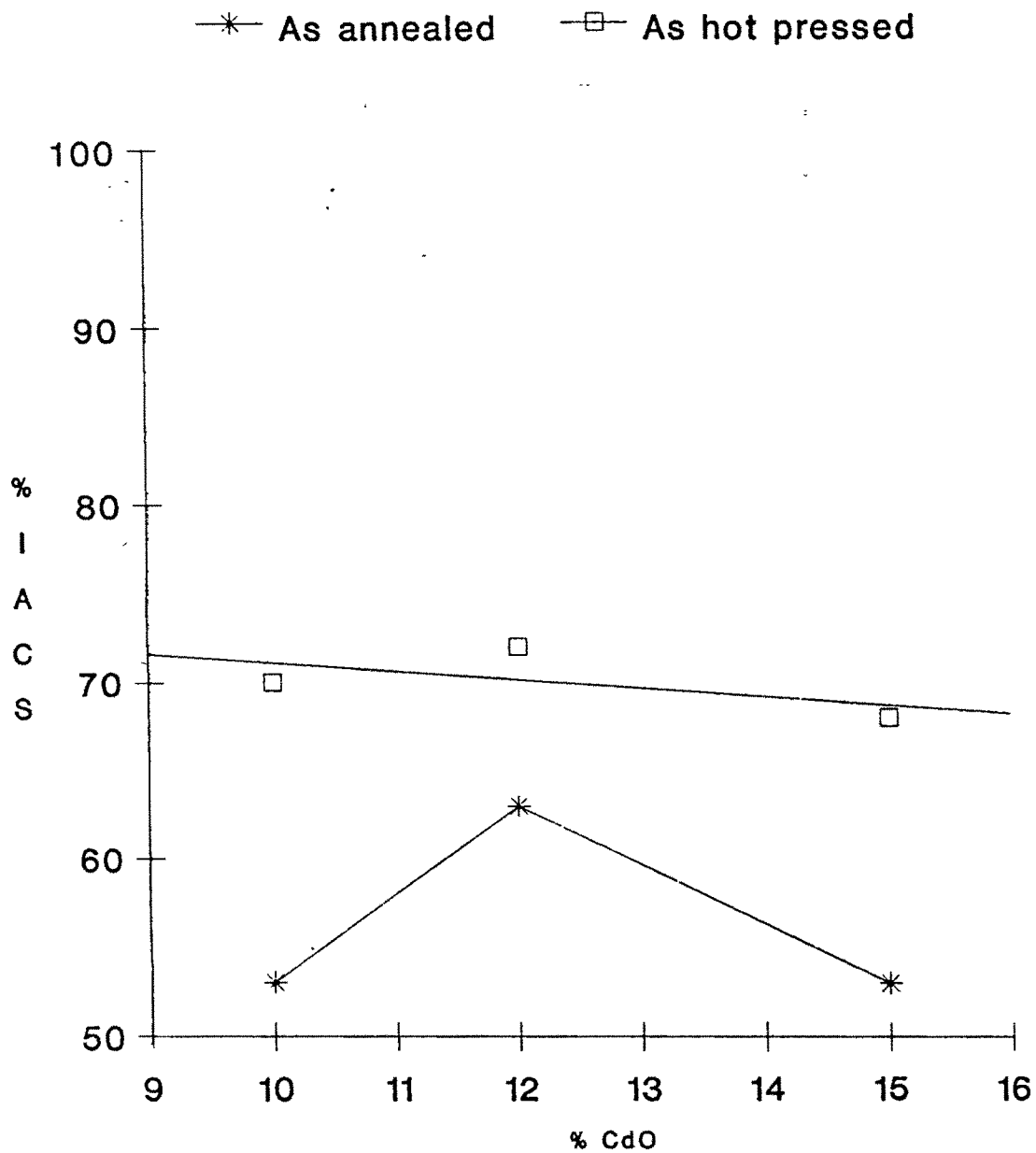
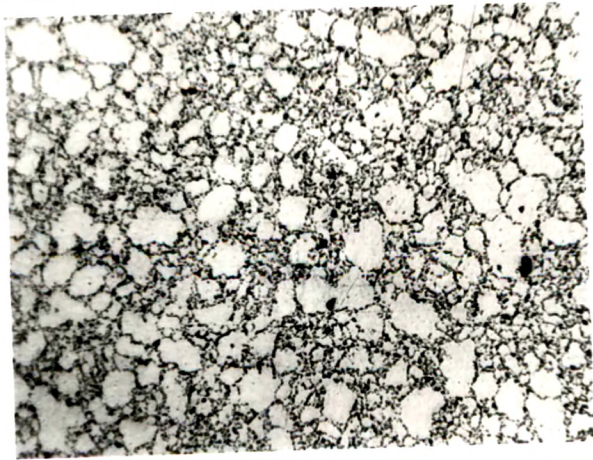


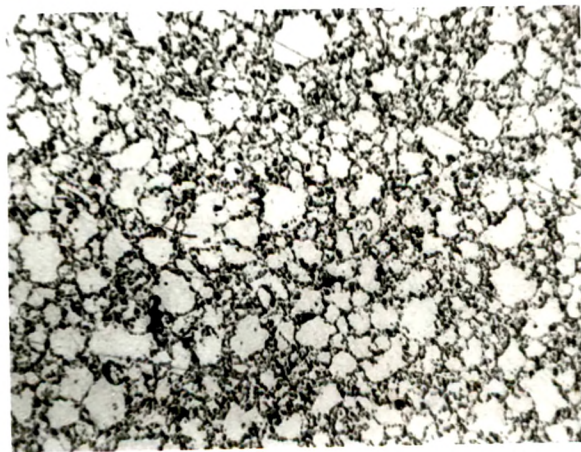
Fig.4.55 : Variation of electrical conductivity with percent oxide phase for Ag CdO (F) system.



a

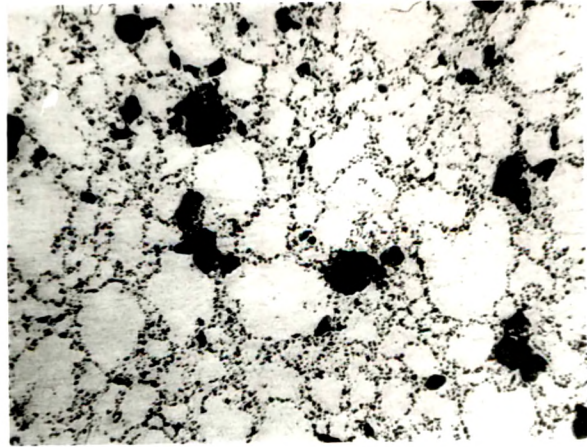


b

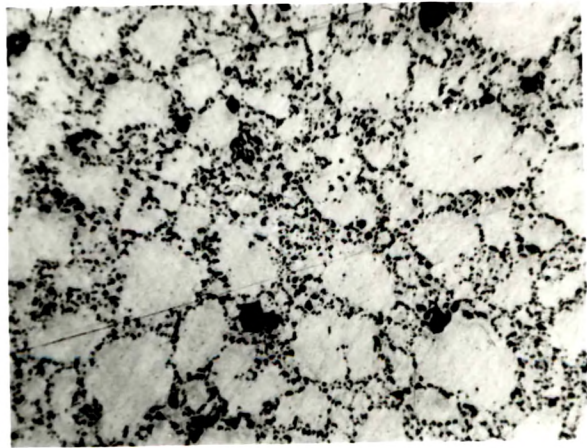


c

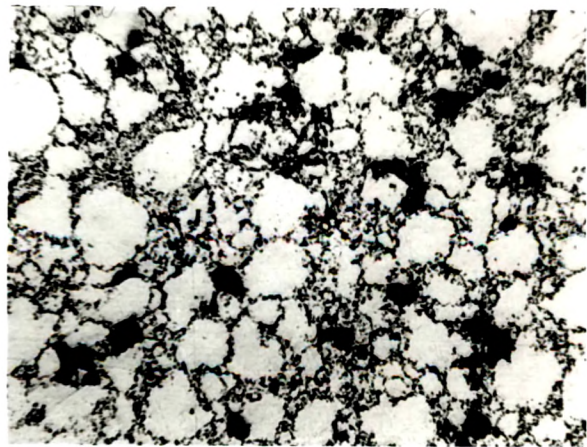
Fig. 4.56 : Optical micrographs for (a) Ag 7.1 ZnO (B), (b) Ag 8.6 ZnO (B) and (c) Ag 10.8 ZnO (B) samples. (100 \times)



a



b

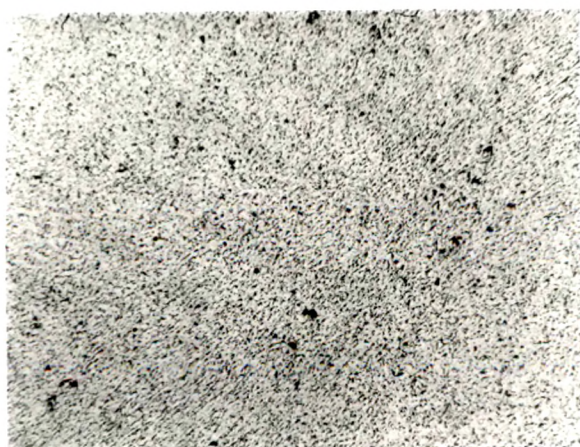


c

Fig. 4.57 : Optical micrographs for (a) Ag 10 CdO (B), (b) Ag 12 CdO (B) and (c) Ag 15 CdO (B) samples. (100 x)



a

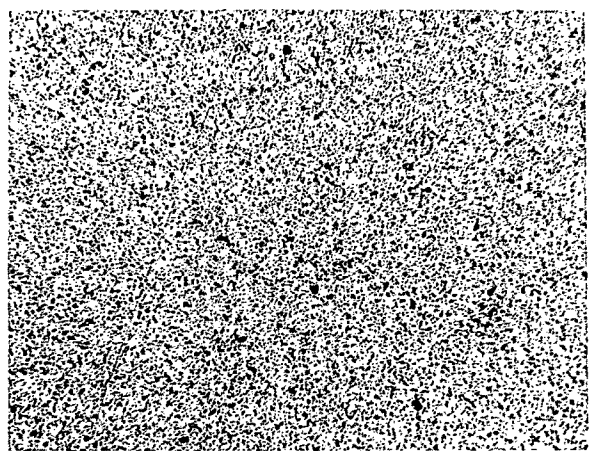


b

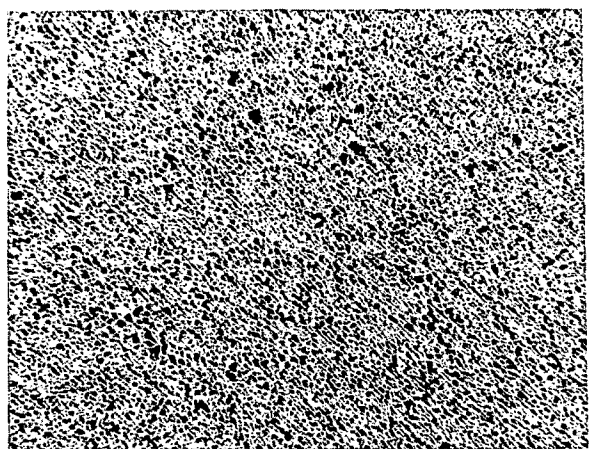


c

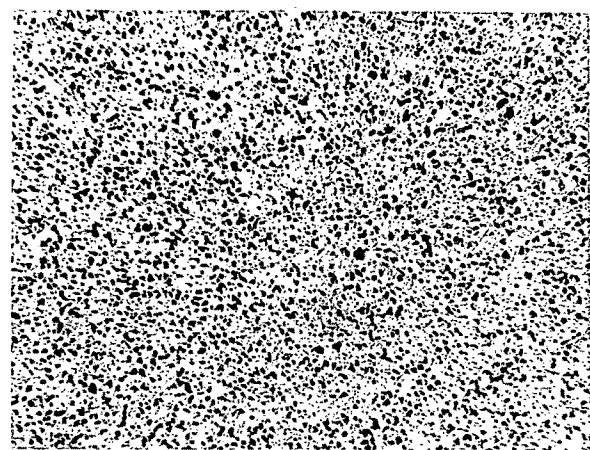
Fig. 4. 58 : Optical micrographs for (a) $\text{Ag}_{7.1}\text{ZnO}$ (C), (b) $\text{Ag}_{8.6}\text{ZnO}$ (C) and (c) $\text{Ag}_{10.8}\text{ZnO}$ (C) samples. (100X)



a



b



c

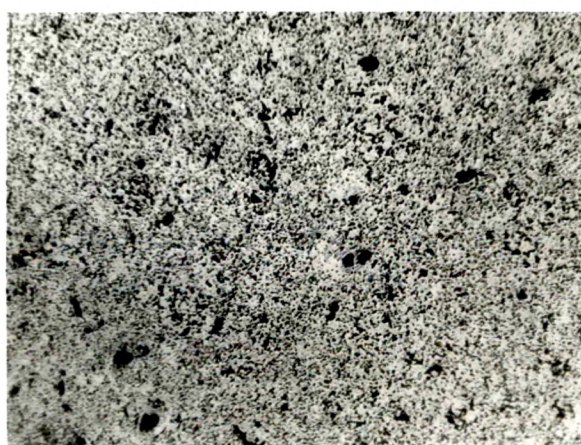
Fig. 4. 59 : Optical micrographs for (a) Ag10CdO (C), (b) Ag12CdO (C) and (c) Ag15CdO (C) samples. (100X)



a



b



c

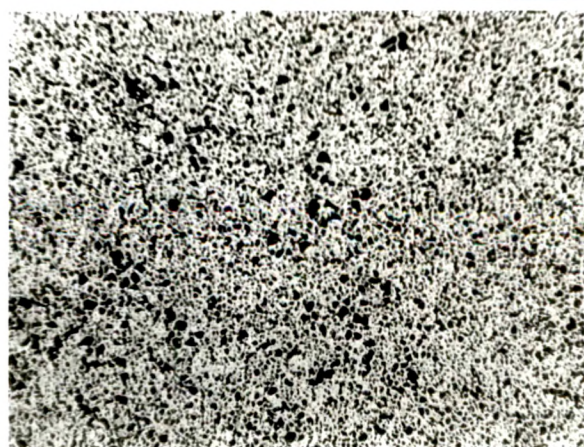
Fig. 4. 60 : Optical micrographs for (a) $\text{Ag}_{7.1}\text{ZnO}$ (E), (b) $\text{Ag}_{8.6}\text{ZnO}$ (E) and (c) $\text{Ag}_{10.8}\text{ZnO}$ (E) samples. (100X)



a

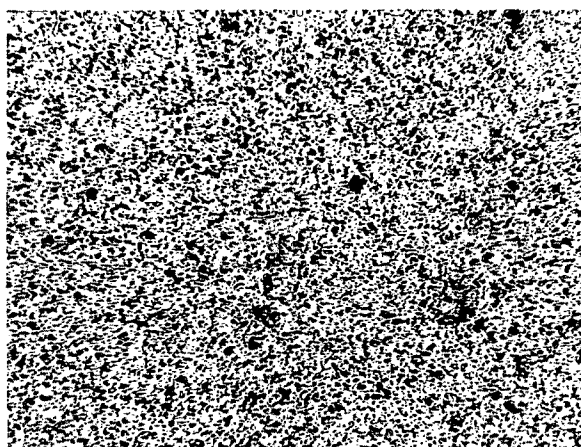


b

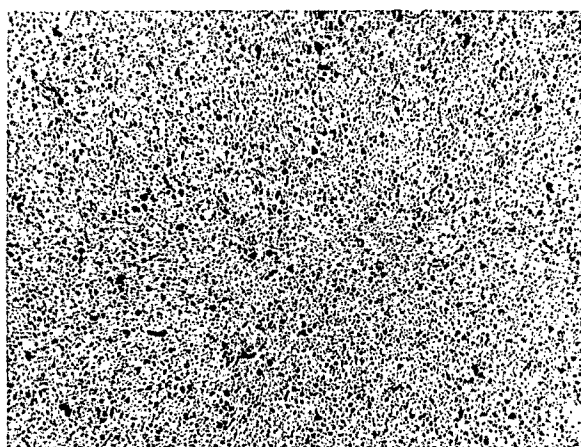


c

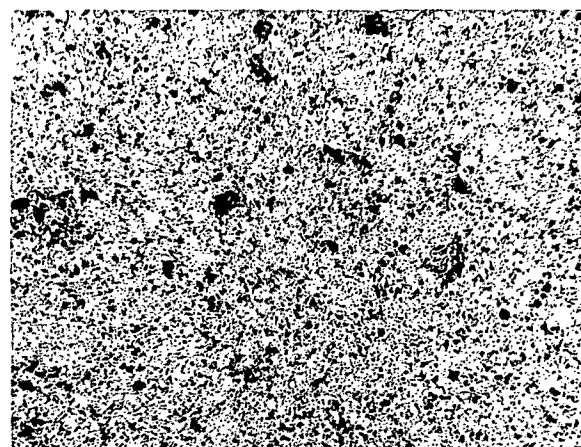
Fig. 4.61 : Optical micrographs for (a) Ag 10 CdO (E), (b) Ag 12 CdO (E) and (c) Ag 15 CdO (E) samples. (100 x)



a

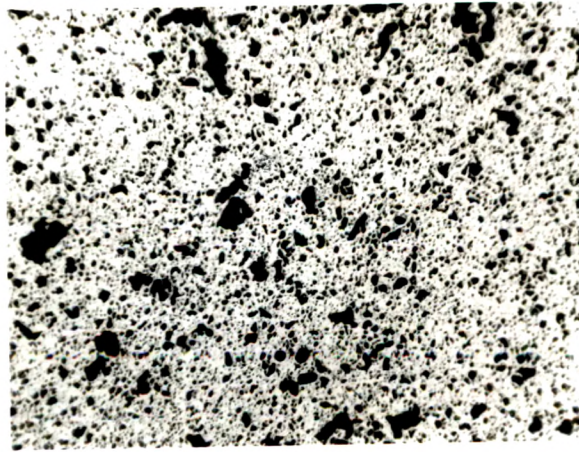


b

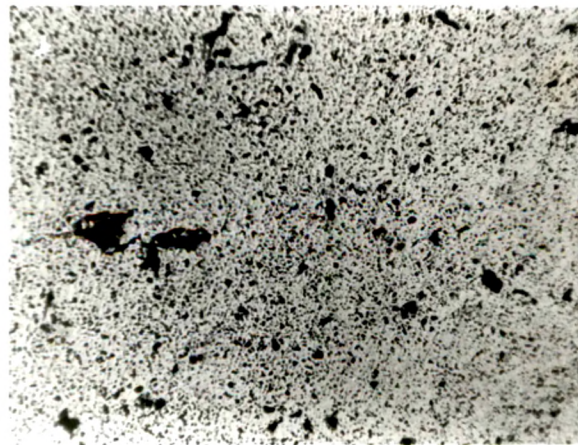


c

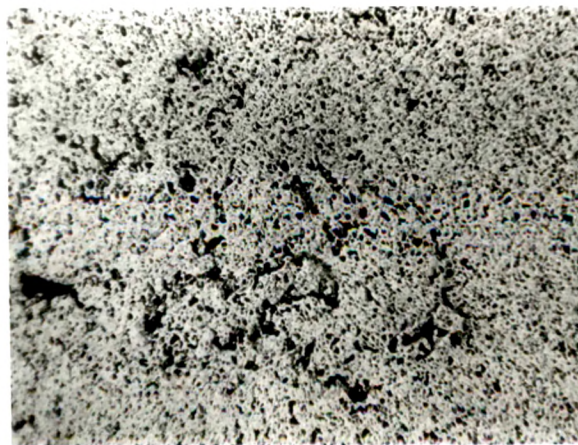
Fig. 4.62 : Optical micrographs for (a) Ag 7.1 ZnO (F), (b) Ag 8.6 ZnO (F) and (c) Ag 10.8 ZnO (F) samples. (100X)



a



b



c

Fig. 4.63 : Optical micrographs for (a) Ag 10 CdO (F), (b) Ag 12 CdO (F) and (c) Ag 15 CdO (F) samples. (100 \times)

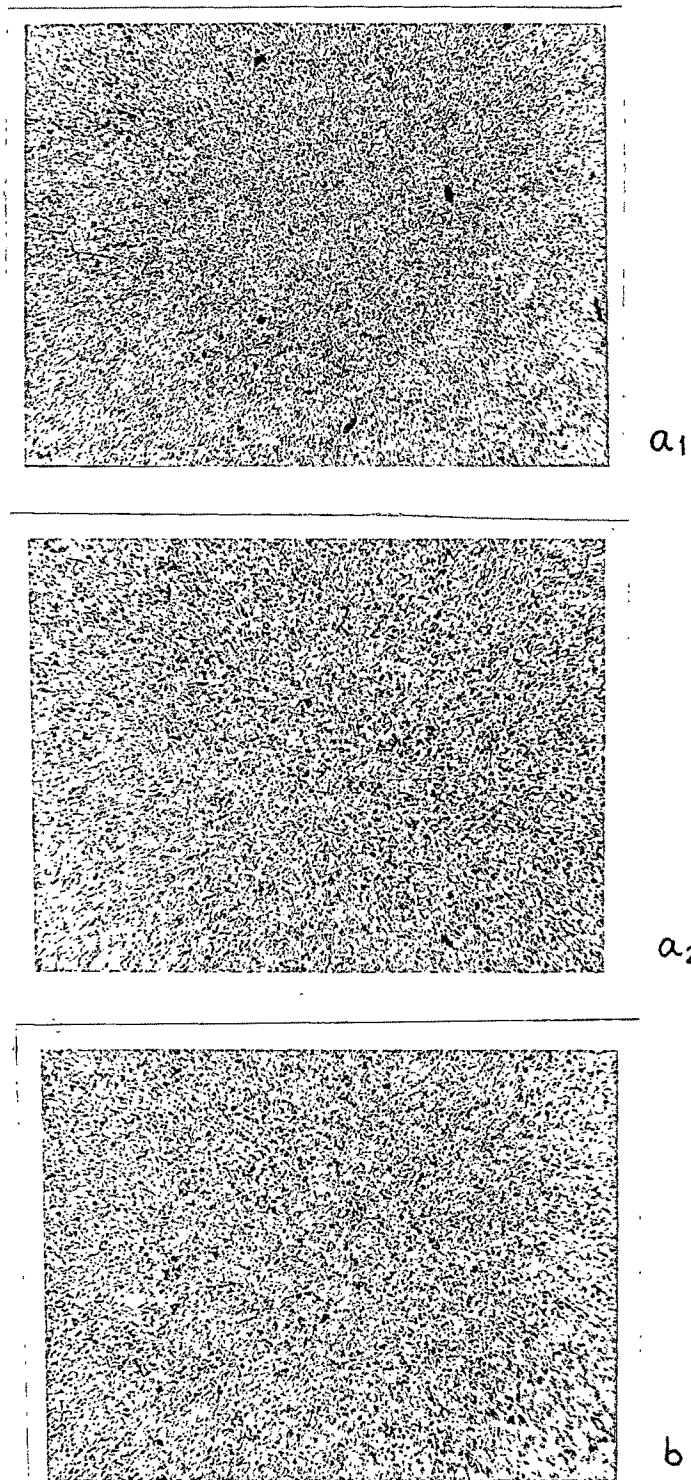


Fig. 4.64 : Optical micrographs for (a) Ag 10.8 ZnO (MA) and (b) Ag 15 CdO (MA) samples. (100 x)

a_1 : condition 1

a_2 : " 2

Large amount of porosity was observed in freeze-dried samples (Fig. 4.62 and Fig. 4.63). Higher porosity in bulk solids of this processing route may be owing to higher microporosity of freeze-dried powders reported earlier during BET specific surface area measurements. As a result of this, freeze-dried samples gave low as-sintered and hot-pressed density, low microhardness and low electrical conductivity compared to other routes.

Fig. 4.64 gives the microstructures for Ag 10.8 ZnO (MA) samples of condition 1 and 2 as well as that of Ag15 CdO (MA). An exceptionally good dispersion of ZnO or CdO in silver-matrix is attained in these samples; once again putting this technique on the forefront of emerging manufacturing processes for Ag-MeO composite contacts.

4.3.2. Quantitative structural evaluation by Image analysis:

Samples prepared for optical microscopy were also subjected to quantitative metallography using Image Analyser. Representative samples of different process routes were subjected to estimations like average area of dispersed oxide-phase particles, average roundness of oxide particles and the feret average. Table 4.14 (a) and 4.14(b) give the values for area fraction computed from these measurements. Table 4.14 (c) and 4.14 (d) give the summary of measurements of average particle roundness and feret average of oxide phase in final hot-pressed compacts of different process routes.

Maximum value of area fraction is obtained in case of compacts processed from mechanically alloyed powders indicative of the best oxide dispersion. Compacts of blending route offered low values because of highly heterogeneous microstructures of these samples as regards the dispersivity of their oxide phase. Very low values of area fraction for compacts of freeze-drying route are in view of their higher porosity levels.

It is worth mentioning here that as per literature [140,141] the area fraction, A_A , the linear fraction L_L , and the point fraction P_p , are equal to each other and to volume fraction V_V .

Maximum roundness for oxide phase is observed for compacts of electroless coating route. The particle roundness depends on particle size : particles tend to sphericity with increasing fineness : and hence for finely dispersed oxide phase, the particle roundness is maximum. The compacts of blending route offered lowest roundness because of coarse and nonequiaxed nature of their dispersed oxide phase.

Table 4.14 (a) Data on area fraction estimation for Ag-ZnO systems

Parameters	Process routes					
	B	C	E	F	MA 1	MA 2
a) Avg area of oxide in mic^2	7 382	1 895	1 127	1 165	1 384	1.309
b) Std deviation	6.757	1 987	1 368	1.229	2 475	2.005
c) No of features accepted in mic^2	405	862	812	1231	2393	1284
e) Total area of features (a x c) in mic^2	30,952 97	7719 05	7719 05	15,438 11	15,438 11	7719 05
f) Area fraction as % [e/d]	2,989 71	1633 49	915.12	1434 12	3311.96	1680 76
	9 66	21.16	11 86	9 29	21 45	21 77

The value of feret average is maximum for compacts of blending route reflecting the coarseness and very high degree of shape anisotropy of oxide phase in these samples. The results for electroless coating, freeze-drying and MA powders are more or less comparable, giving by and large near to equiaxed particle shapes alongwith fine particle size. For an easy interpretation above results are also shown in the form of histograms in Fig. 4.65 to Fig. 4.70.

Table 4.14 (b) : Data on area fraction estimation for Ag-CdO systems

Parameters	Process routes				
	B	C	E	F	MA
a) Avg area of oxide in mic^2	6 758	2 930	1 633	1 228	1.677
b) Std deviation	5 447	4.434	3.343	1.007	2.528
c) No of features accepted	1012	791	768	656	759
d) Total area surveyed in mic^2	61,905.95	15,438.11	7719.05	7719.05	7719.05
e) Total area of features (a x c) in mic^2	6,839.10	2317 63	1254 14	805.57	1272.84
f) Area fraction as % [e/d]	11.05	15.01	16 25	10.44	16.49

Table 4.14 (c) : Data on roundness factor and feret average for different process routes for Ag-ZnO system

Parameters	Process routes					
	B	C	E	F	MA 1	MA 2
(a) Average roundness	72.651	76.110	80.070	78.698	78.558	77.596
(b) Standard deviation	17 246	17 524	14 019	15.470	14.680	16 148
(c) Average feret in mic.	3.531	1.725	1.225	1.266	1.294	1.282
(d) Standard deviation	2.045	1 037	0.713	0 768	0.983	0 924

Table 4.14 (d) : Data on roundness factor and feret average for different process routes for Ag-CdO system

Parameters	Process routes				
	B	C	E	F	MA
(a) Average roundness	72.205	75 645	81.775	81 108	79.960
(b) Standard deviation	15 917	17.097	14.223	13.416	14.563
(c) Average feret in mic	3.279	1.999	1.365	1.306	1.427
(d) Standard deviation	1 548	1.558	1 104	0 640	1.039

In general findings of image analysis offer a close conformance with the measurements for other properties like optical microscopic features, microhardness, apparent density of powders & SEM powder characteristics. Occasional discrepancies amongst the results

- B - Blending route
- C - Coprecipitation route
- E - Electroless coating route
- F - Freeze-drying route
- MA - Mechanical alloying route

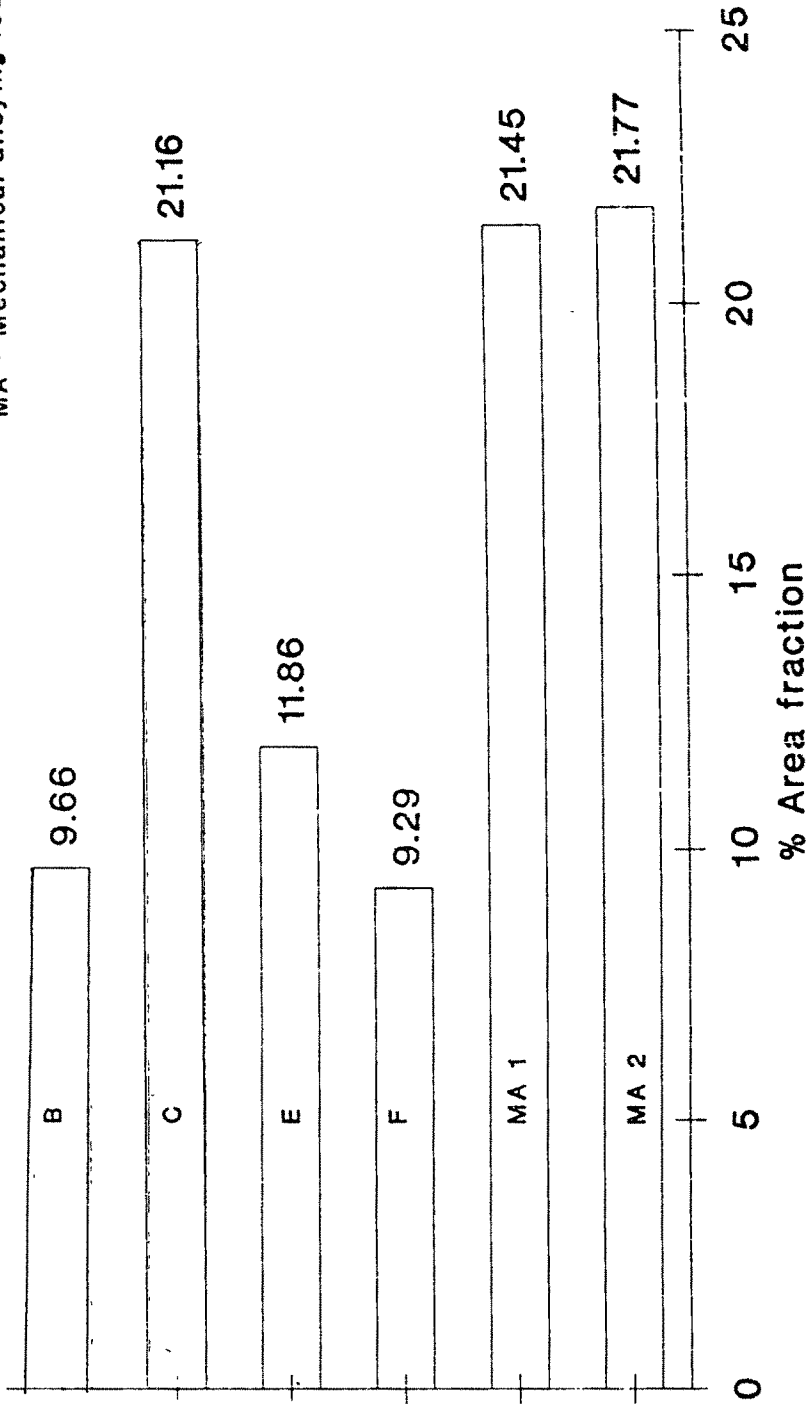


Fig.4.65 : Histograms showing % area fraction for ZnO for different process routes

- B - Blending route
- C - Coprecipitation route
- E - Electroless coating route
- F - Freeze-drying route
- MA - Mechanical alloying route

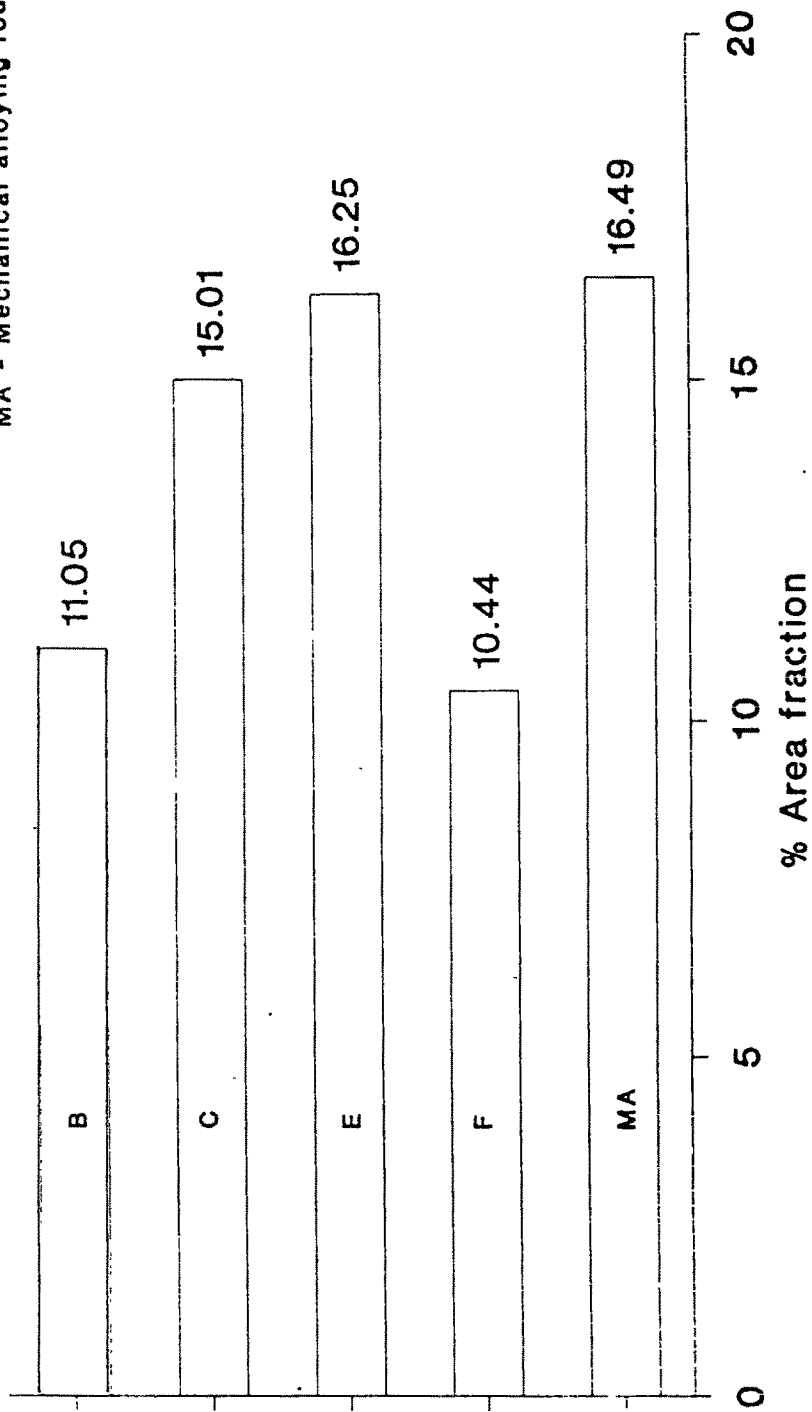


Fig.4.66 : Histograms showing % area fraction for CdO for different process routes

- B - Blending route
- C - Coprecipitation route
- E - Electroless coating route
- F - Freeze-drying route
- MA - Mechanical alloying route

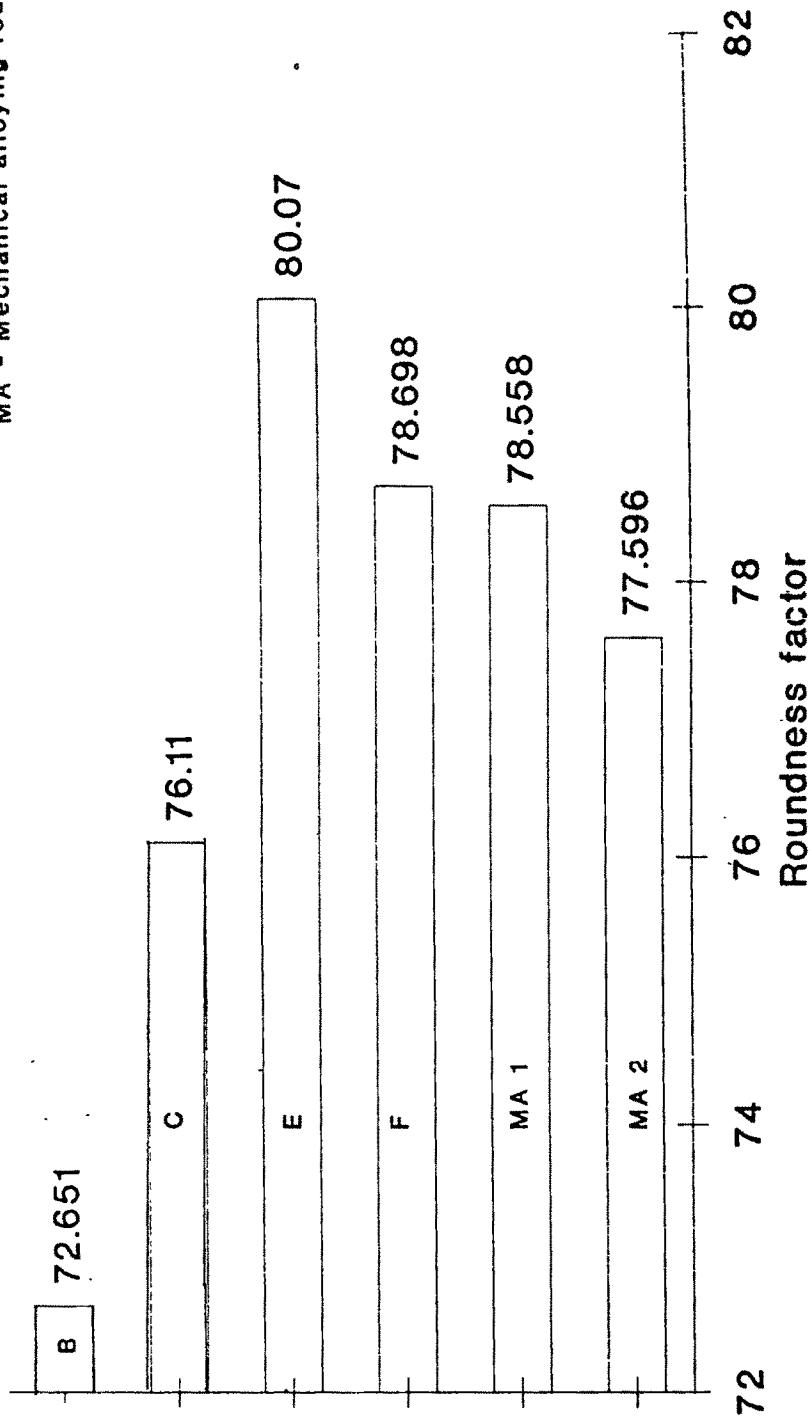


Fig.4.67 : Histograms showing roundness factor for ZnO phase for different process routes

- B - Blending route
- C - Coprecipitation route
- E - Electroless coating route
- F - Freeze-drying route
- MA - Mechanical alloying route

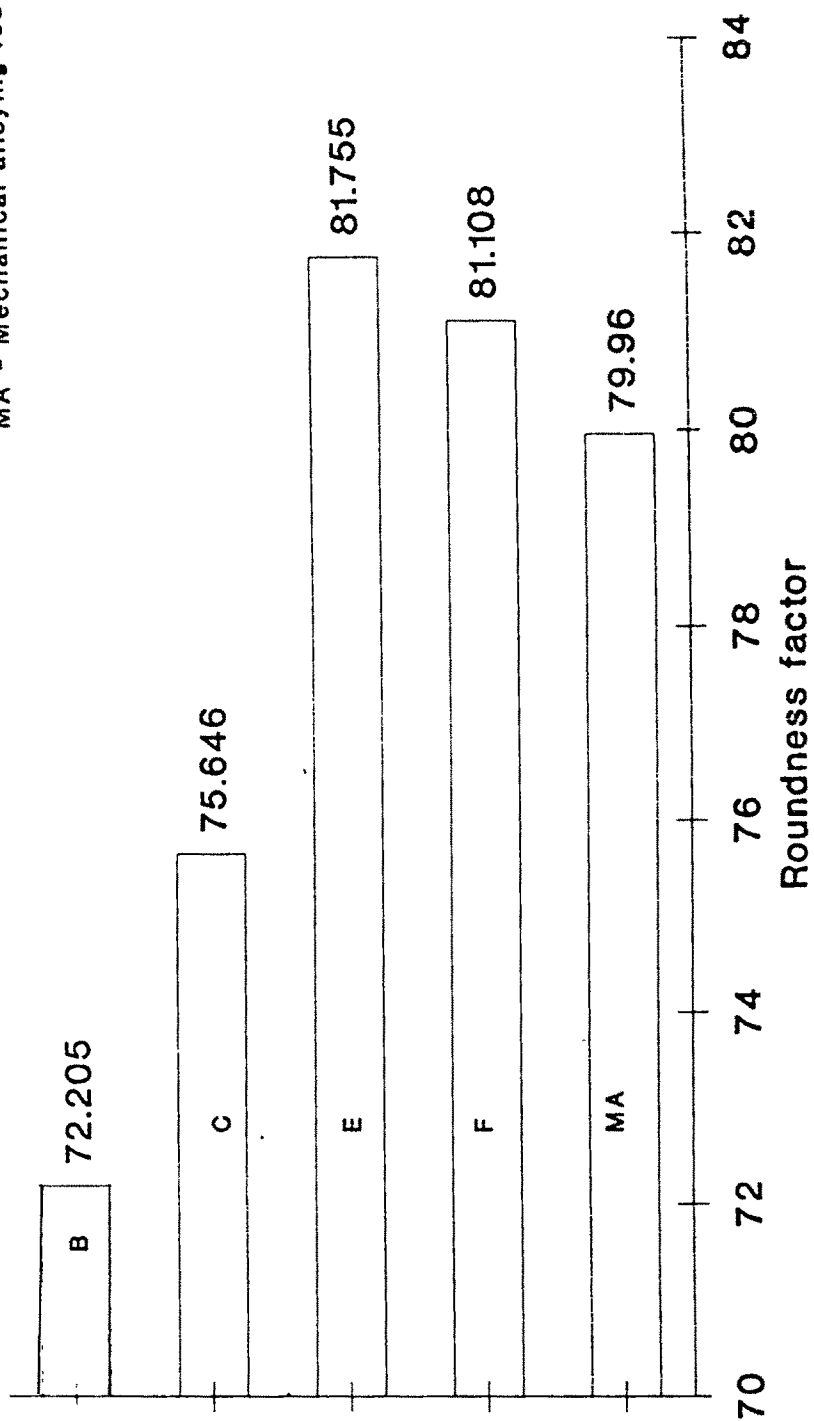


Fig.4.68 : Histograms showing roundness factor for CdO phase for different process routes

- B - Blending route
- C - Coprecipitation route
- E - Electroless coating route
- F - Freeze-drying route
- MA - Mechanical alloying route

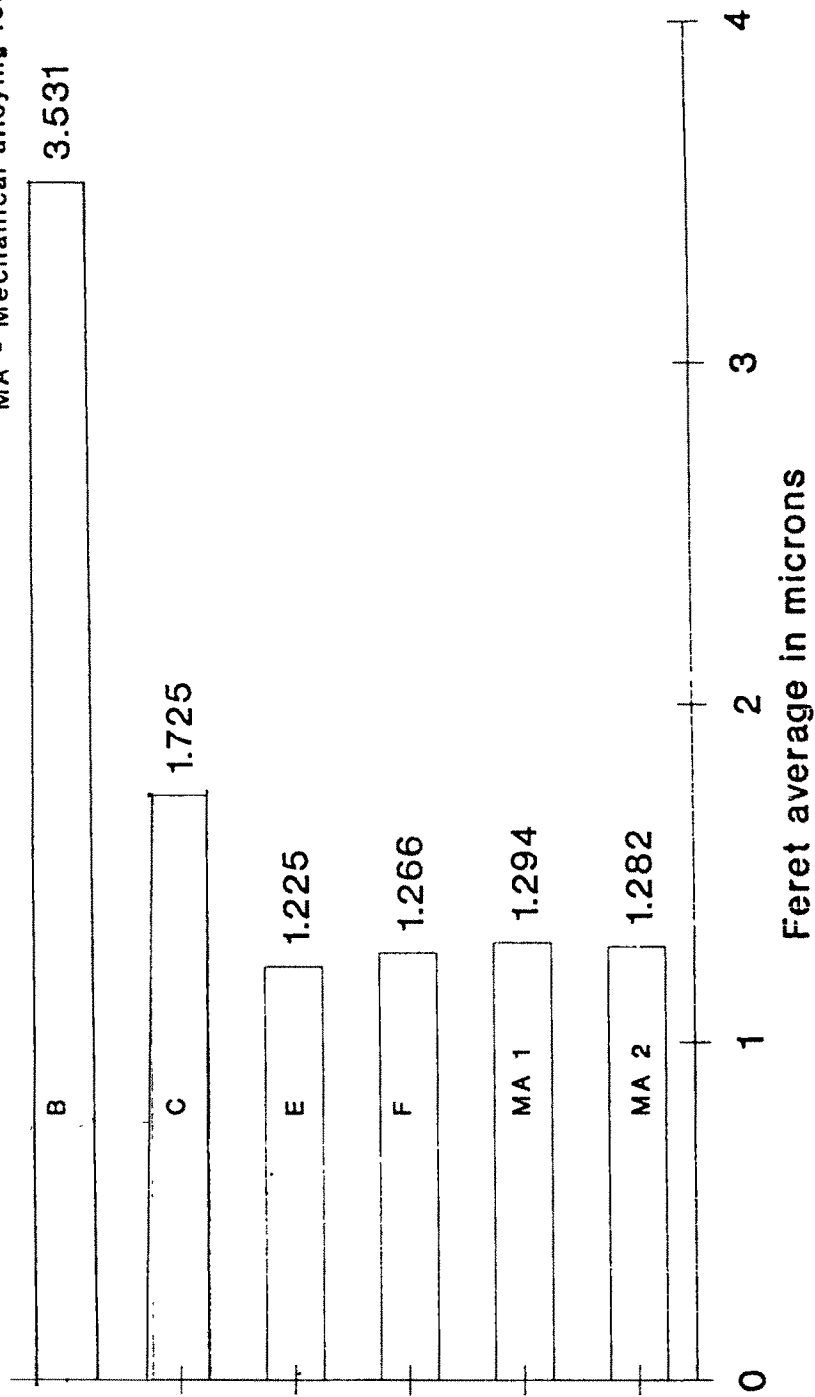


Fig.4.69 : Histograms showing feret average for ZnO particles for different process routes

- B - Blending route
- C - Coprecipitation route
- E - Electroless coating route
- F - Freeze-drying route
- MA - Mechanical alloying route

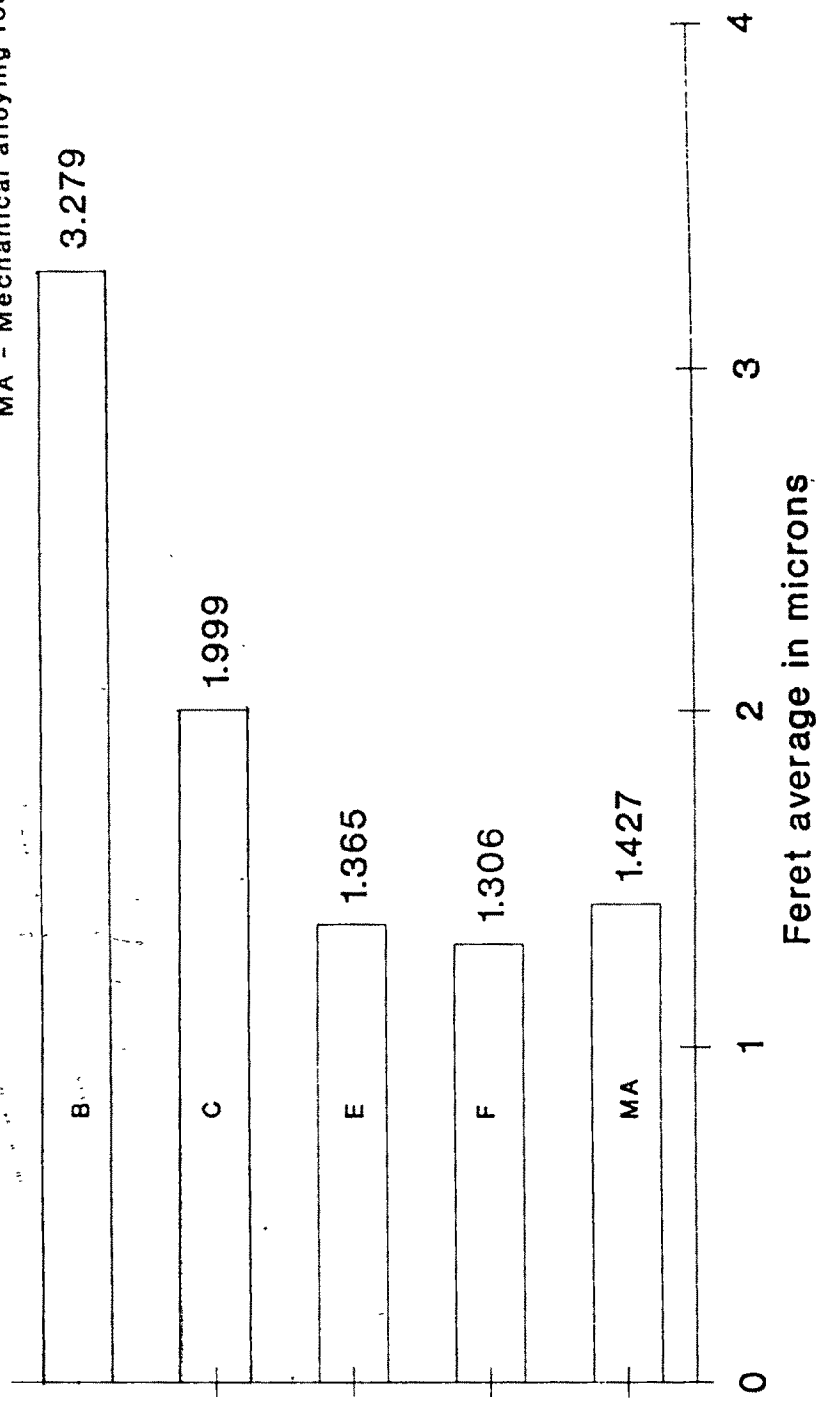


Fig.4.70 : Histograms showing feret average for CdO particles for different process routes

of measured values of image analysis may be attributed to limitations imposed by its measurement steps such as image dilation, image stretching & erosion, setting up of acceptance limits for a feature under study, etc.

4.4 : Effect of Lithium addition on properties of Ag-ZnO system :

The AAS measurements indicated 0.05, 0.09 and 0.096 wt% Li as against the addition of 0.5 wt%, 1.0 wt% and 2 wt% of LiNO_3 to coprecipitated Ag 10.8 ZnO powder samples.

Fig. 4.71 shows the multiple plots for percentage undersize versus particle size in microns for Li-treated and Li-free Ag-ZnO powders. It is evident from these graphs that Li-additions give finer particle size and size distribution. Methanol was used as the carrier liquid during LiNO_3 additions to Ag-ZnO powders. Methanol having less tendency to hydrogen bonding than water, leads to deagglomeration of Li-doped Ag ZnO composite powder particles and hence gives fine particle size distribution to Li-treated samples.

Fig. 4.72 shows XPS survey spectra for Li-treated Ag-ZnO powder sample. The ESCA studies showed that Li-addition improves silver dispersion on zinc oxide surfaces. The surface charging was found to be more for Li-treated samples offering more conductivity to these samples. It was also found from XPS data that the Li-addition results in growth of both silver and zinc. However, the relative growth of zinc particles was greater than that of silver particles for same Li content.

Table 4.15 summarizes the test results for measurement of density, microhardness and electrical conductivity for Li-free and Li-treated Ag-ZnO compacts.

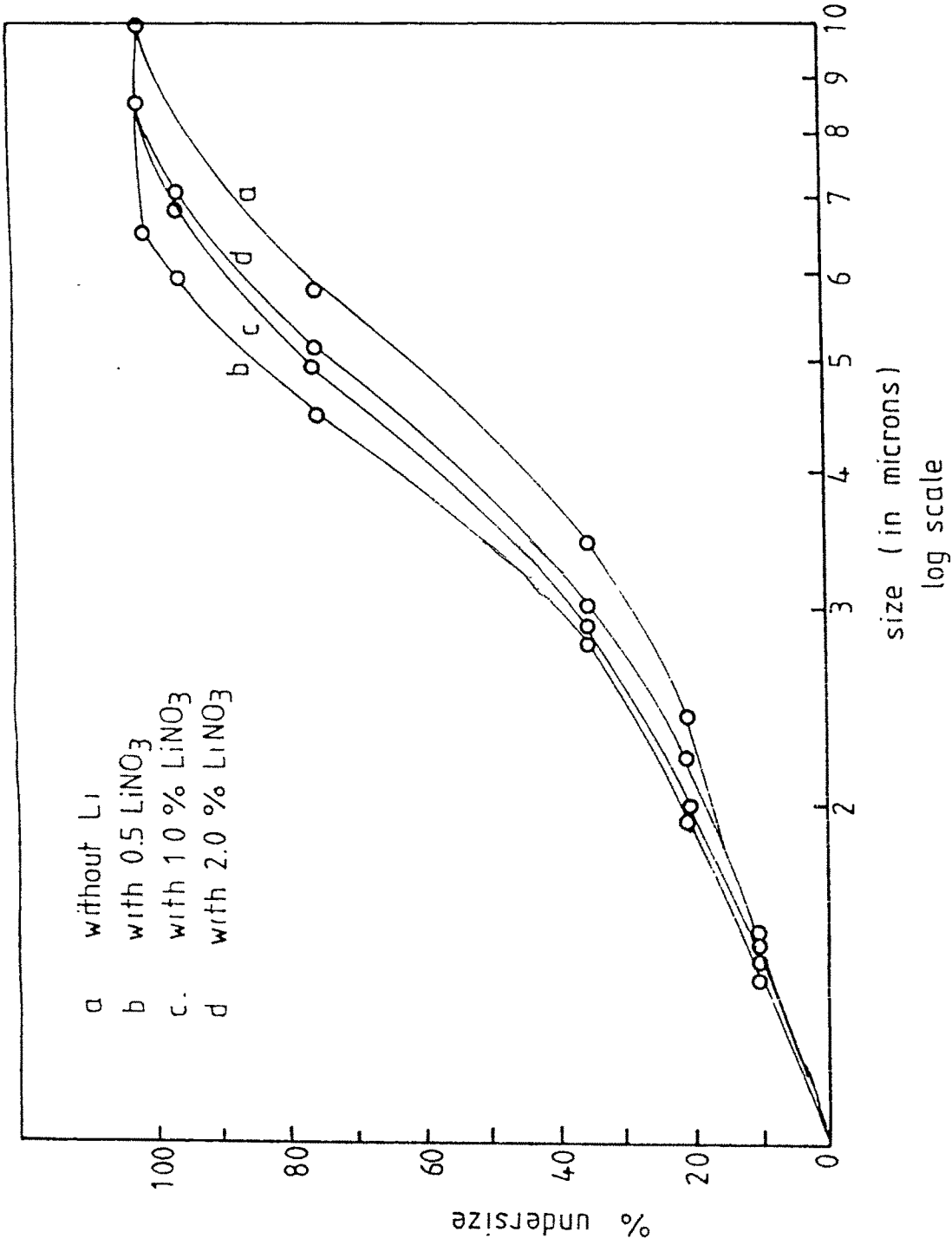


Fig. 4-7: Percentage undersize versus particle size in microns for Ag-ZnO powder samples

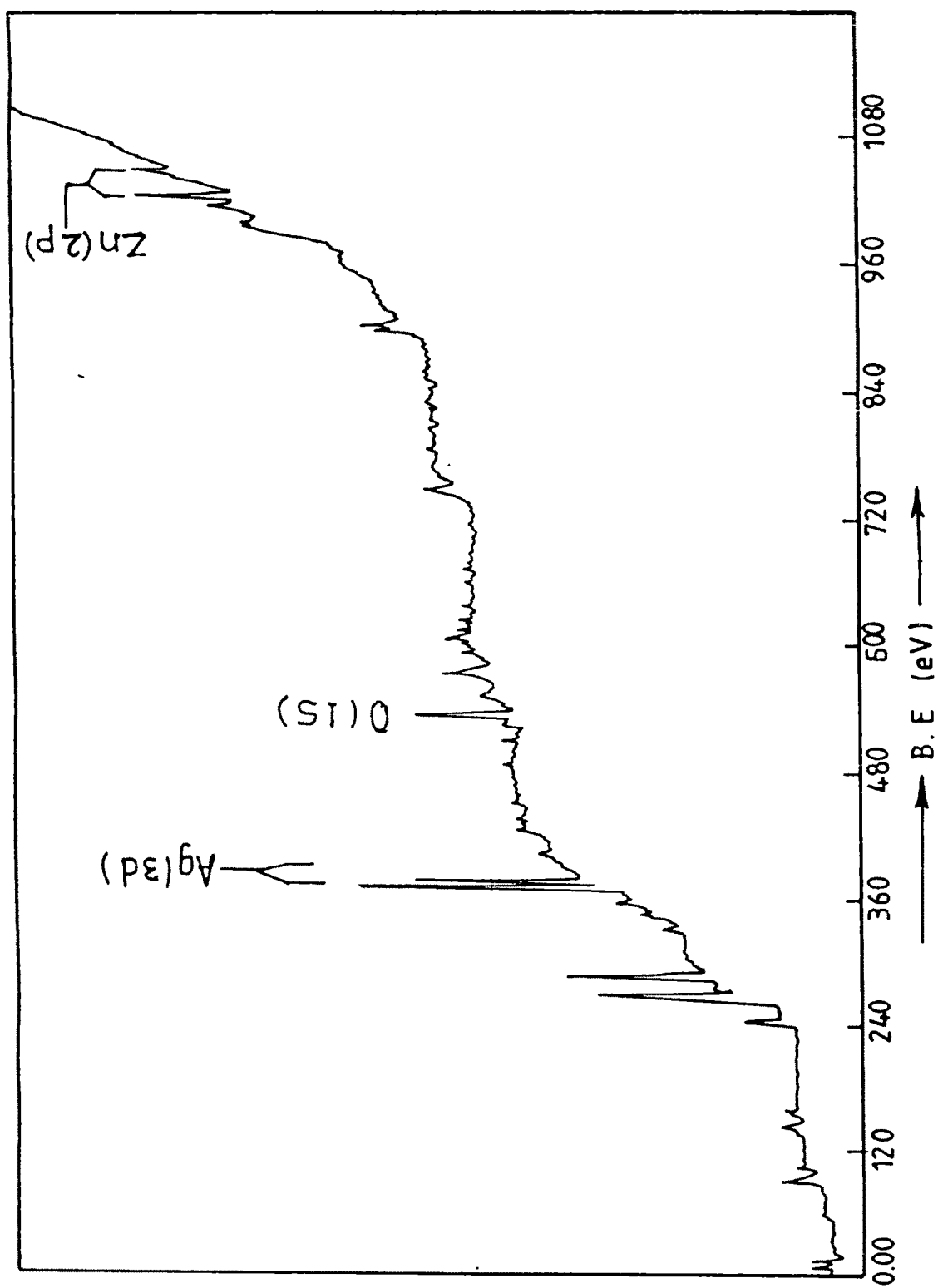


Fig. 4.72 ESCA profile for Ag 10.8ZnO, Li treated powder sample.

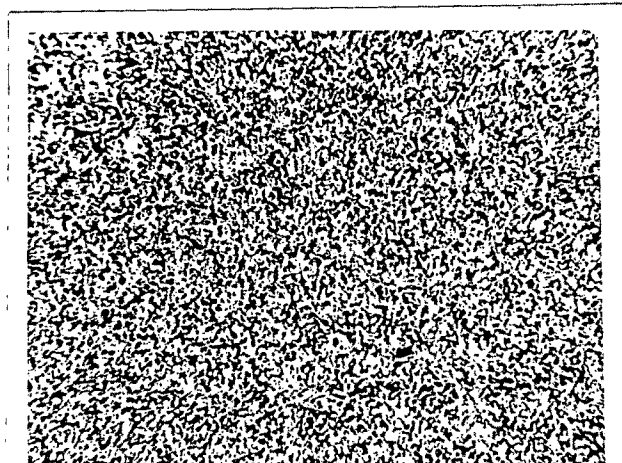
Table 4.15 : Summary of test results for Li-activation studies

Property evaluated	Li as wt% LiNO ₃			
	0.0	0.5	1.0	2.0
Green density (as % T. D.)	49.7	49.7	52.6	52.3
Sintered density (as % T. D.)	66.0	85.2	94.3	87.0
Hot-pressed density (as % T. D.)	98.7	98.4	99.2	98.5
Hardness in kg/mm ²	97.0	97.0	97.0	97.0
Elect. conductivity in % IACS	85	84	87	82

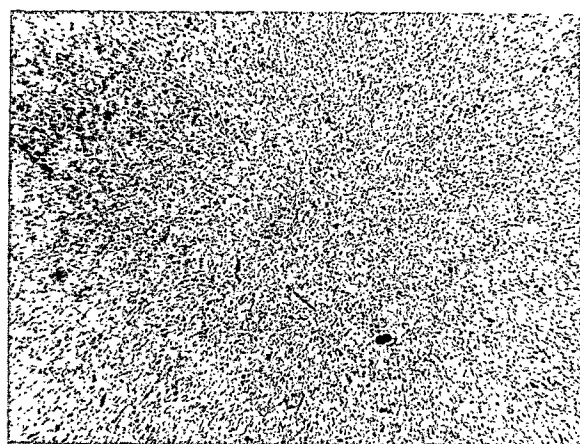
From Table 4.15 it is clear that the Lithium accounts for greater as-sintered density of Li-doped Ag-ZnO compact with max. density achieved at 1% LiNO₃ addition. Role of Lithium may be explained as under.

LiNO₃ during the heating of Ag-ZnO-LiNO₃ green compact decomposes to Li₂O which is expected to react with ZnO forming Li₄ZnO₃ phase. The Li₄ZnO₃ phase formed on heating from 650°C to sintering temperature of 930°C, is supposed to have undergone melting due to its low m.p., imparting the benefits of liquid-phase sintering to Ag-ZnO compact and hence higher as-sintered density.

The XRD analysis of final hot-pressed compacts confirmed the existence of major phases as Ag and ZnO in both Li-free and Li-treated samples. Fig. 4.73 shows the optical micrographs for both Li-free and Li-treated Ag-ZnO hot-pressed compacts. These photographs display finer dispersion of oxide phase in silver matrix for Li-treated sample.



a



b

Fig. 4.73 : Optical micrographs for Ag 10.8 ZnO final hot-pressed compacts
(a) without Li addition and
(b) with 1% LiNO_3 addition.

(100x)

Morphological investigations for dispersed ZnO phase in both Li-treated and Li-free samples, showed greater average roundness count for Li-treated sample. (average roundness of 77.086 for Li-treated sample compared to 72.896 for Li-free sample). The study also gave less feret average for Li-treated sample(2.754 microns) compared to Li-free sample(3.046 microns) conforming to the optical micrograph for Li-treated sample(as shown in Fig. 4.73(b)).

From these preliminary studies, it is clear that Li-addition to Ag-ZnO system offers similar advantages to those for lithium doped Ag-CdO in respect of activation behaviour.

4.5 : Electrical performance evaluation of contacts :

Electrical performance evaluation was done by installing the contact tips developed by different process routes on a commercial contactor of 32 A capacity. No performance evaluation was done on a single-pair test installation (shown in photograph of fig. 3.10) in view of long time periods involved in evaluating atleast 3 pairs for each composition. Not only this, testing on a device like contactor, simulates the actual industrial conditions of performance.

4.5.1 : Performance evaluation of Ag 7.1 ZnO and Ag 10 CdO contacts :

These contacts were evaluated for 100×10^3 number of make and break operations on the test rig developed in the laboratory as shown in Fig. 3.14. Table 4.16 gives the results of contact erosion (measured in terms of weight loss), temperature rise of contacts and welding behaviour over 100×10^3 make and break operations. Ag 7.1 ZnO (C), Ag7.1 ZnO (E) and their equivalent Ag 10 CdO (B) were subjected to evaluation at 10A/230V/cos ϕ 1.0/1 phase AC.

Table 4.16 (a) clearly shows that the contact erosion is more or less same for these three systems under given set of test-conditions. The values obtained are comparable to those reported in the literature. As per the literature the weight loss for fixed contacts for AgCdO system for 50×10^3 operations has been reported to be around 20 mg [103].

Contact resistance in terms of temperature rise is shown in Table 4.16 (b) for these three systems. As per these results, Ag10 CdO (B) showed greater contact resistance and in turn higher temperature rise (10.4°C after 100×10^3 operations as against 5.7°C and 7.1°C for Ag 7.1 ZnO (C) and Ag7.1 ZnO (E) contacts) under similar test conditions. This is expected to be due to relatively non-uniform erosion of AgCdO contact material than that of AgZnO contacts. As per literature, temperature rise for Ag10CdO contacts for 50 A nominal current is reported to be equal to 5°C [82]. Fig. 4.75 shows the variation of contact resistance in terms of temperature rise with number of make and break operations. Contact resistance and hence temperature rise is initially more and then gradually becomes stable.

Though a somewhat higher erosion tendency is displayed by AgZnO systems as compared to Ag CdO system, the smaller value of temperature rise for AgZnO systems indicates a more uniform contact erosion and hence longer life for AgZnO system than equivalent AgCdO system. Fig. 4.74 shows the variation of contact erosion with number of make and break operations.

Table 4.16 : Electrical performance results for Ag 7.1 ZnO (C), Ag 7.1 ZnO (E) and Ag 10 CdO (B) contacts

(a) Contact erosion as a function of make and break operation

Material	Loss in weight (mg)								
	Initial	12.5×10^3	25.0×10^3	37.5×10^3	50.0×10^3	62.5×10^3	75.0×10^3	87.5×10^3	100×10^3
Ag 7.1 ZnO (C)	0.0	3.3	5.1	8.8	10.8	12.2	14.8	17.0	17.9
Ag 7.1 ZnO (E)	0.0	2.5	4.3	5.8	8.5	11.0	13.9	16.8	18.1
Ag 10 CdO (B)	0.0	3.1	4.7	7.1	9.2	10.5	11.9	12.5	17.4

(b) Temperature rise as a function of make and break operation

Material	Initial	Temp rise at fixed contact (OC)							
		12.5 x 10 ³	25.0 x 10 ³	37.5 x 10 ³	50.0 x 10 ³	62.5 x 10 ³	75.0 x 10 ³	87.5 x 10 ³	100 x 10 ³
Ag 7.1 ZnO (C)	-	10.2	5.7	6.0	4.4	6.3	6.6	6.6	5.7
Ag 7.1 ZnO (E)	-	8.5	8.8	7.0	7.5	7.8	7.2	8.0	7.1
Ag 10 CdO (B)	-	10.2	9.2	13.1	10.6	10.3	10.4	10.0	10.4

(c) Weldability test

Material	No. of make and break	Remarks
Ag 7.1 ZnO (C)	100 x 10 ³	No welding
Ag 7.1 ZnO (E)	-	-
Ag 10 CdO (B)	-	-

4.5.2. : Performance evaluation of Ag 8.6 ZnO contacts :

Ag8.6ZnO (C) and Ag 8.6ZnO (E) contacts were evaluated at the Switchgear laboratory of M/S Jyoti Ltd., Baroda at 30A/415V/cosφ 0.95/3 phase AC.

Table 4.17 and Fig. 4.76-Fig.4.78 show the erosion behaviour, contact resistance and temperature rise for these systems. The weight loss due to arc erosion is more for Ag8.6ZnO systems than that for Ag7.1ZnO systems. This is in view of higher test current and voltage employed in this testing. For a given material, the contact erosion increases with increasing arc energy (governed by the product of applied current and voltage during testing).

The values of contact resistance match well with those reported in the literature [105]. No welding was observed over 100 x 10³ operations even for these systems.

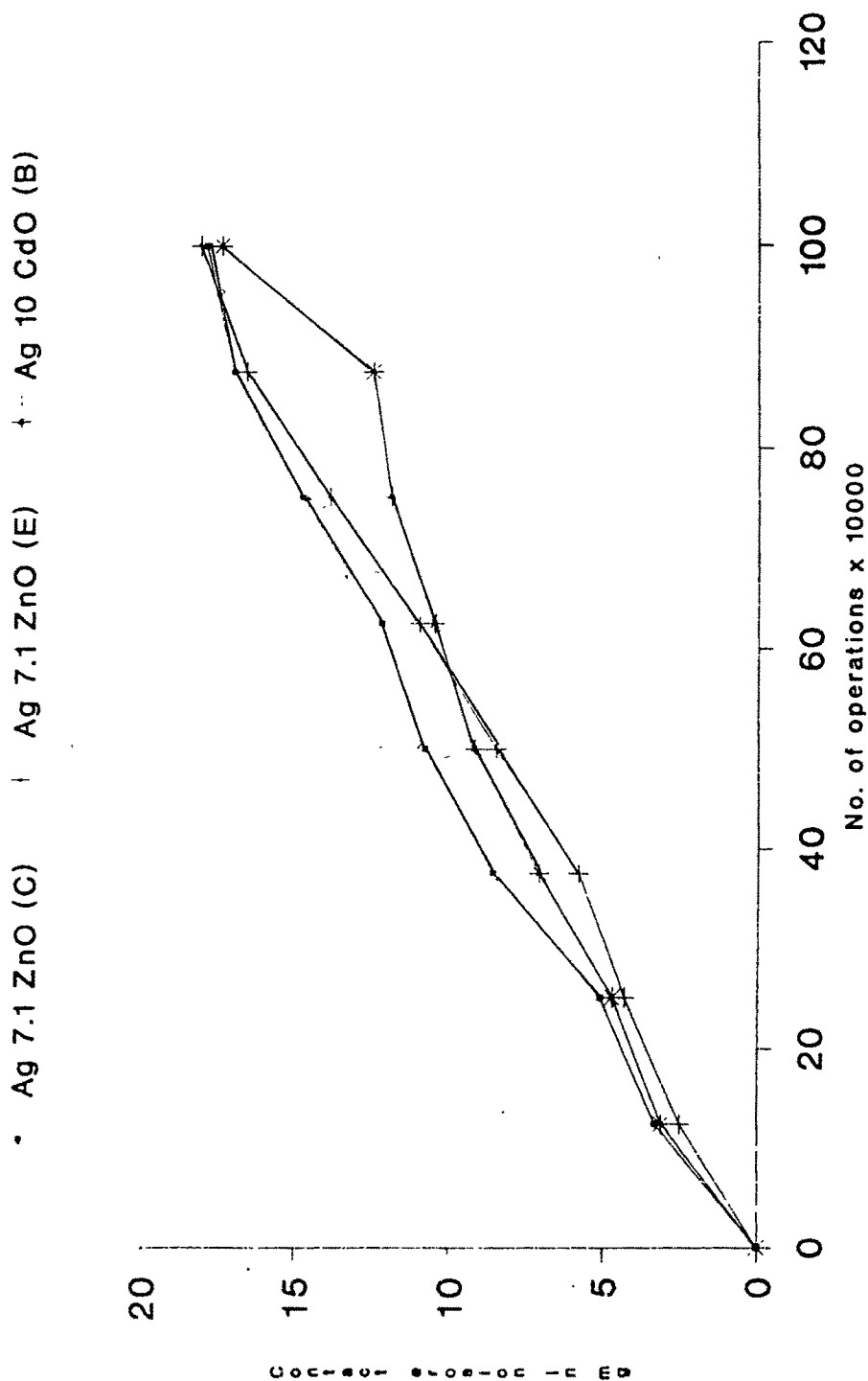


Fig.4.74 : Contact erosion with number of make and break operations for Ag7.1ZnO(C),Ag7.1ZnO(E) & Ag10CdO(B)

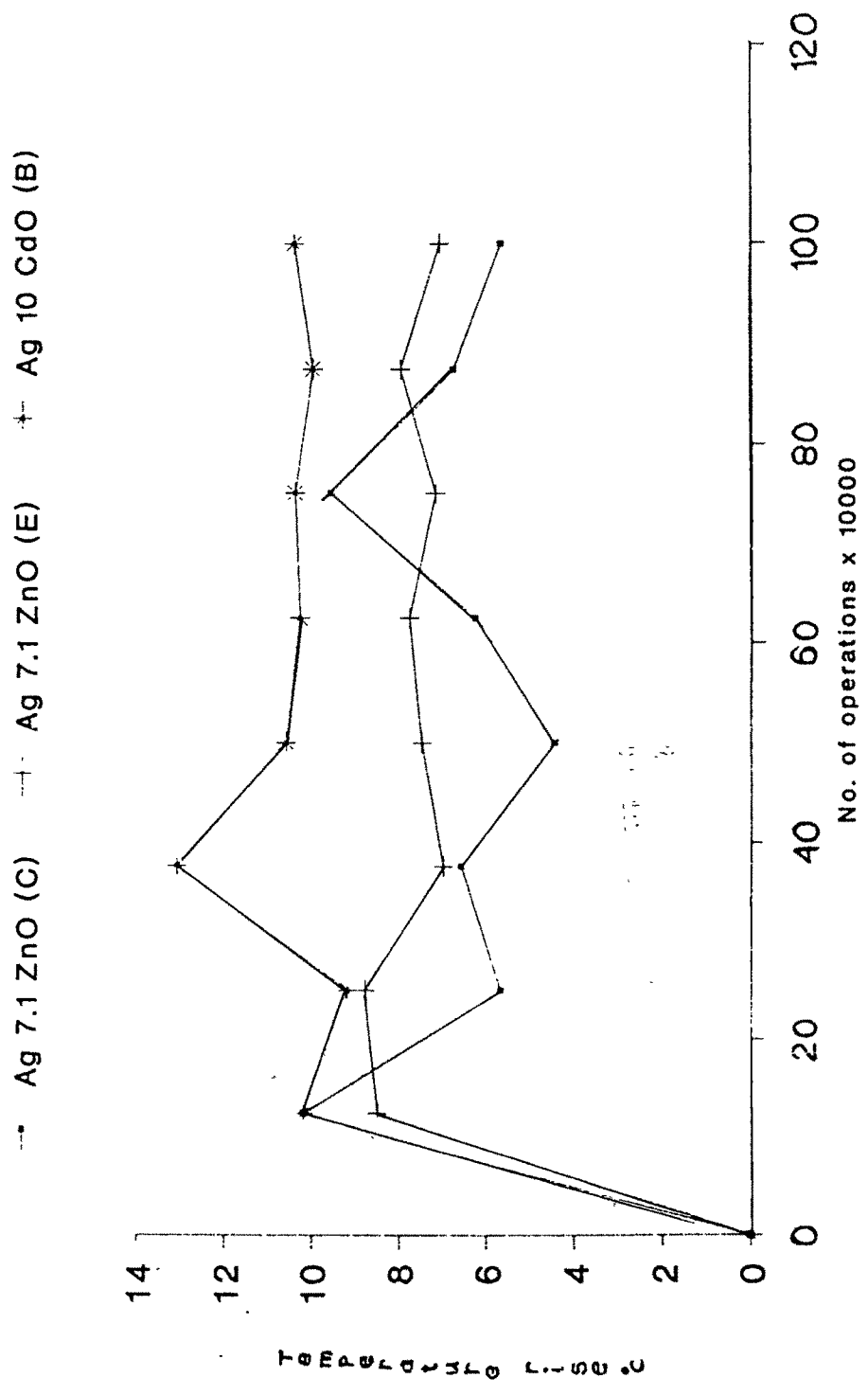


Fig.4.75 : Variation of contact resistance with make & break operations for Ag7.1ZnO(C),Ag7.1ZnO(E) & Ag10CdO(B) (in terms of temp. rise)

Fig. 4.78 gives the temperature rise data for Ag8.6ZnO (C) and Ag8.6ZnO (E) contacts in the form of histograms. The maximum values of temperature rise of 30°C for Ag 8.6 ZnO (C) and 33°C for Ag8.6 ZnO(E) are well within the limits specified by the standards.

Table 4.17 : Electrical performance results for Ag 8.6 ZnO (C) and Ag 8.6 ZnO (E) contacts

(a) Contact erosion as a function of make and break operation

Material	Loss in weight (mg)								
	Initial	12.5 x 10 ³	25.0 x 10 ³	37.5 x 10 ³	50.0 x 10 ³	62.5 x 10 ³	75.0 x 10 ³	87.5 x 10 ³	100 x 10 ³
Ag 8.6 ZnO (C)	0.00	0.15	11.3	12.0	17.0	25.3	29.0	41.3	62.0
Ag 8.6 ZnO (E)	0.00	0.07	11.0	12.7	20.3	31.0	39.0	53.7	73.3

(b) Contact resistance as a function of make and break operation

Material	Contact resistance (m. ohm)					
	Initial	20 x 10 ³	40 x 10 ³	60 x 10 ³	80 x 10 ³	100 x 10 ³
Ag 8.6 ZnO (C)	0.60	1.16	0.74	0.68	0.64	0.64
Ag 8.6 ZnO (E)	0.48	1.23	0.69	0.65	0.70	0.75

(c) Weldability test

Material	No. of make and break	Remarks
Ag 8.6 ZnO (C) Ag 8.6 ZnO (E)	100 x 10 ³ "	No welding "

4.5.3 : Performance evaluation of Ag10.8 ZnO contacts :

Ag10.8 ZnO (C) and Ag10.8 ZnO (E) were evaluated at 15A/230V/cos ϕ 1.0/1phase in AC mode at NML, Jamshedpur. The results of this testing are as per Table 4.18 and Fig. 4.79-4.80. The weight loss due to erosion after 100 x 10³ make and break

• Ag 8.6 ZnO (C) † Ag 8.6 ZnO (E)

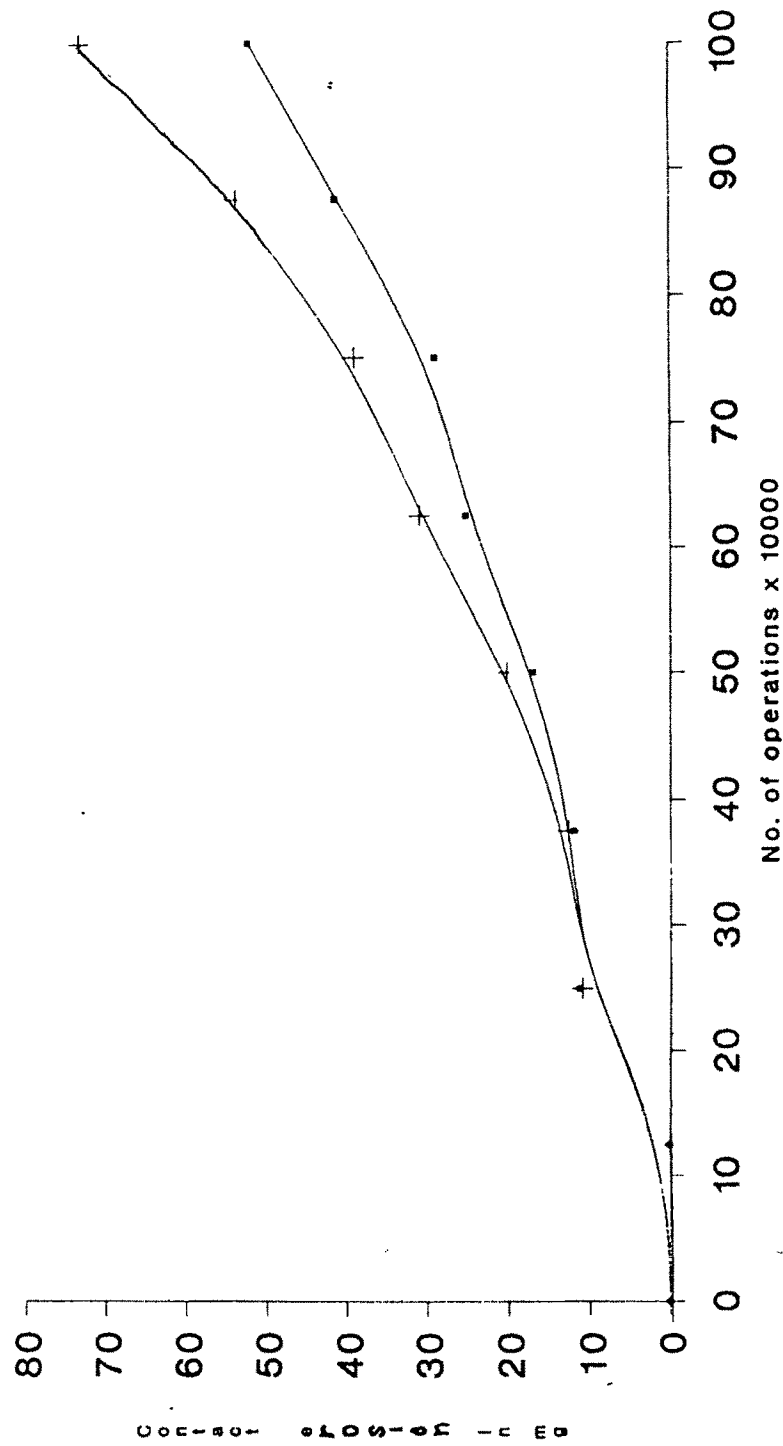


Fig.4.76 : Contact erosion with number of make and break operations for Ag8.6ZnO(C)and Ag8.6ZnO(E)

• Ag 8.6 ZnO (C) | Ag 8.6 ZnO (E)

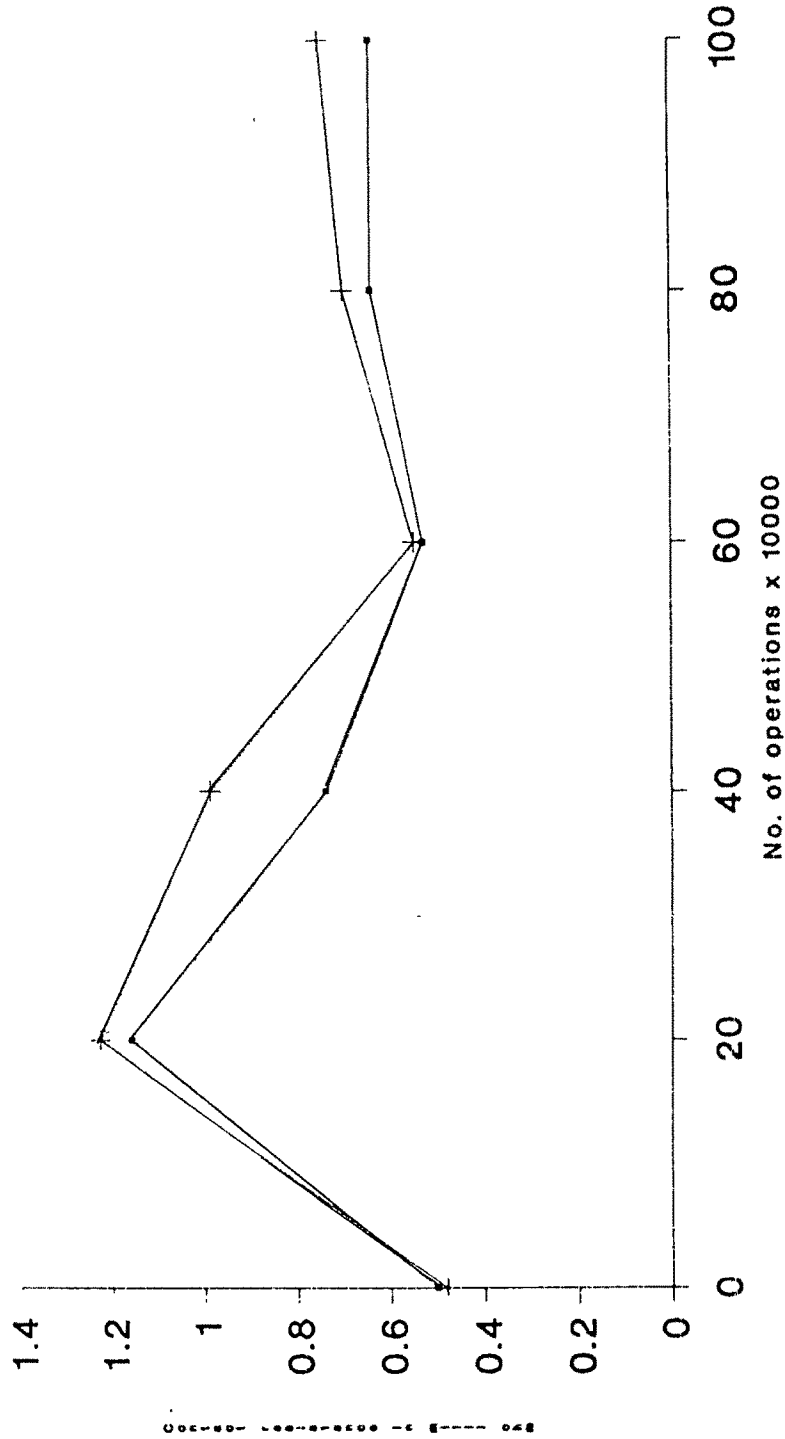


Fig.4.77 : Variation of Contact resistance with number of make & break operations for Ag8.6ZnO(C) and Ag8.6ZnO(E)

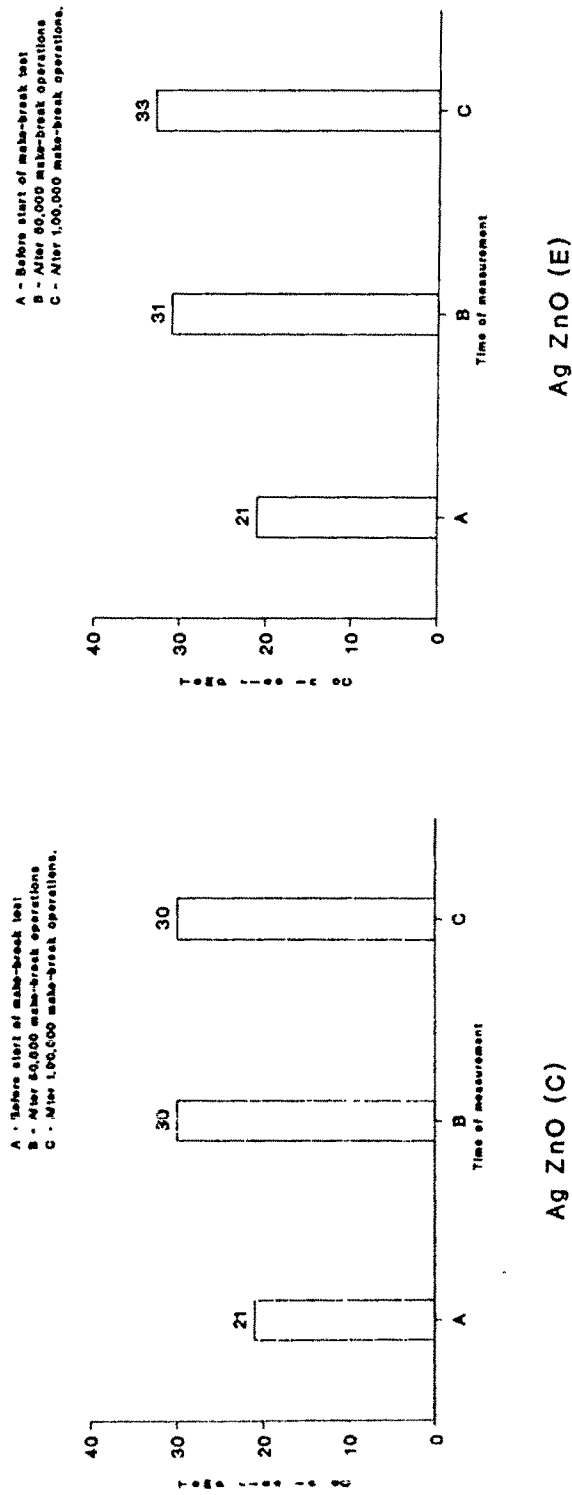


Fig.4.78 : Histograms showing temp. rise for Ag8.6 ZnO(C) and Ag8.6ZnO (E) contacts at different time intervals.

operations was less than 35.0 mg. Relatively higher contact resistance values of 1.31 milli-ohm for Ag 10.8 ZnO (E) and 2.00 milli-ohm for Ag10.8 (C) are in view of greater percentage of dispersed oxide phase. Yet these values are within the acceptable limits.

Table 4.10 : Electrical performance results for Ag 10.8 ZnO (C) and Ag 10.8 ZnO (E) contacts

(a) Contact erosion as a function of make and break operation

Material	Loss in weight (mg)				
	initial	25×10^3	50×10^3	75×10^3	100×10^3
Ag 10.8 ZnO (C)	0.00	6.75	14.80	24.90	32.30
Ag 10.8 ZnO (E)	0.00	3.30	10.70	23.35	34.50

(b) Contact resistance as a function of make and break operation

Material	Contact resistance (m ohm)				
	initial	25×10^3	50×10^3	75×10^3	100×10^3
Ag 10.8 ZnO (C)	0.30	2.93	2.60	3.90	2.00
Ag 10.8 ZnO (E)	0.31	2.10	1.25	3.60	1.31

(c) weldability test

Material	No. of make and break	Remarks
Ag 10.8 ZnO (C) Ag 10.8 ZnO (E)	100×10^3	No welding

4.5.4. : Performance evaluation for Ag10.8 ZnO (MA) contacts :

Ag 10.8 ZnO (MA) contact samples of condition 2 were subjected to electrical performance evaluation as per IEC 947-4-1 for AC-3 utilization category at 30A/415V/cos ϕ 0.45/3 phase AC rating at ERDA, Baroda.

• Ag 10.8ZnO (C) | Ag 10.8ZnO (E)

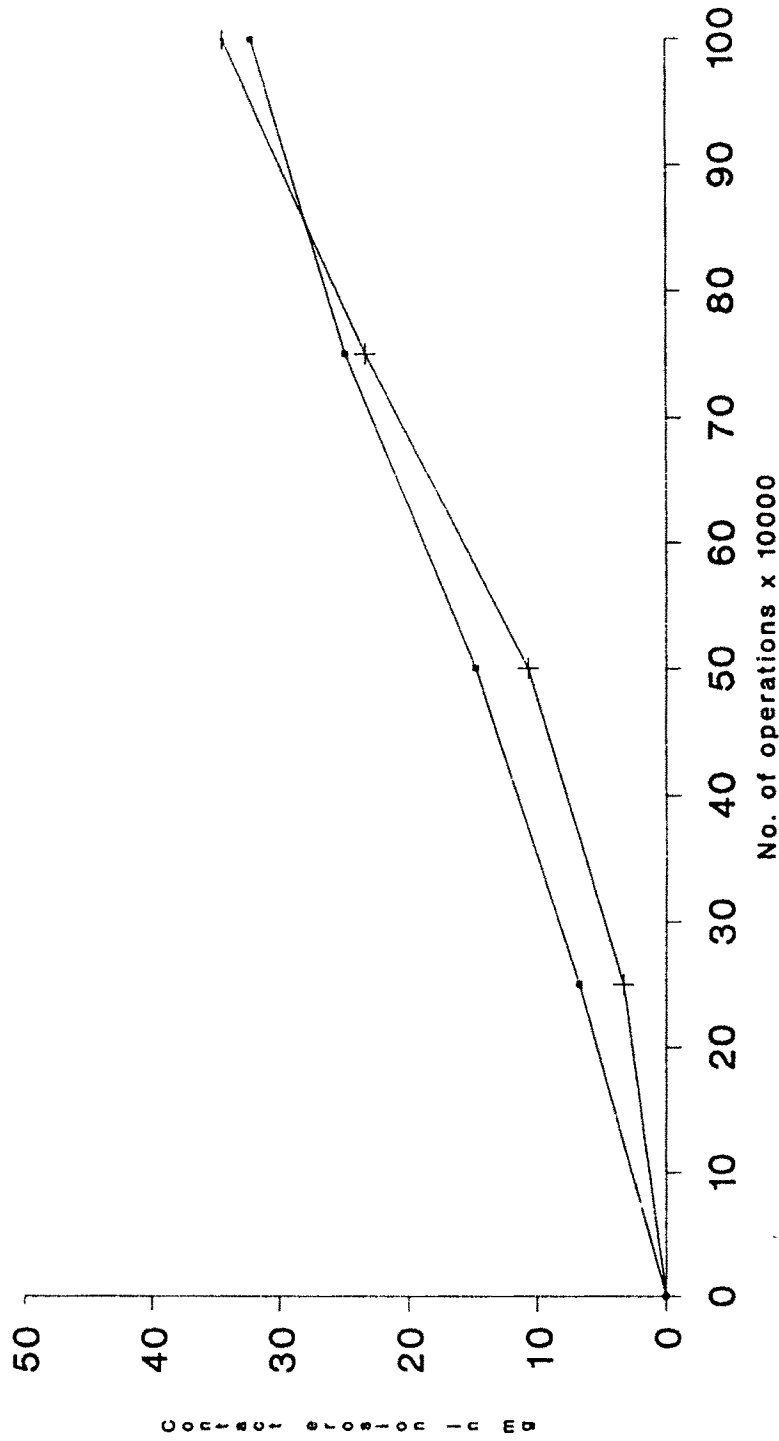


Fig.4.79 : Variation of Contact erosion with number of make & break operations for Ag10.8ZnO(C) & Ag10.8ZnO(E)

• Ag 10.8ZnO (C) | Ag 10.8ZnO (E)

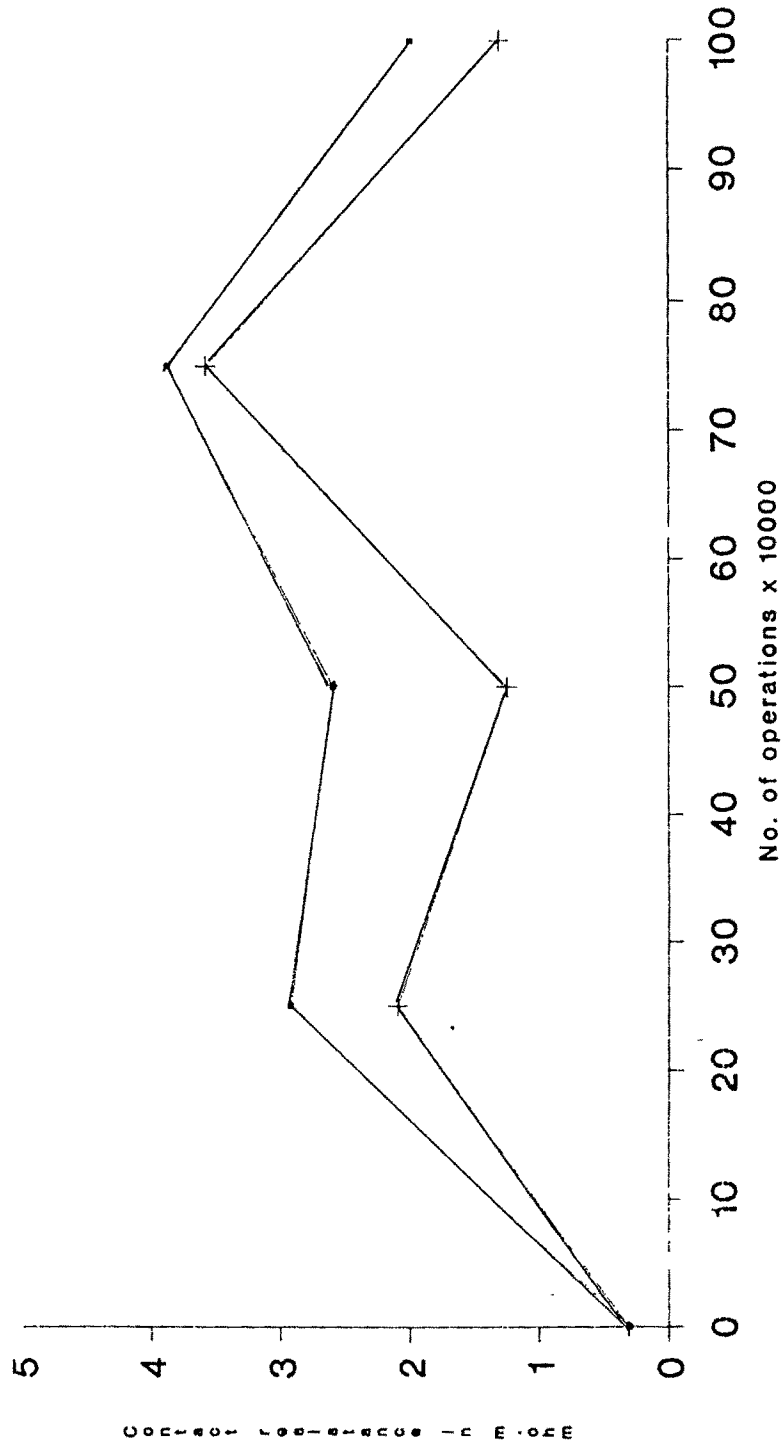


Fig.4.80 : Variation of Contact resistance with number of make & break operations for Ag10.8ZnO(C) & Ag10.8ZnO(E)

Following results were obtained for various tests conducted on ML 2 contactors installed with our Ag_{10.8}ZnO (MA) contact tips.

- (i) Temperature rise of 26.6°C at top terminal and 19.5°C at bottom terminal as against max. permissible value at each terminal equal to 70°C.
- (ii) The contactor (installed with our contact tips) successfully passed through the overload current of 244 A AC for 10 sec.
- (iii) Test contactor successfully withstood the conditions stipulated for both making as well as making and breaking capacity tests with no permanent arcing, no flash over between poles and no welding of contacts etc.
- (iv) During the operational performance test, the test contactor successfully completed 7000 operations under the operating conditions described in section 3.8.3 (iv) for this test.

Finally it may be said that the developed contact tips of Ag 10.8 ZnO (MA) conform to the required quality standards.

4.5.5. : Performance evaluation for Ag_{10.8}ZnO (MA) and Ag₁₅CdO (MA) contacts in DC mode :

DC testing of Ag_{10.8}ZnO (MA) and Ag₁₅CdO (MA) contact samples on a commercial contactor was done at 20A/230V/cosφ 1.0/1 phase using a step-down transformer and bridge-rectifier power supply system.

Erosion in DC mode was found to be much smaller than in AC due to low current-voltage values. In general AgZnO system showed slightly higher erosion and temperature rise than equivalent AgCdO system in DC mode. Table 4.19 and Fig. 4.81 and Fig. 4.82 demonstrate performance of these contacts.

Table 4.19 : Electrical performance results for Ag 10.8 ZnO (MA) and Ag15 CdO (MA) contacts in DC mode

(a) Contact erosion as a function of make and break operation

Material	Loss in weight (mg)					
	initial	1.5×10^3	3.0×10^3	4.5×10^3	6×10^3	7.0×10^3
Ag 10.8 ZnO (MA)	0.00	2.1	2.7	3.3	4.5	5.3
Ag 15 CdO (MA)	0.00	1.1	1.6	2.2	2.5	3.0

(b) Temperature rise as a function of make and break operation

Material	Temperature rise at fixed contact (°C)					
	initial	1.5×10^3	3.0×10^3	4.5×10^3	6×10^3	7.0×10^3
Ag 10.8 ZnO (MA)	0.00	5.52	5.16	6.08	5.72	6.04
Ag 15 CdO (MA)	0.00	5.20	5.84	4.04	3.84	5.05

(c) Weldability test

Material	No. of make and break	Remarks
Ag 10.8 ZnO (MA) Ag 15 CdO (MA)	100×10^3 .	No welding .

From above observations for different material compositions, processing routes and testing conditions it is apparent that the electrical performance of the contact material depends on several factors such as the material of contact; its microstructure in terms of dispersion of oxide phase, type of electrical device used (ie a contactor/relay/switch etc.); operating test parameters like rated current, overload current, applied voltage, power factor, making and breaking force, making and breaking speed, frequency of operation, duration of making current, degree of contact bounce, if any, type of arc-extinction mechanism employed; utilization category etc.

In view of such a high complexity of testing, it is rare to find an exact simile for the findings of this investigation and those reported in the literature. However, by and large the results obtained in this investigation are corroborated by the data reported in the literature by different investigators with few differences here and there.

• Ag 10.8ZnO (MA) + Ag 15CdO (MA)

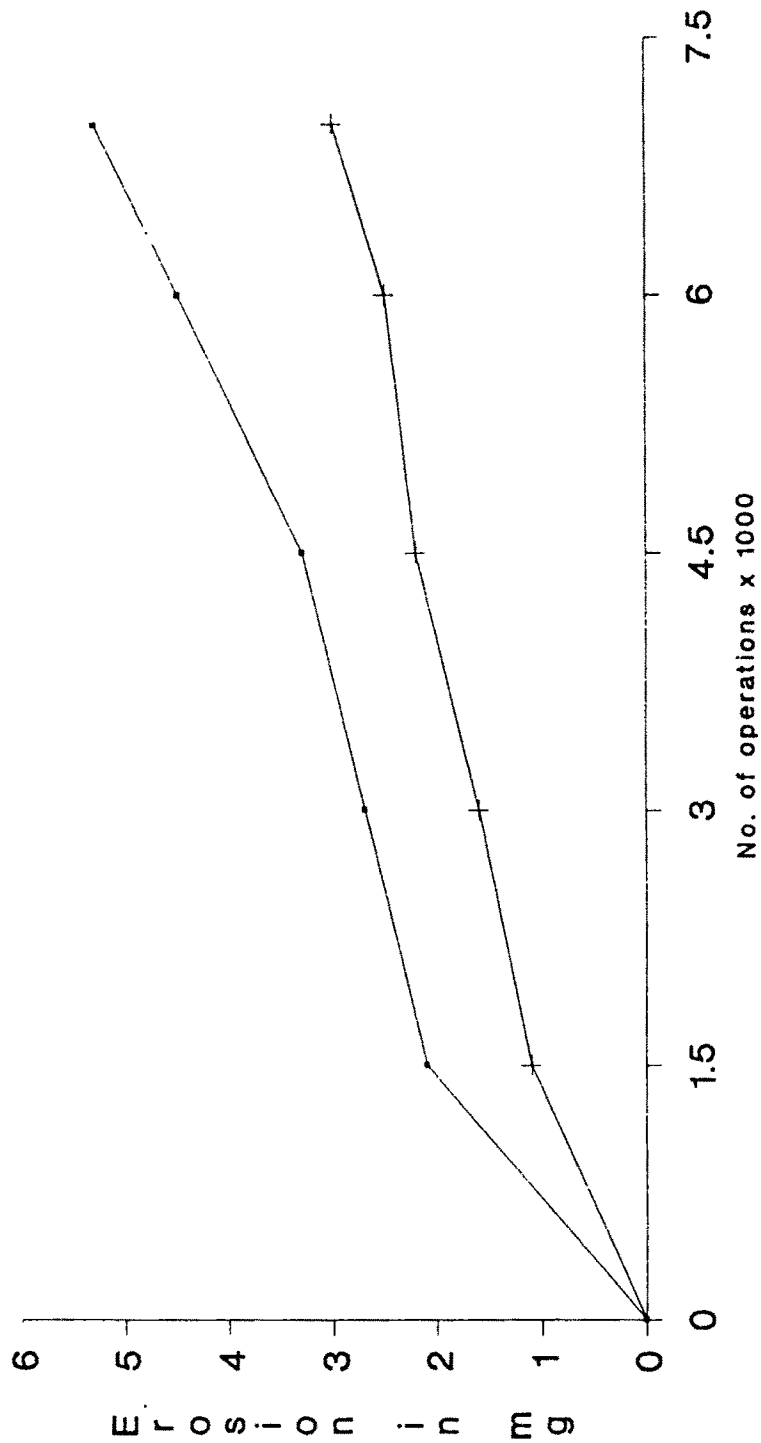


Fig.4.81 : Variation of Contact erosion with number of make & break operations in DC mode for Ag10.8ZnO(MA)&Ag15CdO(MA)

• Ag 10.8ZnO (MA)

+ Ag15CdO (MA)

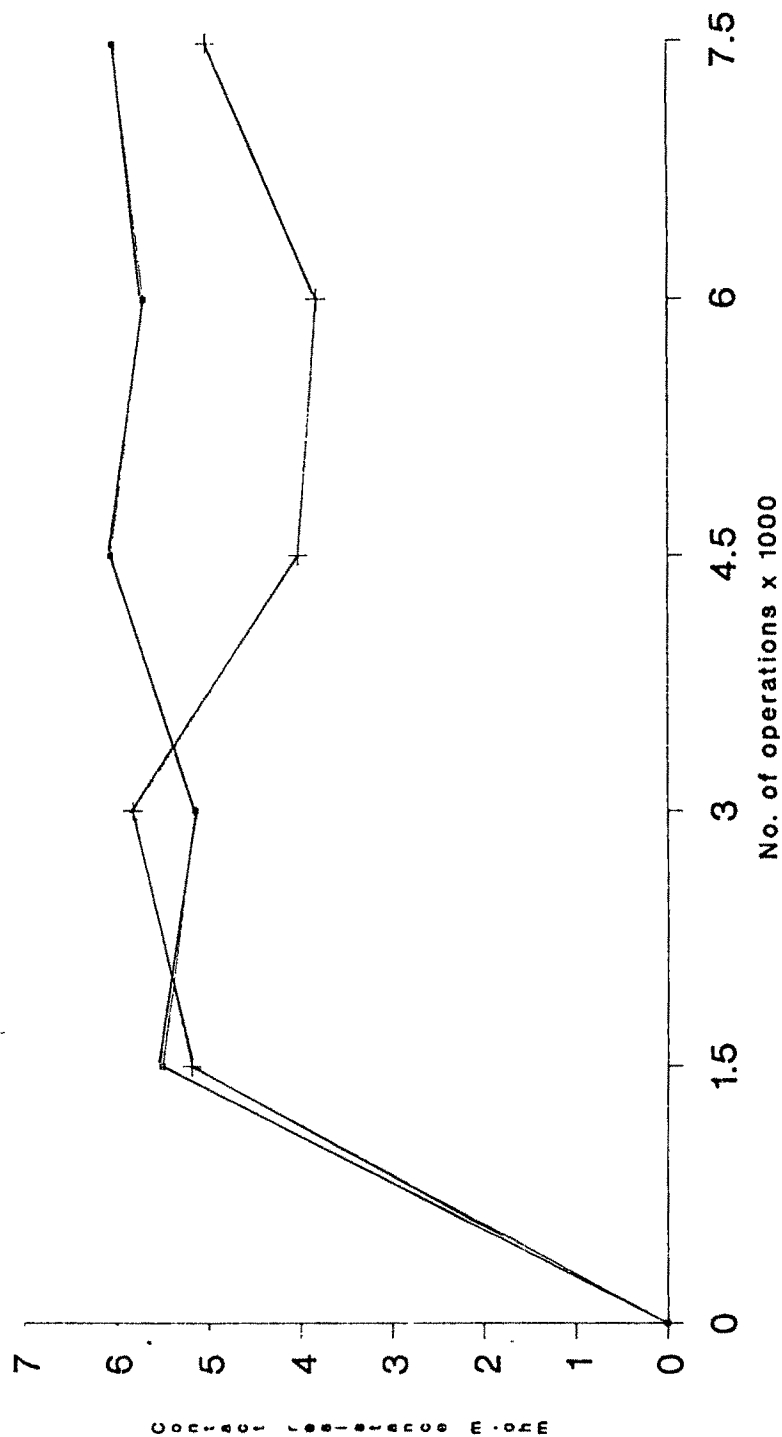


Fig.4.82:Variation of Contact resistance with number of make & break operations in DC mode for Ag10.8ZnO(MA)&Ag15CdO(MA)

The above findings of section 4.1 to section 4.5.5 can be summarized in terms of powder characteristics, the properties of sintered and hot-pressed compacts and the electrical contact performance as under :

(I) Powder characteristics :

It is apparent from the data reported in Table 4.1 (a) and Table 4.1 (b) for atomic absorption spectrometry of Ag-ZnO and Ag-CdO powders of different process routes that it is possible to synthesize Ag-MeO composite powders with controlled amount of trace impurities of Na and K below 50 ppm. Control of alkali metal impurities is essential for better arc erosion resistance and anti-welding properties of contacts.

All the processing routes ensure the production of composite powders having Ag and ZnO or Ag and CdO as the only phases as per their respective XRD profiles (shown in Fig. 4.4 - 4.11)

Tables 4.5 (a) and (b) ; and the histograms shown in Fig. 4.22 (a) to 4.23 (b) clearly display the improved apparent and tap density values for spray-coprecipitated, electroless-coated and the mechanically alloyed Ag-ZnO and Ag-CdO powders. The apparent density for coprecipitated powders was in the range of 1.25 - 1.67 g/cc, that for electroless-coated powders equal to 1.47 - 1.79 g/cc and for mechanically alloyed powders equal to 1.50 - 2.69 g/cc. Similar trend was noticed for tap density also. Tap density for coprecipitated powders varied between 2.27 - 2.77 g/cc, that for electroless coated powders between 2.78 - 3.13 g/cc and for MA powders was equal to 3.13-4.16 g/cc.

Thus mechanically alloyed Ag-ZnO and Ag-CdO powders offered the maximum powder densities.

The particle size analysis for powders of different process routes as per the multiple plots for probability number distribution (Fig. 4.16 – Fig. 4.21) exhibited more or less similar trend for particle size (< 10 microns) and size distribution for powders of different compositions and process routes for Ag-ZnO and Ag-CdO powders.

The coarse granular morphology of MA powders of both Ag-ZnO and Ag-CdO (indicated by SEM micrographs of Fig. 4.37) was suitable for attaining improved packing density. The values for % rise in density on tapping equal to 52.1 % for Ag 10.8 ZnO (MA) powder and 35.3 % for Ag 15 CdO (MA) powder (as per Tables 4.5 (a) and (b) as well as histograms of Fig. 4.24 and 4.25) are indicative of this behaviour.

The value of % rise in density for Ag 10.8 ZnO (MA) powder is superior to those for other process routes whereas that of Ag 15 CdO (MA) compares well with the other process routes. The blending route gave relatively low improvement in density on tapping (with percent rise in density on tapping being only of the order of 28.1 - 37.1 %).

Low apparent density of freeze-dried powders (equal to 0.93 - 1.25 g/cc) and also their low tap density (1.67 - 2.08 g/cc) are attributed to their higher BET surface area (equal to 15.240 m²/g as per Table 4.6) with microporosity as high as 60% as per the analysis of adsorption - desorption isotherms. In turn the low density values are attributed to highly spongy morphology of freeze-dried powders as per SEM micrographs shown in Fig. 4.33 and 4.34.

ESCA studies were done for electroless-coated Ag-ZnO and Ag-CdO powders. Uniform dispersion of silver on ZnO or CdO powder particle surfaces attained by this route is due to higher relative atomic ratios for Ag/Zn and Ag/Cd in composite powders. (equal to 1.30 - 2.33 for Ag/Zn in Ag-ZnO powders and 0.96 - 1.22 for Ag/ Cd in Ag-CdO composite powders as per Table 4.7). Uniform dispersion of silver on oxide phase

particles renders better matrix continuity and thereby improved electrical conductivity (values ranging from 73 to 91 % IACS as per Table 4.7).

Experiments on mechanical alloying of Ag 10.8 ZnO and Ag 15 CdO composite powders by attrition milling showed progressive reduction in relative peak intensity value for ZnO, CdO and Ag peaks and a proportionate increase in the value of FWHM for Ag (200) lines, as reported in Tables 4.2 - 4.4 and Fig. 4.12 - 4.15. These changes are as - expected for MA process for ductile-matrix composite system involving mechanical alloying of metal oxide with silver-matrix.

(II) Properties of sintered and hot-pressed compacts :

On the basis of results of density measurement given in Tables 4.11 (a) and (b), it can be said that it is possible to get final hot-pressed density > 98 % of theoretical by processing routes like mechanical alloying, spray-coprecipitation and conventional PM route of blending. These values are comparable to those reported in the literature. For example, typical density values for Ag 10CdO and Ag 15CdO reported are 10.0 g/cc (98.04 % of theoretical) and 9.8 g/cc (97.42 % of theoretical), respectively, as per Stevens [11]. Low values of hot-pressed density (87.8 - 96.8 % theoretical) for Ag ZnO (F) and Ag CdO (F) compacts and also (96.3 - 98.4 % of theoretical) for Ag ZnO (E) and Ag CdO (E) compacts are in view of presence of porosity in these compacts as revealed by their respective optical micrographs in Fig. 4.60 - 4.63.

Better microhardness values were obtained for final hot-pressed compacts of electroless coating route and MA route (85 - 93 kg/mm² at 65 g load as per histograms given in Fig. 4.46 and 4.47). The value of 106 kg / mm² for microhardness of compacts of MA route is substantially higher than values reported in the literature. As per the reports of R. K. Dubey and coworkers [13], microhardness for Ag 10 CdO, Ag 13 CdO and Ag 15 CdO compacts in cold-worked condition is 85, 85 and 88 VPN, respectively. Improved

microhardness of compacts of MA route is because of fine and uniform dispersion of oxide phase in silver-matrix for these compacts as per their optical micrographs given in Fig. 4.64. This is essential for improved resistance of contact material to mechanical wear during make and break operations.

Microhardness as low as 71-77 kg/mm² in case of compacts of conventional PM route of blending is as a consequence of non-homogeneity in dispersion of oxide phase developed in compacts of this route leading to the formation of silver-islands as per their microstructures (see Fig. 4.56 and Fig. 4.57).

The electrical conductivity data reported in Tables 4.13 (a) and (b) for Ag-ZnO and Ag-CdO compacts clearly show an acceptable level of conductivity for samples of blending, coprecipitation, electroless-coating and mechanical alloying routes (conductivity obtained for final hot-pressed compacts ranged from 72 % IACS to 91 % IACS units). They are in close conformance with the literature data. As per Appendix A1, the electrical conductivity values reported in ASM Handbook on 'Powder Metallurgy' vol. 7 (vide ref. [1]) for Ag 10 CdO are of the order of 72-85% IACS and for Ag 15 CdO are equal to 55-75 % IACS (large variation in quoted values may be due to difference in the processing routes adopted). Relatively lower electrical conductivity (63 - 78 % IACS) for samples of freeze -drying route is in accordance with their higher porosity level. (as per optical micrographs of Fig. 4.62 and 4.63)

Optical microscopy of hot-pressed compacts revealed fine and uniform dispersion of ZnO or CdO in silver matrix for compacts of coprecipitation and MA routes. Whereas the conventional PM route of blending gave non-uniformity in oxide phase dispersion (see optical micrographs of Fig. 4.56 to 4.63). Relatively higher porosity observed in optical micrographs for compacts of electroless coating and freeze-drying routes is

supposed to be the cause of their inferior physical and electrical properties as per earlier discussion.

Oxide-phase morphology (in terms of its degree of dispersion and shape) was quantitatively evaluated using image analysis method. As per Tables 4.14 (a) and (b), the values of % area fraction for oxide phase equal to 21.77 % and 16.49 % for Ag ZnO (MA) and Ag CdO (MA) compacts as against the values of 9.66% and 11.05% in Ag ZnO (B) and Ag CdO (B) compacts are indicative of superior dispersion of oxide-phase in silver matrix for compacts of MA route than those of blending route.

More rounded morphology of oxide phase in compacts of electroless-coating , freeze-drying and MA routes is reflected by the measured values of roundness factor for their oxide phases. Roundness factor for oxide particles in compacts of Ag ZnO and Ag CdO is only ~ 72 for blending route whereas it is around 77-81 for other routes (Table 4.14 (c) and (d)). Roundness of oxide phase particles indirectly correlates to the particle fineness. The particles tend to sphericity with increasing fineness.

Sameway, low feret average value of about 1.2 - 1.4 (as per Table 4.14 (c) and (d)) for oxide phase in compacts of electroless-coating, freeze-drying and MA routes as against a value of 3.3 - 3.5 for oxide phase in conventional route of blending, indicates finer and more isotropic nature of oxide phase for former routes than for blending route.

(III) Electrical contact performance evaluation :

The review of data for evaluation of contact performance leads to following inferences:

The weight loss due to arc erosion depends on the value of rated current employed during test. For instance, the weight loss due to arc erosion is 18.1 mg for Ag 7.1 ZnO (E) tested at 10A current ; 34.5 mg for Ag 10.8 ZnO (E) tested at 15A and 73.3 mg for

Ag 8.6 ZnO (E) contacts tested at 30A rated current over 100×10^3 make and break operations. Thus amount of wt. loss due to arc erosion increases with increasing current. The weight loss due to arc erosion for Ag 12 CdO contacts at 20A rated current under resistive load of power factor 1.0 after 100×10^3 contact operations comes to about 55 -60 mg as per the reports of K.Basu [142] on LCIE's life-test studies for electrical contacts.

During and on completion of 100×10^3 make and break operations for contact testing under several current-voltage combinations in these studies, no welding of contacts was recorded. Thus an excellent anti-welding behaviour was displayed by all the systems under investigation. This behaviour is comparable to the details reported in the literature [105], according to which no welding for Ag CdO or AgZnO samples was found after 50×10^3 make and break operations.

The property, contact resistance or resultant temperature rise, was also evaluated as a function of number of make and break operations during contact performance evaluation. In general, the contact resistance is high during early stages of make-break operations ; subsequently decreases and becomes more or less stable. The contact resistance for a system under a given set of test condition increases with increasing percentage of oxide phase. In present investigation, the contact resistance after 100×10^3 make and break operations for Ag 8.6 ZnO (E) system is 0.73 m.ohm whereas that for Ag 10.8 ZnO (E) it is 1.31 m.ohm. The value of contact resistance as per K. Basu's report [142] for similar test conditions comes to around 1.5 m.ohm for Ag 12 CdO contact material.

A separate evaluation carried out (as discussed in sect. 3.8.3 (iv)) on the Ag 10.8 ZnO (MA) contacts developed during this investigation gave encouraging results. The contact evaluation as per IEC 947-4-1 under AC-3 utilization category at 30A/415V/0.45 cos ϕ for 7000 make and break operations showed temperature rise at

contact terminals equal to 26.6°C (max.) as against the permissible limits of 70°C as per the standards. Lower temperature rise means lower contact resistance. The contactor in this evaluation successfully passed through the overload current test of 244 A (8 times the rated current) for 10 sec. as per IEC specifications and successfully completed 7000 make and break operations (as against the minimum required number of 6000 operations) without any permanent arcing, flashover between the poles and contact welding.

These results clearly indicate the possibility of replacement of Ag-CdO by an environment friendly Ag-ZnO system without any compromise in its contact performance in general.